UNIVERSITY OF TRENTO

Department of Industrial Engineering

Doctoral School in Materials, Mechatronics and System Engineering
XXXV Cycle

Multifunctional polymeric foams: preparation, characterization, and environmental aspects

Francesco Galvagnini

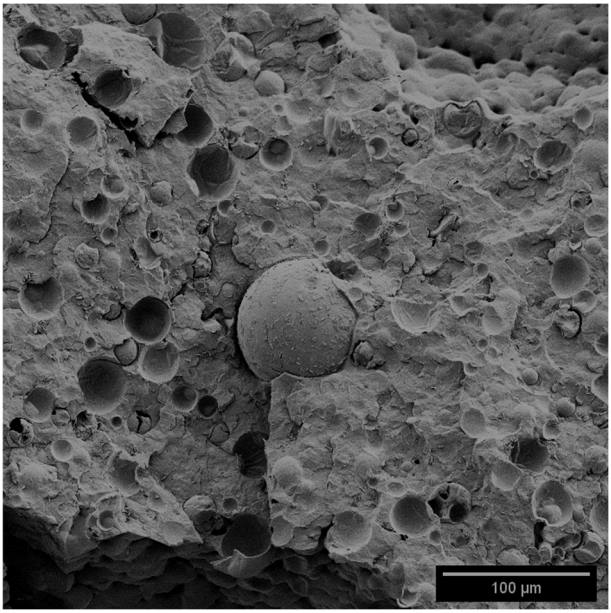

Multifunctional polymeric foams: preparation, characterization, and environmental aspects

Francesco Galvagnini

E-mail: francesco.galvagnini@unitn.it/

Approved by:

Prof. Andrea Dorigato, Advisor
Department of Industrial Engineering
University of Trento, Italy

Prof. Luca Fambri, Advisor
Department of Industrial Engineering
University of Trento, Italy

PhD. Commission:

Prof. Stefano Pandini
Department of Mechanical Industrial Engineering
Università degli studi di Brescia, Italy

Prof. Dr. Volker Altstaedt
Department of Polymer Engineering
University of Bayreuth, Germany

University of Trento,

Department of Industrial Engineering

Date

Abstract

Syntactic foams (SFs) are characterized by a unique combination of low density, high mechanical properties, and low thermal conductivity. Moreover, these properties can be tuned to specific applications. In contrast to traditional foams, where porosity is formed during the foaming process, porosity in syntactic foams can be obtained simply by incorporating pre-formed bubbles. Because of their high chemical stability and buoyancy, these type of foams found their first application in the marine industry. Nowadays, they are utilized in many other fields, such as in the aerospace and automotive industry. In this work, the multifunctionality of epoxy-based and polypropylene (PP)-based SFs was increased by including a microencapsulated Phase Change Material (PCM), able to impart Thermal Energy Storage (TES) capability at phase transition temperatures of 43 °C and 57 °C. The rheological, morphological, thermal, and mechanical properties of the prepared materials were systematically investigated. A final comparison of the two systems was performed to obtain a better comprehension of their potential in emerging industrial applications.

Contents

List of Figures

List of Tables

List of Acronyms

TES	Thermal energy storage
AN	Acrylonitrile
APTES	γ-Aminopropyl-Triethoxysilane
D50	Mean particle size
DGEBA	Diglycidyl ether of Bisphenol A
DMTA	Dynamic mechanical thermal analysis
DSC	Differential scanning calorimetry
EDA	Ethylenediamine
EMI	Electromagnetic interference
EP	Epoxy
FE-SEM	Field emission SEM
HDPE	High density polyethylene
HGMs	Hollow glass microspheres
HMs	Hollow microspheres
LDPE	Low density polyethylene
LFA	Light flash analysis
LHS	Latent heat storage
LLDPE	Linear low-density polyethylene
MA-g-PP	Anhydride-grafted-polypropylene
MAN	Methacrylonitrile
MF	melamine-formaldehyde resin
MMSFs	Metal matrix syntactic foams
PA	Polyamides
PC	Polycarbonates
PCMs	Phase change materials
PET	Polyethylene terephthalate
PF	Phenol formaldehyde
PMMA	Polymethylmethacrylate
PP	Polypropylene
PS	Polystyrene
PTFE	Polytetrafluoroethylene
PVC	Polyvinylchloride
SEM	Scanning electron microscopy
SFs	Syntactic foams
SHS	Sensible heat storage
TCHS	Thermochemical heat storage
TDI	Toluene-2,4-diisocyanate

TGMDA	Tetraglycidyl methylene dianiline
UF	Urea-formaldehyde

List of Symbols

a_{cN}	Charpy impact strength	[J/m^2]
c_p	Specific heat capacity	[J/(g·K)]
c_{p30}	Specific heat capacity at 30 °C	[J/(g·K)]
E_a	Activation energy of crosslinking	[J]
E_C	Compression elastic modulus	[MPa]
E_C/ρ	Specific compression elastic modulus	[MPa/(g/cm^3)]
E_t	Tensile elastic modulus	[MPa]
E_t/ρ	Specific tensile elastic modulus	[MPa/(g/cm^3)]
E'	Storage modulus	[MPa]
E'/ρ	Specific storage modulus	[MPa/(g/cm^3)]
E"	Loss modulus	[MPa]
G_{IC}	Critical strain energy release rate	[J/m^2]
G'	Storage shear modulus	[MPa]
G"	Loss shear modulus	[MPa]
k_E	Einstein coefficient (2.5 for spheres)	[-]
K_{IC}	Plane-strain fracture toughness	[MPa·m$^{0.5}$]
m	Mass	[g]
Q	Heat	[J]
R	Universal gas constant	[J/(mol·K)]
R^2_{adj}	Goodness of fit	[-]
$S_{y.x}$	Residual standard error	[specific]
T	Temperature	[°C]
tanδ	Loss tangent	[-]
T_c	Crystallization temperature	[°C]
T_f	Final temperature	[°C]
T_g	Glass transition temperature	[°C]
t_{gel}	Gel time	[s]
T_i	Initial temperature	[°C]
T_m	Melting temperature	[°C]
$t_{26–55}$	Time from 26 to 55 °C	[min:s]
t_{55-26}	Time from 55 to 26 °C	[min:s]
t_{35-80}	Time from 35 to 80 °C	[min:s]
$t_{80–35}$	Time from 80 to 35 °C	[min:s]
$VC_{\%}$	Void content	[%]

α	Thermal diffusivity	[m^2/s]
$\dot{\gamma}$	Shear rate	[1/s]
ΔH	Latent heat	[J/g]
ΔH_c	Crystallization enthalpy	[J/g]
ΔH_m	Melting enthalpy	[J/g]
ε_B	Tensile strain at break	[mm/mm]
ε_y	Tensile strain at yield	[mm/mm]
η	Viscosity	[Pa·s]
λ_c	Thermal conductivity of the composite material	[W/(m·K)]
λ_g	Thermal conductivity of glass	[W/(m·K)]
λ_h	Thermal conductivity of the contained gas	[W/(m·K)]
λ_{HGM}	Thermal conductivity of HGMs	[W/(m·K)]
λ_m	Thermal conductivity of the matrix	[W/(m·K)]
λ_{30}	Thermal conductivity at 30°C	[W/(m·K)]
ρ_{exp}	Pycnometric density	[g/cm^3]
ρ_{th}	Theoretical density	[g/cm^3]
σ_B	Tensile stress at break	[MPa]
σ_C	Maximum compressive stress	[MPa]
σ_y	Tensile stress at yield	[MPa]
σ_{20}	Compressive stress at 20% of strain	[MPa]
ϕ_g	Volume fraction of glass in HGMs	[-]
ϕ_h	Volume fraction of empty space in HGMs	[-]
ϕ_{HGM}	Volume fraction of HGMs in the composite	[-]
χ	Packing factor of the HGMs	[-]

Chapter 1 - Aim of the work

1.1 Motivation and objectives

One of the emerging technologies for more effective use of energy resources is Thermal Energy Storage (TES), which enables the temporary storage of excess heat that may be released when the demand for thermal energy outweighs its supply. Organic Phase Change Materials (PCMs), such as paraffin waxes, are among the most promising materials for TES in the low-medium temperature range (0-100 °C). These store heat when they melt and release it upon crystallization. PCMs are applied for thermal management applications, such as controlling the indoor environment in buildings or preventing the overheating of batteries and other electronic devices, because they can store a significant amount of latent heat at a nearly constant temperature. As a result, they are frequently used to maintain the temperature in a specific interval. PCMs can be "shape-stabilized" in porous materials or nanofiller networks, or they can be enclosed in macro, micro, or nanoshells, to avoid their leakage above the melting point. Generally, TES systems represent a supplementary component to be added to the main structure of a device. In applications where weight and volume savings are critical design parameters, embedding heat storage/management functionality directly into structural or semi-structural materials would be advantageous. Polymer matrix composites have the potential to be designed as multifunctional materials with both structural and non-structural functionalities in this context.

When lightness is a requirement, foams play an important role thanks to their high specific volume and specific strength. A special class of foams to be considered, especially when compressive strength is needed, is that of syntactic foams (SFs). Unlike traditional foams, where porosity is generated during the foaming process, in syntactic foams porosity can be obtained simply by incorporating pre-formed bubbles. When incorporated into a matrix, they can reduce the overall density and the thermal conductivity of the system. This class of foams found its first application in the marine field, thanks to their elevated chemical stability and buoyancy, but later they were also applied in many other fields like automotive, construction, and aerospace. One of the most utilized bubbles in SFs are the Hollow Glass Microspheres (HGMs), thanks to their simple production and low cost. By varying the HGM diameter, shell thickness, volume fraction, and surface reactivity, the final properties of the resulting SFs can be finely tuned.

Lightweight polymer composites with good mechanical properties and TES capability may find applications in a wide variety of technical fields, including the automotive industry, where the diffusion of lightweight structures may complicate

thermal management of the environment in the cockpit, and the portable electronics industry, where the reduction in volumes and masses also limits the space available for the cooling system. Although in the scientific literature there are many examples of polymers containing PCMs, little has been done to comprehensively investigate their mechanical properties and to improve them with the addition of reinforcing agents.

Therefore, the goal of this PhD Thesis is to develop multifunctional polymeric-based syntactic foams incorporating encapsulated organic PCMs, to design novel systems coupling structural/semi-structural functions and heat storage/management capabilities. Because this research topic has not yet been systematically addressed in the scientific literature, this work highlights the advantages and disadvantages of two different systems, prepared by using a thermoplastic (polypropylene (PP)) and a thermosetting (epoxy (EP)) matrix, also defining the formulations with the highest potential in terms of mechanical and TES properties synergism.

1.2 Thesis outline

This PhD Thesis is divided into 6 Chapters.

Chapter 2 - presents a detailed literature review on the TES technology, with a special focus on the different classes of PCMs and their applications. This Chapter also provides a review of the HGMs world, concerning their manufacturing and application fields.

Chapter 3 - describes the materials and the experimental techniques used to characterize the produced foams.

Chapter 4 - and Chapter 5 - report the results of the rheological, morphological, thermal, and mechanical analyses of the epoxy/HGMs/PCM and PP/HGMs/PCM systems, respectively. In both of them, the correlation among the considered properties were also depicted in the conclusion sections.

Lastly, Chapter 6 - contains concluding remarks, a comparison between the two systems, and the main recommendations for future research on this topic.

Chapter 2 - Background

2.1 Syntactic foams

2.1.1 Introduction

Syntactic foams are composite materials that have two phases: one is a continuous phase that composes the matrix (usually polymeric), and the other is made up of rigid hollow particles. These composite materials were created to reduce density without sacrificing mechanical properties. The research began with the aim of finding new low-density materials for marine, automotive, and aerospace applications, but it was then applied also to other fields, such as thermal insulation in buildings and packaging [1,2]. Because of the decrease in density caused by the insertion of hollow elements, these materials are classified as foams. It is particularly important to distinguish between two types of foams, on the basis of the type of porosity. Open porosity is constituted by interconnected holes, while close porosity is made by confined hollow spaces, like in the case of syntactic foams. Close-cell porosities are suitable for thermal insulation because they do not allow the free movement of air within the foam, while open-cell porosities are typically used for sound insulation [3].

Numerous materials can be used as a matrix for hollow particles, ranging from metals to polymers and even ceramics. This, combined with the variation in filler content, allows for the creation of syntactic foams with a wide range of properties [4–6]. Of course, the recyclability of the final foam will depend on the chosen matrix. From an industrial perspective, only thermoplastic-based SFs seem to be easily recyclable, while the other matrixes show hard challenges like the high cost and low volume available. There is the possibility of recycling the filler (when made of glass) in the case of thermosetting matrixes by burning the polymeric part and leaving the rest [6]. This procedure is also commonly used for recycling glass fibers from thermosetting composites.

2.1.2 Applications

Syntactic foams are becoming more popular in a variety of fields of application due to their unique properties. Among these characteristics, the adaptability of the properties stands out. This is thanks to the fact that the matrix and sphere materials, as well as sphere dimensions, surface condition, and eventually the presence of other fillers, can all be finely tuned[7,8]. Furthermore, in most cases, the manufacturing process is straightforward and rather simple. In most cases, low-cost polymers are used as matrices, filled with borosilicate glass spheres, making SFs

relatively inexpensive. In terms of properties, syntactic foams can withstand relatively high compressive stresses (especially the hydrostatic ones). They are good thermal insulators and have a high resistance to water absorption and degradation, if the matrix is carefully selected [9]. Furthermore, one of the most important characteristics of SFs is their low density. Weight reduction is a significant achievement in many manufacturing fields like aerospace but also automotive. Then, syntactic foams can be considered a suitable material wherever there is a need to reduce the weight of moving components while maintaining a certain set of properties [8,10–12]. Another fascinating aspect is that of recyclability. Meeting the new standards for reducing plastic pollution has become a top priority for many countries. As already said, SFs may be a fully recyclable class of material due to the use of two components: a polymeric matrix (made of recyclable thermoplastic polymer) and glass microspheres. These two materials are very different and can be quite easily separated (for example through flotation) [3].

2.1.2.1 Marine applications

The low density and good mechanical resistance to hydrostatic compressive stresses of syntactic foams make them an excellent candidate for marine applications. They are particularly popular as buoys for both surface and depth see conditions. Engineered Syntactic Systems LLC (Massachusetts, USA), for example, commercially produces a wide range of syntactic foams that can be used as buoys at various depths [13]. Figure 2-1 depicts a syntactic foam umbilical buoyancy. Aside from low density, thermal insulation is used for pipeline and subsea hardware insulation [14]. When the fluid temperature falls below a certain critical value, long underwater oil transfer systems can become clogged by the formation of paraffines and hydrates. This is why SFs are used for thermal insulation in underwater applications [13]. They can also be used as acoustic insulators in sound recorders, which are used to monitor biological sounds below sea level [15]. This material was chosen not only for its soundproofing capabilities but also for its compressive resistance and ability to resist aggressive environments, such as seawater.

Figure 2-1 DeepWater Buoyancy Inc. syntactic foam solution for deep see applications.

2.1.2.2 Aerospace applications

Because of their low weight and tailorable properties, syntactic foams have found their way into aerospace applications [16]. Companies such as Boeing Co have already developed SFs that are now used in their manufacturing lines. The Boeing Phantom Works R&D division developed patented thermoplastic syntactic foam to reduce electromagnetic interference of communication antennas, which are incorporated into the wings of the F/A-18E/F Super Hornet carrier-based aircraft [17,18]. Hohe et al. investigated the potential of sandwich composites with a SF core in aerospace applications [19]. Characterization tests revealed promising results in terms of perforation resistance and impact strength, thermal and acoustic insulation, and vibrational damping.

2.1.2.3 Automotive

The SFs capability of reducing weight and post-mold contractions seemed enticing for their application in automotive. Some original equipment manufacturers (OEM) are considering the use of thermoplastic syntactic foams for specific components like the air filter box, active grid shatter, and cowl grille. Even if the material is more expensive than "classic" materials like polypropylene with 20 wt% of talc (PP-T20), the reduction in weight could lead to an almost equal price per component with better features. To give an example, Ford is actually using thermoplastic based syntactic foams to manufacture their cowl grilles.

2.1.3 Microspheres

Microspheres play the role of filler in syntactic foams and are responsible for density reduction. Because of their hollow morphology, they are extremely lightweight. Depending on the application and on the matrix, there are numerous

options available, including glass, polymers, and ceramic microspheres of various dimensions and densities. Table 2-1 contains a list of microspheres commonly utilized in SFs.

Table 2-1 Different kinds of microspheres utilized in syntactic foams.

Microspheres	***Avg. Diameter μm***	***Density g/cm³***	***Matrix***	***Ref.***
Poly methyl methacrylate (PMMA)	0.2	0.40	PP/EPR	[20]
Hollow glass microspheres (HGMs)	60.0	0.15	Epoxy resin	[21]
HGMs low density (LD)	70.0	0.12	PMMA	[22]
HGMs medium density (MD)	45.0	0.37	PMMA	[22]
HGMs high density (HD)	18.0	0.60	PMMA	[22]
Fly ashes cenospheres	63.0	0.40	HDPE	[23]
Expanded perlite	3500.0	0.18	Aluminum A356	[24]

From Table 2-1 it is clear that there are various types of spheres commercially available with different dimension, density, and chemical composition. In particular, a relationship between particle dimensions and density can be noted. By increasing the particle diameter, thinning of the sphere wall occurs, therefore lowering the density.

2.1.3.1 Hollow Glass Microspheres (HGMs)

Hollow Glass Microspheres are, as the name implies, hollow spheres with micrometric dimensions made of boro-silicate glass. They can be filled with air or gas and frequently appear as a white fine powder. Their history begins in the 1930s when the 3M Srl Company produced solid glass beads used in reflective road paints from common window glass scraps. 3M used the same glass beads in 1950 to create special reflective sheets (called "Army Cardboard" at the time) to reduce night-time accidents among military vehicles during the second world war. However, the panels did not meet the brightness requirements, so 3M decided that the technology needed further development. At that point, a closer inspection revealed a series of micro-bubbles near the surface of the beads, reducing the brightness of the reflected light. The storage of crushed glass feed particles in a humid environment for an extended period determined the conditions that induced the formation of these bubbles. Shortening the storage time was enough to resolve this issue and meet the brightness requirements.

Nevertheless, it was demonstrated that the production of hollow glass spheres, which 3M had been interested in since 1930, was feasible. A patent application was filed in 1963 for the production of hollow microspheres from glass and phenolic

resins using a two-step melting and forming process. This commercial development opened up a lot of different solutions and applications, including the production of hollow spheres from fly ashes (a coal combustion by-product) [25]. These are known as cenospheres, they have a higher density than normal HGM and are typically composed of alumino-silicate materials. When compared to conventional HGMs, the external surface is riddled with flaws. However, this disadvantage is offset by improved composition [23,26].

There are several types of commercially available HGMs with varying densities and dimensions, as shown in Table 2-1. This is accomplished by varying the ratio between the wall thickness and diameter of the bubbles, resulting in a wide range of densities. According to Ozkutlu et al., when producing HGM syntactic foams, flexural strength is heavily influenced by HGM density. In particular, it appeared to be enhanced with increasing density, most likely due to the higher crushing resistance [22]. Furthermore, spheres with thicker walls tend to withstand and survive the melting processing typically used in the production of syntactic foams at a higher rate [27,28]. The failure load as a function of the HGMs wall thickness is shown in Figure 2-2.

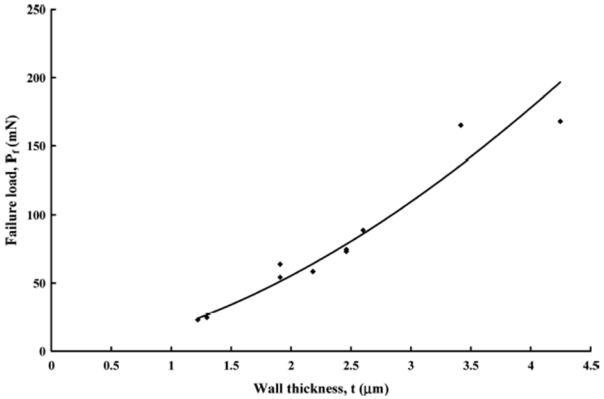

Figure 2-2 HGMs failure load vs wall thickness [28].

Of course, the presence of glass defects could result in the HGM failing before its time, but modern HGM manufacturing techniques allow for almost defectless bubbles. The survival rate can be then calculated by comparing the expected density calculated theoretically (for example, using the rule of mixture) and the experimental density. If the true value is greater than the expected one, HGM has been broken during processing [29].

The bulk isostatic compression strength of HGMs is an important mechanical property that is commonly measured. This is a parameter that is determined by the diameter and wall thickness of the spheres. There are several methods for determining HGM's compressive behavior. One of them involves subjecting a group of spheres to high isostatic pressure and then measuring the survival rate. The spheres are first placed inside a rubber container filled with glycerin, which is then placed inside a pressure chamber. Glycerin is used because it is one of the least compressible fluids. The measurement itself begins by pressurizing the chamber to a predetermined pressure and simultaneously recording volume and pressure. The process is then repeated with a higher value of pressure, while volume and pressure are again evaluated. Finally, a plot of pressure as a function of volume, like that shown in Figure 2-3, can be obtained. In this way, two sets of data will form two curves: the first is known as the collapse curve, and the second one is known as the compression curve [84-86] useful to determine the percentage of collapsed HGMs in the test. Percent volume survival ($V_{survival}$) calculations shown in Equation ((2-1).

$$V_{survival} = 1 - \left(100 \cdot \left(V_t \cdot \frac{V_1 - V_2}{V_{ap} - V_m}\right)\right) \tag{2-1}$$

Where V_t is the total volume collapse calculated by the difference in the collapse and compression curve values at zero pressure; V_1 and V_2 are the volume values of the compression and collapse curves, respectively, at the pressure of interest; V_{ap} is the volume occupied by the HGMs, and V_m is the volume of the wall material.

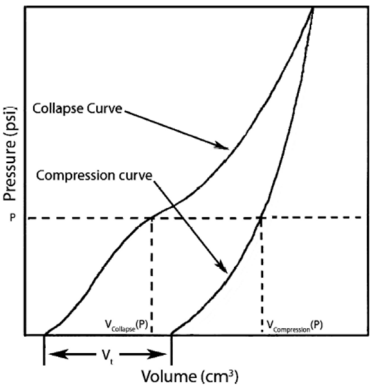

Figure 2-3 An example of bulk isostatic compression test curves [27].

Uniaxial compression testing of individual HGMs is another mechanical characterization technique commonly used for these materials. It is carried out by testing the compression resistance of a single sphere with a modified nano-indenter. This is a newly developed technique that employs a cylindrical sapphire indenter with a diameter of 90 μm, while the sphere rests on an aluminum polished surface and serves as the compression plate. The alignment of the indenter is critical to achieve precise uniaxial testing of the sphere, and it is obtained by using an optical microscope. This technique measures not only the ultimate compressive stress of HGM but also the load and displacement at failure, as well as the work of fracture (calculated as the area under the load-displacement curve). The pseudo-stiffness (k) can be calculated using the initial linear relationship between load and displacement. The results of this test revealed an unusual aspect that was not highlighted by common bulk isostatic compression tests. There is a positive relationship between fracture work and failure load and sphere diameter. This means that HGM with larger diameters (and thus generally thinner walls) would sustain higher loads and energy of fracture in comparison to smaller spheres, which contrasts with the results of bulk isostatic compression and this is due to two reasons. First, HGMs with larger diameters (and thus thinner walls) have a lower number of defects and flaws than thicker spheres, and second, increasing the diameter of the sphere increases its radius of curvature, allowing for a larger contact area between the plates and the HGMs. This results in a more evenly distributed load [26,30,31].

Boro-silicate glass or aluminum-silicates are commonly used to make HGMs. When these fillers are inserted inside polymers, they can be considered thermally stable materials. Thermal characterization demonstrates how the thermal transitions of glass occur at relatively high temperatures. The glass transition temperature (T_g) is around 600 °C, while the melting temperature (T_m) of pure silica is 1710 °C. Despite having one of the highest melting temperatures (between 325 and 335 °C) [32], T_m of polytetrafluoroethylene (PTFE) is still much lower than those found in glass [26].

The thermal conductivity of HGMs is a difficult parameter to measure, both in the case of a single sphere (due to its small dimensions) and in powder form (because of the trapped air between spheres). For this reason, thermal conductivity (λ_{HGM}) is typically calculated by using theoretical models [33–35]. The series model reported in Equation (2-2) is the simplest expression.

$$\lambda_{HGM}(T) = \left(\phi_g \cdot \lambda_g(T)\right) + \left(\phi_h \cdot \lambda_h(T)\right) \quad (2\text{-}2)$$

Where ϕ_g and ϕ_h are respectively the volume fraction of glass and interior empty space (containing gas), and λ_g and λ_h are respectively the values of thermal

conductivity of glass and inner gas. However, this series model produces too simplistic results and frequently underestimates the actual value of conductivity. As a result, a more sophisticated flux-law model can be used to predict thermal conductivity of HGMs. A Maxwell flux model, as described in Equation (2-3), can be used [26]:

$$\lambda_{HGM}(T) = \lambda_g(T) \cdot \frac{\lambda_h(T) + 2\lambda_g(T) - 2\phi_g\left(\lambda_g(T) - \lambda_h(T)\right)}{\lambda_h(T) + 2\lambda_g(T) + \phi_h\left(\lambda_g(T) - \lambda_h(T)\right)} \tag{2-3}$$

The values of thermal conductivity of the glass and the contained gas depend on the considered temperature.

When incorporating HGMs inside a resin, it can be possible to estimate the thermal conductivity of the resulting composite material (λ_c) by using the Nielsen model reported in Equations (2-4), (2-5), (2-6), and (2-7). This model takes into account not only the shape of the particulate filler used (in the case of HGM, the shape is spherical) but also the packing factor [35–37].

$$\lambda_c = \lambda_m \frac{1 + A\,B\,\phi_{HGM}}{1 - B\,\Psi\,\phi_{HGM}} \tag{2-4}$$

$$A = k_E - 1 \tag{2-5}$$

$$B = \frac{(\lambda_{HGM}/\lambda_m) - 1}{(\lambda_{HGM}/\lambda_m) + A} \tag{2-6}$$

$$\Psi = 1 + \phi_{HGM} \frac{1 - \chi}{\chi^2} \tag{2-7}$$

Where λ_m is the thermal conductivity of the matrix, λ_{HGM} is the thermal conductivity of the HGMs, ϕ_{HGM} is the HGM volume fraction, k_E is the Einstein coefficient (equal to 2.5 for spherical rigid particles suspended in a matrix), and χ is the packing factor for HGMs (for spheres around 0.63).

2.1.3.2 Production methods

Concerning the manufacturing of hollow microspheres (HMs), there is a distinction between cenospheres and synthetic HMs. The first are made of aluminosilicate from fly ashes (a byproduct of coal combustion). They have a variable composition and are filled with air or an inert gas [38]. Because their properties are highly unpredictable, a controlled process is required. The second starts with the typical glass production technology, thus making the manufacturing process much easier.

Modern processes are based on the formation of a solid phase at the boundary between a droplet or a solid particle and the surrounding medium. The core is removed once the outside wall has been formed. The most important methods for producing HMs are reported in the following list [39]:

- *High-temperature smelting*
  It involves blowing a powdery precursor into a stream of hot gas or flame. This precursor is primarily made up of silica, inorganic components, and a blowing agent. When exposed to high temperatures, the thermal decomposition of the blowing agent allows cavities to form inside the spheres. Following this reaction, the formed spheres are quenched with water.

- *Spray and dipping technologies*
  A colloidal or molecular dispersion of a film-forming substance in a suitable medium is the starting point for the process. The solution is then atomized by a nozzle, resulting in droplets of liquid. These are then placed in a hot gaseous atmosphere, which causes the solvent to evaporate, causing the outer walls to form.

- Emulsion processes
  These methods typically involve the emulsification of a water-based inorganic solution in an organic phase. This allows for the dispersion of single droplets within a continuous medium. Water is removed from the emulsion by diffusion or evaporation. This method can be used to create polymeric hollow microspheres.

- Coating in suspension and fluidized beds processes
  Both of these processes entail coating solid template particles to create a surrounding wall. Evaporation or pyrolysis is then used to remove the sacrificial core. The dimensions of the spheres that can be obtained differ between the two processes. Fluidized bed processes necessitate proper particle fluidization, which is difficult for spheres with dimensions less than 50 μm. As a result, this process can produce spheres with dimensions ranging from 100 to 3000 μm.

2.1.4 Matrices

Syntactic foams are composite materials composed of hollow elements embedded in a matrix that can be polymeric, metallic, or ceramic. Polymeric matrices are the most widely used, because of their easy processability and lower material and

manufacturing costs [25,40–43]. Figure 2-4 depicts an overview of the various types of matrices used in the production of syntactic foams.

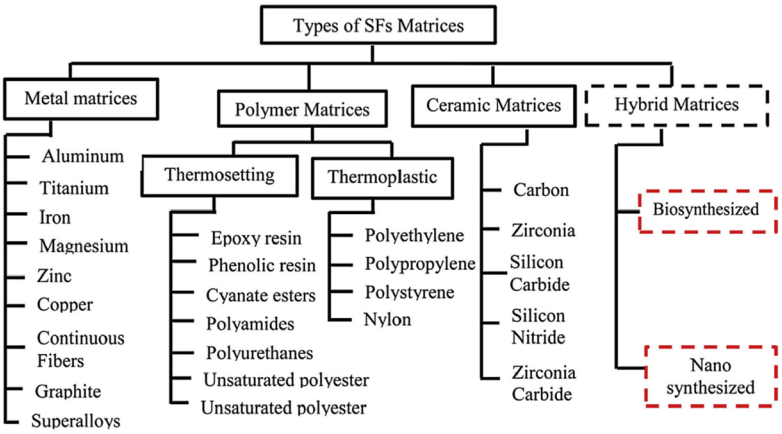

Figure 2-4 Overview of matrices utilized for syntactic foams production [3].

2.1.4.1 Thermosetting matrices

Thermosetting polymers have a structure in which polymeric chains are crosslinked together following a hardening procedure obtained through curing. This irreversible process involves the reaction of the resin and a curing agent, which may be aided by heat or radiation. The starting materials are liquids, and as the crosslinking reaction progresses, their viscosity increases as well until its flow is stopped. Aside from an increase in viscosity, heat evolution and the loss of potentially volatile components occur during curing. Once the two components are combined, the time available for shaping is limited. In general, all these parameters are often provided by the resin manufacturer [44]. The Pot Life is the time after which the viscosity of the resin doubles. The Gel Time is the time required for a resin to reach the point at which it will be defined as solid and no longer as viscous material, and thus it is no longer workable. Working Life is a parameter defined by the manufacturer representing the practical resin working time. Shelf Life is the time that precursors can be stored without losing their chemical reactivity.

These materials are distinguished by their high stiffness, high glass transition temperature, good dimensional stability, thermal stability, and chemical resistance. Epoxy resins, phenol-formaldehyde (PF) resin, polyurethanes, phenolic resins, are examples of thermosetting polymers. For syntactic foams, thermosetting matrices, particularly epoxy resins, are among the most commonly used [4,40,45,46].

Epoxy resins have found their way into a wide range of applications, including adhesives, aerospace, automotive, sports equipment, biomedical systems, and so on. Epoxy resins are organic liquid pre-polymers that have a low molecular weight and contain multiple epoxide groups. Various hardeners can be used to induce crosslinking, and different properties can be achieved depending on the type of resin and curing agent [47]. A schematization of the epoxide group is shown in Figure 2-5.

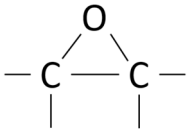

Figure 2-5 Epoxy group schematization

Commercial epoxy matrices are typically made up of one major and two minor epoxy prepolymers, as well as one or two curing agents. Minor epoxies are used to adjust viscosity and/or improve temperature resistance, toughness, and moisture absorption. Diglycidyl ether of Bisphenol A (DGEBA) and tetraglycidyl methylene dianiline (TGMDA) are the most commonly used major epoxies, particularly in the aerospace industry. Diluents are used in small amounts (3-5%) in the epoxy formulation to reduce curing shrinkage, increase shelf and pot life, and control the exothermicity of the curing reaction. Butyl glycidyl ether, cresyl glycidyl ether, phenyl glycidyl ether, and aliphatic alcohol glycidyl ethers are common diluents [48].

Higher temperatures and longer curing times in an epoxy resin result in a higher crosslink density and thus a higher glass transition temperature, especially if the precursors have high functionality (e.g., four reactive end groups per molecule). Toughening agents can be added to the resin to prevent excessive brittleness, but this may result in lower thermal resistance [48].

2.1.4.2 Thermoplastic matrices

Thermoplastic polymers are plastics that, in principle, can be shaped and remelted an infinite number of times. In practice, the cycles are limited by the thermal degradation of the polymers. These plastics can be amorphous, with only a glass transition temperature (T_g), or semi-crystalline, with both T_g and melting temperature (T_m). These polymers can also be distinguished, from a molecular structure point of view, by linear or branched chains that can be ordered, allowing the formation of crystalline domains. Because of their lack of crystalline structure, amorphous thermoplastic polymers are frequently transparent and have a lower

resistance to chemical attacks [49]. Thermoplastic polymers can be synthesized through polymerization processes in which monomers with functionality (F) equal to 2 react with various mechanisms:

- *Chain Polymerization reaction:* it can be free radical, ionic, ring opening, living, and others.
- *Polycondensation reaction.*
- *Polyaddition reaction:* that includes catalytic reaction (Ziegler-Natta) and isocyanate reactions.

Polyethylene (HDPE and LDPE), polystyrene (PS), polypropylene (PP), polyvinyl chloride (PVC), polyamides (PAs), polycarbonate (PC), polymethyl methacrylate (PMMA) are examples of thermoplastic polymers. Regarding syntactic foams, the research with thermoplastic polymers is more limited with respect to thermosetting matrices, because thermosets are generally easier to process. Despite this, studies on HDPE, PP, and PMMA have shown promising results in terms of density reduction without compromising mechanical properties [20,22,25,29,50,51].

Polyolefins are primarily HDPE, LDPE, PP, and their copolymers produced by the polymerization of unsaturated aliphatic hydrocarbons. LDPE was the first commercially important polyethylene produced by free radical polymerization, which created branched macromolecules. Later, HDPE was synthesized through Ziegler-Natta polymerization, which allowed for longer linear chains and, as a result, higher density due to the presence of a catalyst. Figure 2-6(a,b) depict the polyethylene repeating unit and the chain morphologies of LDPE, LLDPE, and HDPE.

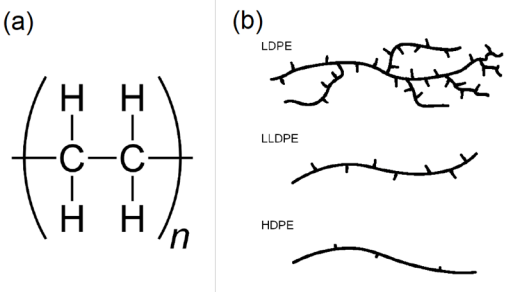

Figure 2-6 (a) repeating unit of polyethylene, and (b) structure of different types of polyethylene.

Polyethylene terephthalate (PET) is another important thermoplastic polymer. It is considered as one of the most important engineering polymers due to its widespread

use. Thanks to its excellent tensile and impact strength, clarity, processability, and chemical resistance it is commonly employed in many applications, particularly in plastic bottle manufacturing. In addition to these characteristics, its recyclability, combined with its dominance in the single-use plastic containers market, makes it the most recycled polymer [52].

Isotactic polypropylene (PP) is a thermoplastic polymer of the polyolefins group discovered in 1954 by Professor Giulio Natta in Milan, Italy [53]. Tacticity, which describes the characteristic stereochemistry of chiral centers inside a macromolecule, is an important concept for this plastic. It refers to the position of the methyl group of each repeating unit with respect to the main carbon chain in polypropylene [54]. Three possible configurations can be identified in isotactic, syndiotactic, and atactic, as reported in Figure 2-7(a,b).

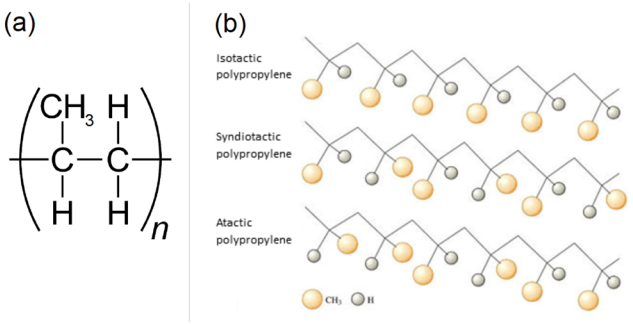

Figure 2-7 (a) PP repeating unit, and (b) tacticity in polypropylene

When it first appeared, PP was distinguished by the presence of isotactic, syndiotactic, and atactic domains, indicating that it was polyhedric. However, thanks to catalyzed processes, it was possible to obtain a dominant isotactic behavior [55]. PP is created through the polymerization reaction of propylene [47]. The reaction can be catalyzed by Ziegler-Natta (isotactic), metallocene (syndiotactic), or free radical polymerization (atactic). Isotactic PP is the most technologically and commercially important type of polypropylene. It has a typical crystallinity value from 40 to 60%, a melting temperature between 150-170 °C, a glass transition temperature of -10 °C, and a decomposition temperature of 240 °C. Its low density (0.9 g/cm^3) makes it one of the most lightweight thermoplastic polymers. It has good chemical resistance as well as mechanical properties due to its relatively high crystallinity, with a tensile modulus of up to 1.5 GPa and tensile strength around 30 MPa. Extensive research on commercially available PP enabled the achievement of a wide range of melt flow indexes , ranging from 1.9 to 31.0

g/10 min (at 230 °C, 2.16 kg) [56]. This can be a significant advantage during the processing phase because it allows for the selection of the appropriate polypropylene based on the desired value of melt viscosity.

2.1.4.3 Metallic matrices

Metal matrix syntactic foams (MMSFs) are made by dispersing hollow particles within a metallic matrix [57,58]. The inserted hollow particles give the composite closed-cell porosity, allowing for lighter materials than the matrix alloy [59]. These MMSF composite foams have found their way into the automotive and marine industries due to their high energy absorption, heat insulation, specific stiffness, and damping capabilities [60–62]. In recent years, several MMSFs have been investigated with different matrixes like aluminum [63–68], steel [69–72], or magnesium [73–76], with promising results. Recently, also MMSFs with zinc have been developed [59,77].

2.1.4.4 Ceramic matrices

Ceramic-based syntactic foams are used in energy storage systems, automotive, aerospace, and the building industry. Because the matrix is made of ceramic materials, it can withstand harsh environmental conditions such as temperature and chemical presence [78].

2.2 Thermal Energy Storage (TES) technology

Many efforts have been made to improve energy efficiency in both the domestic and industrial environment to reduce greenhouse gas emissions and fossil fuel consumption. Wasting less energy requires less intensive energy production. However, thermal energy management remains an important aspect in this time-consuming and lengthy search for alternative and efficient technologies. Using thermal energy storage (TES) materials, that can store and release heat when needed, is a strategy that is gaining popularity. A sub-class of these materials is the Phase Change Materials (PCMs). They have a high enthalpy of fusion, which allows them to store and release a large amount of energy as latent heat during melting and solidification [79].

2.2.1 Introduction

Concerns about the depletion of fossil fuels, climate change, and greenhouse gas emissions have recently attracted the attention of researchers, industries, and

governments in developing technologies for more efficient energy use. As fossil-fuel-based energy production strategies have recently been linked to environmental pollution and global warming, the research attention has shifted to sustainable and renewable energy sources such as solar, wind, and geothermal energy [80]. The high initial plant costs and the intermittent nature of these sources are the two main barriers to their widespread adoption. If technological progress mitigates the first issue, increasing energy storage technologies can provide an effective solution to source intermittency. Because the amount of solar energy varies on a daily and seasonal basis, and wind and geothermal power can be unpredictable, energy production plants must be supplemented with energy storage systems to provide a significant and consistent output even during off-peak periods [80]. When used in buildings, vehicles, and industrial applications, energy storage systems can benefit the use of conventional energy sources as well [80,81]. In the transport industry, for example, improved battery performance could encourage the use of electric vehicles, reducing demand for traditional fuels. Energy storage systems can help to reduce equipment sizes and initial and maintenance costs, increase plant flexibility and efficiency, and reduce the need for emergency power generators that consume primary energy sources. [81,82].

2.2.2 Thermal energy storage (TES) concept

Thermal energy storage (TES) is the temporary storage of heat that can be used later and/or in a different location. The TES systems are intended to reduce the mismatch between thermal energy availability and demand, thereby contributing to waste heat recovery and more efficient use of intermittent energy sources [83]. In comparison to the other energy storage systems, heat (or cold) storage has longer storage times and a higher efficiency [80].

TES technologies are classified based on how the internal energy of the storage medium varies. Thermal energy can be stored and released by varying the temperature of a material (sensible heat storage SHS), changing the endo/exothermic phase of a material (latent heat storage LHS), or through thermochemical reactions (thermochemical heat storage TCHS). The choice of one TES system over another is influenced by several factors, including the required heat storage period (hours, months, or days), economic considerations, working temperature, and available volume. Table 2-2 contains a list of the main parameters of the various TES systems [84]. Despite the fact that the TCHS system has a higher energy density per unit mass and volume and a higher efficiency, its technological maturity is lower than that of the other two classes, and some recent reviews on the topic suggest that significant efforts should be made to develop advanced materials and produce efficient prototypes [85]. LHS systems, on the other hand, such as

underground thermal energy storage and domestic hot water storage, are characterized by low risk and high commercialization potential [80].

Table 2-2 Main features of sensible, latent, and thermochemical TES technologies [84].

TES system	*Capacity kWh/t*	*Efficiency %*	*Storage period h, d, m*	*Cost (2017) €/kWh*
Sensible heat storage (SHS)	10-50	50-90	d/m	0.1-10
Latent heat storage (LHS)	50-150	75-90	h/m	10-50
Thermo-chemical heat storage (TCHS)	120-250	75-100	h/d	8-100

2.2.3 Sensible heat storage (SHS)

SHS materials, as previously stated, are based on the storage of thermal energy by heating a solid or a liquid. The amount of heat (Q) that can be stored is determined by the specific heat capacity (c_p), mass (m), and temperature interval (T_f - T_i) of the material and can be calculated by using Equation (2-8).

$$Q = \int_{T_i}^{T_f} m\, c_p\, dT = m\, c_p\, (T_f - T_i) \tag{2-8}$$

It should be noted that c_p depends on the temperature [86]. Because of its low cost and high specific heat (4.18 J/g·K), water is frequently used as a medium in this type of TES system. This technology has found its way into active heating systems in the form of water-filled panels and solar heating systems [79,87].

2.2.4 Latent heat storage (LHS)

LHS materials, on the other hand, use the latent heat (ΔH_m) of phase transitions (for example, from solid to liquid) to store energy. They deal with solid-solid, solid-liquid, and other transitions. This TES system deals with PCMs, which can provide higher energy storage density with a narrower temperature range than SHS. Equation (2-9) can be used to calculate the storage capacity of LHS [88].

$$Q = \int_{T_i}^{T_m} m\, c_p\, dT + m\, \Delta H_m + \int_{T_m}^{T_f} m\, c_p\, dT \tag{2-9}$$

2.2.5 Classification of PCMs

Phase change materials (PCMs) collect numerous types of substances different in nature that work similarly, and for this reason, there are several ways to categorize them. Firstly, they can be simply classified according to their melting temperature [86–89].

- Low-temperature PCMs (less than 15 °C) are used in air conditioning and the food industry.
- Medium-temperature PCMs (between 15 and 90 °C) are typically employed in solar, medical, and construction applications.
- High-temperature PCMs (above 90 °C) are mostly used in solar plants and automotive and aerospace applications.

PCMs are also categorized based on the type of phase transition, as reported in Figure 2-8.

In comparison to other transitions, liquid-gas and solid-gas have high latent heat values. Unfortunately, due to their difficult management, their use is impractical. PCMs characterized by solid-solid and solid-liquid transitions with a much more limited volume expansion are a more popular choice. In addition, solid-solid transition PCMs can also provide an added benefit by avoiding technical difficulties associated with the presence of the liquid phase, despite having a lower latent heat.

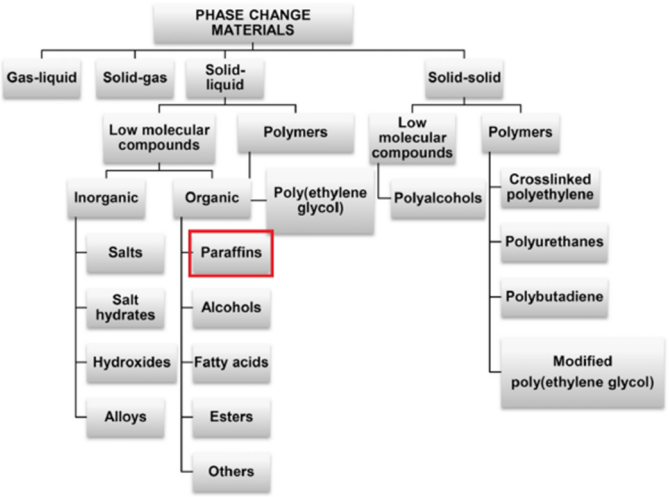

Figure 2-8 Classification of PCMs

Organic and inorganic solid-liquid PCMs compounds are both available. Paraffins are particularly interesting because of their wide range of operating temperatures. These materials are classified as low molecular compounds because they are made

up of saturated hydrocarbons, with the formula C_nH_{2n+2}. The majority of them are non-toxic and non-hazardous to the environment. Paraffines have a relatively high TES density with low thermal conductivity. This could slow charging and discharging processes, necessitating a larger surface area [86,88,89]. The melting temperature of paraffins unusually depends on their molar mass. Furthermore, the ability to select different phase transition temperatures makes them extremely versatile and simple to select based on the application. The average length of the hydrocarbon chain influences the melting temperature and heat of fusion. It is possible to tune both of these parameters by modulating the molecular weight, and it is frequently obtained by mixing paraffines. A review of the performance of n-paraffin waxes as PCM can be found in the studies conducted by He et al. on Hexadecane, tetradecane, and their mixtures. The results demonstrated a high heat of fusion as well as adequate stability and repeatability even at elevated heating/cooling cycles [90]. Furthermore, the melting and freezing of the PCM occurs over a temperature range rather than at a fixed temperature. Volume expansion and contraction were also evaluated, with less than 10% contraction during solidification.

Interactions with other materials may occur when working with these PCMs. Metal coupling is considered safe because it does not promote corrosion or other phenomena. However, with polymers, the situation is more complicated. Because of chemical affinity and similarity, PCM can cause polymer softening, particularly in polyolefins. PCMs are encapsulated to avoid also this phenomenon [91–94].

2.2.6 Encapsulation technologies

Microencapsulation is a process in which a specific material, which serves as the core, is contained within a particle that serves as the external shell [93]. It is performed on PCMs for the following reasons: it increases the heat transfer area, reduces chemical interaction with the surrounding environment, and aids in volume control when a phase transition occurs. Microencapsulation is a technique that is now widely used in industries such as food and agriculture, pharmaceuticals, cosmetics, and textiles [95–100]. It has obtained more attention in recent years for PCMs as well [98,101–108], even if its use in thermal energy management applications is still limited due to the high costs involved. In terms of materials, the following are commonly used as shells for the microcapsules: urea-formaldehyde resins (UF), melamine-formaldehyde resins (MF), and polyurethanes [87,93,106]. There are various methods that can be used to achieve encapsulation. The following paragraphs contain some additional information about common shell-forming techniques.

2.2.6.1 Coacervation

It is defined in colloidal chemistry as the separation of two phases through the modification of the environmental conditions (pH, temperature, or solubility). The method involves the deposition of a coacervated polymer (rich in colloids) around the active component (the core). The mechanism is controlled by complex ionic interactions between charged macromolecules present in the solution that eventually form the shell itself. Coacervation is one of the most effective methods of encapsulation and it is widely used in the food and pharmaceutical industries. Gelatin, various proteins, Arabic gum, and cellulose are examples of shell materials that can be used [109]. Figure 2-9 shows a scheme of the working principle of coacervation.

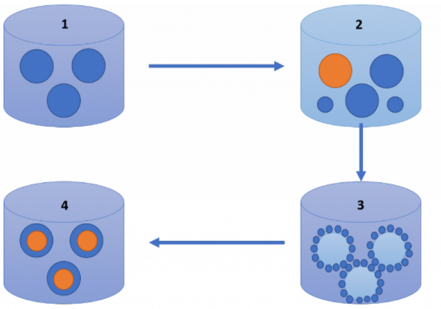

Figure 2-9 Representation of the coacervation process, (1). Dissolution of the polymer, (2) formation of immiscible phases, (3) deposition of liquid coating on core material, and (4) rigidization of coating.

2.2.6.2 Suspension polymerization

This method creates polymeric microcapsules by dispersing a monomer (in the form of liquid droplets) within a stabilizing medium (usually water) as shown in Figure 2-10. The polymerization initiator can also be found within this dispersion. Because the goal is to form an external shell around the PCM, the free radicals required for polymerization are generated at the interface between the medium and the suspended oil droplets. To accomplish this, the initiator must be of the appropriate polarity. Examples of this process can be found in the work of Sànchez et al. [110] where they obtained a polystyrene shell or by Jonsson et al. [111] where they developed a copolymer shell in Acrylonitrile/methacrylonitrile (AN/MAN).

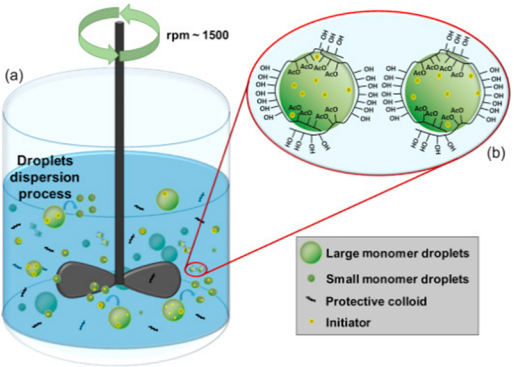

Figure 2-10 Suspension polymerization scheme [112]

2.2.6.3 Emulsion polymerization

This is a heterogeneous free radical polymerization in which a hydrophobic monomer is emulsified in water, as shown in Figure 2-11. The reaction begins with a water-insoluble initiator. Styrene, butadiene, acrylonitrile, and methacrylate ester monomers are examples of commonly used monomers. This polymerization process is rather complex because the nucleation, growth, and stabilization of polymer particles are controlled by a combination of factors that regulate free radical polymerization and colloidal phenomena [113]. Zhang et al. used emulsion polymerization to create a Polystyrene/Cellulose Nanocrystal Hybrid Shell for PCMs with promising results [114].

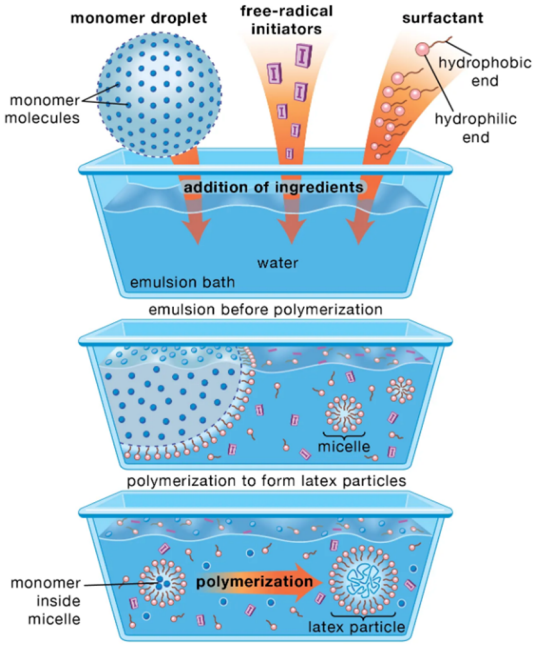

Figure 2-11 Emulsion polymerization scheme (by Encyclopædia Britannica) [115].

2.2.6.4 Polycondensation

Interfacial polycondensation is a popular encapsulation method that is distinguished by its ease of use, high reaction rates, and low penetrability of the resulting shells. The core materials are formed into droplets in this process via emulsion in an aqueous solution containing a dissolved reactive monomer that serves as the shell. When the reaction begins, a thin monolayer membrane forms around the core droplets, and the shell is formed as a result of the polycondensation reaction [116]. The shell can be made from a variety of materials, including polyurethane, polyurea, polyamide, and amine resin, using this technique. Using an interfacial polycondensation method, Liang et al. were able to encapsulate butyl stearate (PCM) inside polyurea microcapsules. The monomers chosen for the shell formation are toluene-2,4-diisocyanate (TDI) and ethylenediamine (EDA) [83].

2.2.7 Applications

The construction industry is a significant user of Phase Change Materials [102,117–121]. It is demonstrated in the literature how, by employing these PCM-based

thermal energy management systems, it is possible to reduce energy consumption in areas where temperature changes significantly during the day-night cycle. Feldman et al. [122] in 1990 investigated the effects of incorporating butyl stearate (PCM) into gypsum during the conventional mixing stage with water. The results demonstrated the viability of this method for obtaining thermal energy storage capability. An important aspect to consider is the effective thermal comfort enhancement that these systems can provide. Kuzink et al. [123] investigated this by monitoring a renovated office building with PCM wallboards in the lateral walls and ceiling for about a year. Two rooms were specifically controlled: one with PCM and one without. The results showed an increase in thermal comfort due to improved control of both walls and air temperature. Another intriguing application is in thermo-solar energy systems [124–130]. PCMs, in particular, are commonly used to store solar heat collected during the day for use during the night. These systems are typically coupled with a solar water heater. Fazilati et al. [131] used an encapsulated paraffin PCM to store energy on a solar water heater. The results showed a nearly 40% increase in energy storage density and a 15% increase in energy storage efficiency.

Another intriguing application is the incorporation of PCMs into textile fabrics, which results in the creation of smart textiles that aid in the regulation of body temperature and are especially useful in extreme weather conditions. NASA developed one of the first examples of PCM-enhanced textiles. Nonadecane was added to garment fabrics (e.g., space suits) to reduce the impact of the extreme temperature changes to which astronauts are subjected during space missions [132]. Such intelligent thermoregulating textiles were later used to improve the thermal comfort of mountain outdoor clothing and apparel, as well as blankets, mattresses, and pillowcases [79].

Electronic devices are well known to be temperature sensitive, as their performance and lifetime span are entirely dependent on maintaining them within a specific temperature range, with special care taken to avoid overheating. As electronic components have become more sophisticated in terms of electronics while shrinking in size, the risk of overheating has increased. Without a proper thermal management system, heat generation and temperature rise can degrade performance, cause critical components to fail, and reduce user-device interaction comfort [133]. As roughly 55% of electronic component failures can be attributed to high-temperature issues or inadequate thermal management, overheating is one of the most frequent reasons for the failure of electronic components [134]. According to research, a 1°C drop in temperature can reduce failure rates by up to 4%, whereas a 10 to 20 °C rise can double the likelihood of failure [134]. Tan and Tso [135] conducted ground-breaking experimental research on the use of PCMs in

mobile electronic devices, evaluating the effectiveness of a passive cooling unit based on n-eicosane for the thermal control of small hand-held personal computers (personal digital assistants). The PCM was housed in an aluminum case and placed beneath heaters that mimicked the heat generation units of such a device, namely the processor and other integrated circuit packaging. The authors concluded that the PCM units were required to keep the device's working temperature below an acceptable threshold of 50 °C and that the efficacy of the heat storage unit was determined not only by the amount of PCM but also by its orientation, which determined the heat flux distribution throughout the device.

Aside from the construction materials field, there are surprisingly few publications on materials designed to combine structural and TES functions. Wirtz et al. [136] presented one of the first reported examples, a sandwich structure made of graphitic foam impregnated with paraffin (T_m=56 °C) as the core and carbon/epoxy laminates as the skin, intended for thermal management of electronic devices. The graphitic foam served two purposes: it immobilized the molten paraffin and increased thermal conductivity, while the carbon/epoxy skins increased flexural stiffness. The higher the foam porosity, the more paraffin that can be accommodated into the foam pores, and the lower the foam's mechanical properties. As a result, even though the carbon-fiber-based skins were the main enhancers of the mechanical performance of the entire sandwich structure, the foam porosity was the main parameter dominating the balance between the core mechanical properties and the overall TES performance, which acted competitively in this system. Several other studies on carbon foams as shape-stabilizers for organic PCMs have been published in the literature, but they are mostly used to improve thermal conductivity, with little attention to mechanical performances [137–139].

2.3 Multifunctional syntactic foams

The combination of different properties in one material that allows it to perform different tasks without the use of additional components is known as multifunctionality. Thermal stability, sensing functions, electrical conductivity, energy storage (electrical and thermal), electro-magnetic interference (EMI) shielding, and self-healing are some of the properties developed in the field of multifunctionality [140,141]. Because of multifunctionality, it is possible to reduce the number of devices and components in a given system, allowing for mass, volume, and cost savings. Furthermore, one of the goals in the design of multifunctional materials is to achieve the additional function without compromising other properties and structural capabilities. Different materials are

combined to achieve such coexistence, resulting in the field of composite materials. Polymeric matrix composites are an advantageous choice due to their inherent characteristics such as low density, processability, low cost, and mechanical resistance. Carbon fiber reinforced composites are a popular class of multifunctional composite materials [142]. Aside from their light weight and mechanical properties, their electrical properties are also intriguing. This is because carbon fibers, unlike the equally popular glass and Kevlar fibers, are electrically conductive. However, the insertion in a non-conductive polymeric matrix causes conductivity to be dependent on the arrangement and microstructure of the reinforced composite. Furthermore, this electrical conductivity allows for the shielding of electromagnetic radiation, which is used for both radio wave absorption and reflection [141].

The work of Akbar et al. [143] was focused on the development of a wing box with electrical energy harvesting capabilities. Because of the presence of embedded piezoelectrical materials, this structural component can collect electrical energy. H. Kim et al. [144] investigated the fatigue resistance and life of components that could be used to conduct electricity as well as being part of the load bearing structure, which is another example of multifunctionality in the field of electrical properties.

Another intriguing property is self-healing, which refers to the material's ability to heal itself after being damaged. To accomplish this, four techniques are used: encapsulated healing agents, thermoplastic polymers, and solvents [141].

The multifunctionality considered in this work is related to Thermal Energy Storage capability together with lightness. This was accomplished through the use of Phase Change Materials, which effectively store and release thermal energy by utilizing the latent heat of solidification/fusion in syntactic foams well known to be lighter and more stable from a geometrical point of view. The resulting composites would consider epoxy and polypropylene resins as matrix to cover both thermosets and thermoplastics. By incorporating HGMs, several advantages can be mentioned other than lightness, like a low thermal expansion coefficient and thermal conductivity useful in injection molding to lower the cycling time. The incorporation of PCMs in such foams could give them an extra property useful for the thermal management of the components.

Therefore, this research intends to investigate and better understand the resulting combination of properties provided by these novel composites, as well as the specific uses they may have.

Chapter 3 - Experimental Part

This Chapter introduces all of polymer matrices, reinforcements, and PCMs used in this Thesis and characterization techniques utilized to investigate the properties of the prepared SFs. The sample preparation methods and the description of the specimens for each test will be reported in Chapter 4 - and Chapter 5 - .

3.1 Materials

The present section lists the materials employed in this Thesis, divided into matrices, PCMs, hollow glass microspheres (HGMs), compatibilizer, and silane.

3.1.1 Matrices

3.1.1.1 Epoxy resin

Elantas Europe Srl (Collecchio, Italy) kindly provided the epoxy resin Elan-tech® EC 157 and the hardener Elan-tech® W342. According to the datasheet, this epoxy system is ideal for producing high-performance structural composite parts of small and medium size using the hand lay-up process. The producer indicated in the datasheet a resin/hardener mass ratio of 100:30. Table 3-1 and Table 3-2 report the viscosity and density of the two precursors from the technical datasheet. The initial mixture's viscosity is in the 200-600 mPa·s range with a pot life of 30 min. After 2.5 hours the mixture reaches the gelation time. The fully cured product exhibits a glass transition temperature of 80-110 °C and a flexural elastic modulus of 3.1-3.3 GPa.

Table 3-1 Properties of Elan-tech® EC 157 resin from technical data sheet.

Property	*Value*	*Unit*	*Test method*
Viscosity (25°C)	700 ± 100	mPa·s	EN13702-2
Density (25°C)	1.15 ± 0.01	g/cm^3	ASTM D 1475

Table 3-2 Properties of Elan-tech® W342 hardener from technical data sheet.

Property	*Value*	*Unit*	*Test method*
Viscosity (25°C)	50 ± 20	mPa·s	EN13702-2
Density (25°C)	0.95 ± 0.01	g/cm^3	ASTM D 1475

3.1.1.2 Polypropylene

Lyondell-Basell (U.S.) provided the polypropylene used in this work, Moplen HP456J, in form of granules. This product is a polypropylene homopolymer designed for extrusion and thermoforming operations, with technical data sheet characteristics listed in Table 3-3.

Table 3-3. Properties of polypropylene Moplen HP456J from technical data sheet. (*T = 23 °C, testing speed = 50 mm/min).

Property	*Value*	*Unit*	*Test method*
Melt flow rate (5 kg / 230 °C)	3.4	g/10min	ISO 1133-1
Density	0.90	g/cm^3	ISO 1183-1
Melting temperature	170	°C	ISO 11357
Flexural modulus	1500	N/mm^2	ISO 178
Tensile stress at yield*	34	N/mm^2	ISO 527-1,2
Tensile stress at break*	21	N/mm^2	ISO 527-1,2
Tensile strain at yield*	11	%	ISO 527-1,2
Tensile strain at break*	200	%	ISO 527-1,2
Vicat grade (A50)	156	°C	ISO 306
Deflection temperature (0.45 MPa)	91	°C	ISO 75B-1,2

3.1.2 Phase Change Materials (PCMs)

In this thesis, two different encapsulated Phase Change Materials (PCMs) were used, the MPCM43D and MPCM57D. They were chosen for their melting point in the 40-60 °C range, which may be useful for applications in the thermal management of food packages, electronic devices, and automotive components. This melting temperature range was also chosen since these PCMs are solid at room temperature.

Microtek laboratories Inc. (Dayton, USA) provided MPCM43D, which has a density of 0.9 g/cm^3 and a mean size of 17-22 µm. The melamine-formaldehyde shell, which accounted for 15% of the total mass, ensured thermal stability up to 250 °C. The melting temperature of the paraffinic core was 43 °C, with a melting enthalpy of 190-200 J/g.

MPCM57D were again provided by Microtek laboratories Inc. (Dayton, USA). The technical data sheet was not provided by the manufacturing company. The shell was composed of melamine-formaldehyde and delivers thermal stability up to 250 °C, while the paraffinic core possessed a melting temperature of 57 °C. More features were investigated through characterization techniques such as pycnometry and differential scanning calorimetry (DSC). The capsules showed a melting enthalpy

of 207 J/g and a density of 0.94 g/cm^3. Figure 3-1 shows the MPCM57D as received. Mechanical sieving was used to study the microcapsules size distribution, as reported in Figure 3-2. The resulting mean size was 43 ± 13 µm.

Figure 3-1 Paraffin microcapsules MPCM57D (Microtek Laboratories Inc), as received.

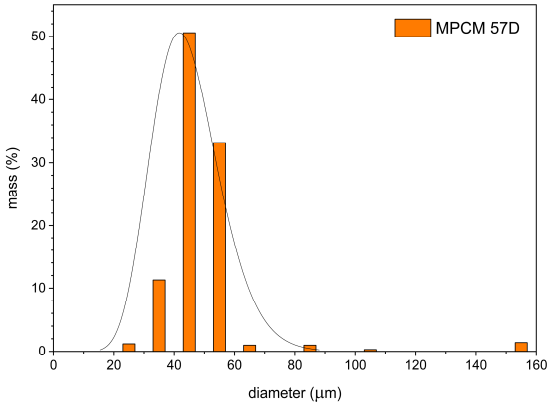

Figure 3-2 MPCM 57D particle size distribution obtained from sieving process.

3.1.3 Hollow glass microspheres (HGMs)

There are various solutions on the market, for this Thesis two different types of hollow glass microspheres, K15 and iM16K, were chosen. These were both supplied by 3M Italia Srl. (Pioltello, Italy) as dry powder.

K15 HGMs were made of soda-lime-borosilicate glass and had a density of 0.15 g/cm^3, a mean particle size (D_{50}) of 60 µm, a thermal conductivity of 0.055

W/(m·K), and a crush strength (90% survival) of 2.07 MPa, according to the producer's technical datasheet. These HGMs were chosen due to their low density which maximizes the lightness of components. Mechanical sieving was used to study the powder's size distribution, as reported in Figure 3-3. The sieves used were: 150, 100, 80, 63, 50, 40, 32, and 25 µm.

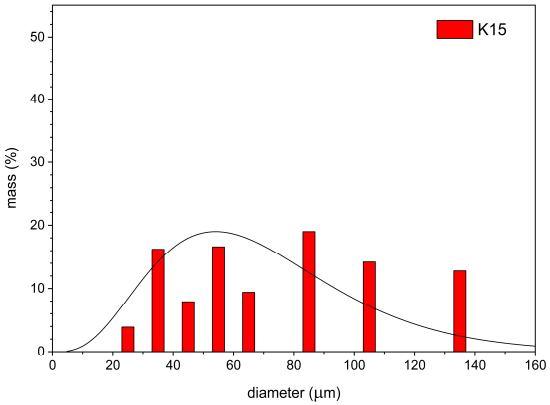

Figure 3-3 K15 HGMs particle size distribution obtained from sieving process

iM16K HGMs were made of soda-lime-borosilicate glass, as K15 microspheres, but because of their high wall thickness/diameter ratio, they showed a higher density (0.45 g/cm^3) and crush strength (90% survival near 110 MPa). They had a D_{50} mean particle size of 27 µm and a thermal conductivity of 0.153 W/(m·K). Figure 3-4 reports a picture of iM16K HGMs as received from the producer. A granulometric analysis was also performed on these microspheres, as reported in Figure 3-5.

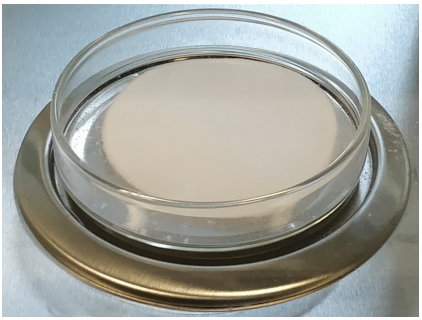

Figure 3-4 iM16K HGMs as received.

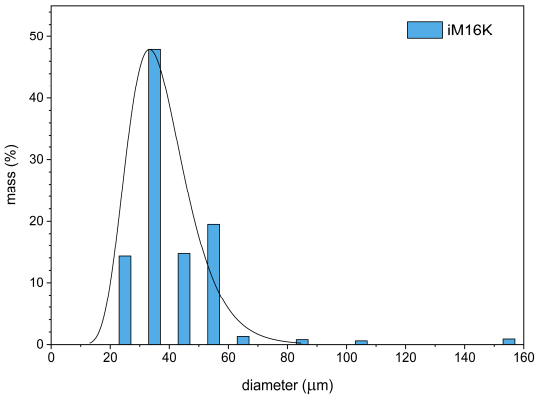

Figure 3-5 iM16K HGMs particle size distribution obtained from sieving process.

3.1.4 Compatibilizer

Due to the difficulties in obtaining good adhesion between polypropylene and HGMs the use of a compatibilizer was necessary, as also reported in the work of Gogoi et al. [145]. The compatibilizer used in this work was a maleic anhydride-grafted-polypropylene (MA-g-PP), commercially known as Compoline CO/PP H60, supplied by Auserpolimeri srl (Italy). This coupling agent is a polypropylene that has been modified with maleic anhydride and is commonly used as a compatibilizer in glass fiber filled polypropylene composites. It is used to maintain excellent adhesion between matrix and fillers, resulting in improved mechanical properties. Table 3-4 shows the properties of this compatibilizer based on the technical datasheet provided by the producer.

Table 3-4 Properties of Compoline PP/H60 compatibilizer from the technical datasheet

Property	*Value*	*Unit*
Melt flow index (230 °C, 2.16 kg)	180	g/10 min
Flexural modulus	1500	MPa
Melting temperature	160	°C
Graft level	High	-
Density	0.87	g/cm^3

3.1.5 Silane

As suggested by Gogoi et al. [145] and also by Kumar et al. [25] and by Huang et al. [146], silanes play a vital role in connecting the glass surface with the compatibilized matrix, improving the adhesion and consequently the mechanical properties. Figure 3-6 schematizes a general silane molecule where "X" are the hydrolyzable groups that, in presence of water, hydrolyze becoming capable to bond with -OH groups already present on the surface of glass, while "Y" is an organofunctional group that is compatible with the polymeric matrix.

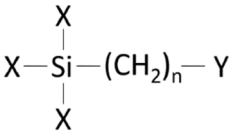

Figure 3-6 Schematization of a general silane organic molecule.

The chosen silane is γ-Aminopropyl-Triethoxysilane (commonly abbreviated as APTES), which is a popular choice for this type of application. The chemical structure of APTES is shown in Figure 3-7. The organofunctional group is represented by an amine group, while the hydrolyzable elements are constituted by ethoxy groups. It is a liquid with 0.946 g/ml of density and it boils at 217 °C.

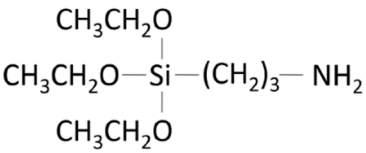

Figure 3-7 Schematization of γ-Aminopropyl-Triethoxysilane (APTES).

3.2 Experimental techniques

This section describes the general experimental techniques used to analyze the prepared materials. The techniques applied to a specific system will be described in the Chapter 4 - (for epoxy/HGM/PCM SFs) and Chapter 5 - (for PP HGM/PCM SFs).

3.2.1 Rheological properties

The rheological properties play an important role in determining the processing window of thermosetting and thermoplastic materials. Rheological analysis allows

the determination of properties like the viscosity (η) as a function of the shear rate ($\dot{\gamma}$) through flow sweep tests, as well as the storage and loss dynamic shear modulus (G' and G" respectively) through frequency sweep tests. Discovery HR-2 rheometer from TA instrument (USA), reported in Figure 3-8, was used to perform the measurements. For both thermosetting and thermoplastic composites, a plate-plate configuration was utilized, by using disks with a diameter of 25 mm and setting a gap of 1 mm.

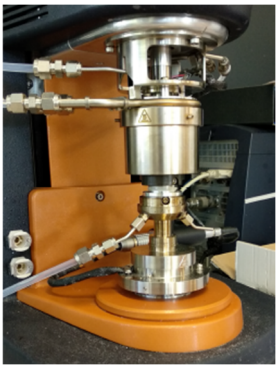

Figure 3-8 Plate-plate rheometer (DHR-2) used for the rheological measurements.

Flow sweep tests measure how viscosity (η) changes within a shear rate ($\dot{\gamma}$) window. The upper plate spins from low to higher frequencies to see how the analyzed material responds to the imposed stresses. In the case of epoxy/HGM/PCM composites, the shear rate sensitivity was measured between 0.1 and 1 1/s on non-cured compositions at a constant temperature of 30 °C. In the case of PP/HGM/PCM samples, disks of 25 mm in diameter were tested at 200 °C in a shear rate interval between 0.01 and 200 1/s.

In Frequency sweep tests the upper plate continuously changes the spin direction with a predetermined frequency, to determine the viscoelastic response of the material at a specific temperature and shear stress. For thermosetting systems, it also allows the determination of the gel time (t_{gel}), which is defined as the time at which the curve of the shear storage modulus (G') intercepts the curve of the shear loss modulus (G"). The Arrhenius equation was used to calculate the activation energy of crosslinking (E_a), as shown in Equation (3-1).

$$E_a = R\left(\frac{d\left(ln\, t_{gel}\right)}{d(1/T)}\right) \tag{3-1}$$

where R is the universal gas constant, equal to 8.314 J/(mol·K), and T is the testing temperature in K.

For Epoxy/HGM/PCM systems, the rheological behavior of non-cured mixtures has been measured at 70 °C, 80 °C, 90 °C, and 110 °C by using a maximum shear stress of 1000 Pa at a constant frequency of 1 Hz. This test was carried out on four uncured compositions, allowing the gel time (t_{gel}) to be determined.

For PP-based SFs the tests were conducted on disk samples at 200 °C with an oscillation frequency between 0.1 and 600 rad/s, with a fixed strain amplitude of 1%. Three specimens for each composition were tested.

3.2.2 Morphological properties

3.2.2.1 Density

Density measurements were used to determine the pore volume fraction in the prepared SFs. The experimental density was measured via helium pycnometry (ρ_{exp}). A small amount of material was tested using a Micromeritics AccuPyc 1330TC (Micromeritics Instrument Corp., USA) helium pycnometer at 23.0 °C, by using a 1 cm^3 testing chamber. For each composition, one specimen was tested 30 times, and the experimental density was determined as the average values of these measurements. The instrument used is shown in Figure 3-9.

Figure 3-9 Helium pycnometer (Micromeritics AccuPyc 1330TC).

In addition, the theoretical density values (ρ_{th}) were also calculated by using the mixture rule, as reported in Equation (3-2).

$$\rho_{th} = \sum_{i=1}^{n} \rho_i \cdot \phi_i \qquad (3\text{-}2)$$

Where ρ_i is the pycnometric density of the i-th component, and ϕ_i is its volume fraction. The void content ($VC_{\%}$) was then calculated by using Equation (3-3).

$$VC_{\%} = \frac{\rho_{th} - \rho_{exp}}{\rho_{th}} \cdot 100 \quad (3\text{-}3)$$

3.2.2.2 Light microscopy (LM)

In order to understand the morphology and size distribution of PCM capsules and HGMs within the matrix, optical microscopy was used. The samples were incorporated inside a small cylinder of epoxy resin that, after curing, has been polished on one surface. The microscope used was a Zeiss Axiophot (Carl Zeiss AG, Germany) optical microscope, equipped with an Epiplan Neofluar objective and a digital camera, as reported in Figure 3-10.

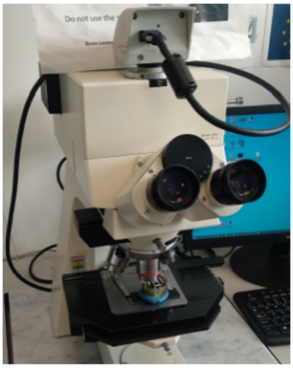

Figure 3-10 Zeiss Axiophot light microscope.

3.2.2.3 Scanning electron microscopy (SEM)

SEM micrographs were acquired to investigate the microstructure and morphology of syntactic foams. SEM investigation was performed on cryofracture surfaces, obtained by fracturing the specimens after soaking them in liquid nitrogen for at least 5 minutes. This analysis was carried out with a Zeiss Supra 60 field-emission scanning electron microscope (FE-SEM) operating at 3.5 kV. As all the investigated samples were not good electrical conductors, a thin layer of Pt-Pd was sputtered on their surface to render them conductive. Figure 3-11 reports the picture of the instrument used.

Figure 3-11 Scanning Electron Microscope Zeiss Supra 40 SEM.

3.2.3 Thermal and thermo-mechanical properties

3.2.3.1 Differential scanning calorimetry (DSC)

Differential scanning calorimetry is essential for determining material thermal properties, such as melting and crystallization enthalpies (ΔH_m, ΔH_c) and temperatures (T_m and T_c), glass transition temperatures (T_g), and specific heat capacity (c_p). Figure 3-12 shows the Mettler DSC30 instrument (Mettler Toledo LLC, Columbus, OH, USA) used to investigate these properties, testing specimens in aluminum crucibles under a nitrogen flow of 10 mL/min. 40 mg of material was inserted in 160 µl aluminum crucibles for epoxy/HGM/PCM samples, and 10 mg in 40 µl aluminum crucibles for PP/HGM/PCM samples. Three scans were performed at a heating/cooling rate of 10 °C/min in a temperature range between 10 and 160 °C for the epoxy-based syntactic foams, and between -50 and 220 °C for PP-based syntactic foams. One specimen for each composition was tested.

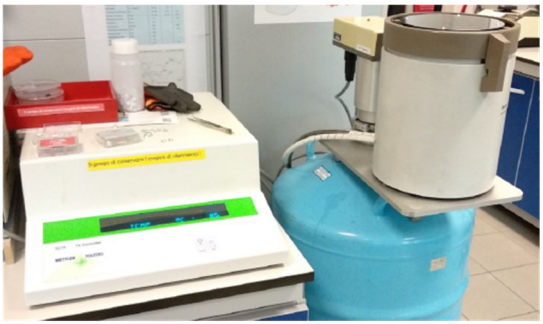

Figure 3-12 Differential scanning calorimetry Mettler DSC30 calorimeter

For epoxy matrix composites, the specific heat capacity at 30 °C (c_{p30}) was calculated from the DSC thermograms in the first heating scan by dividing the specific heat flow by the heating rate at 30 °C. Although this method did not meet the ASTM E-1269 standard, the c_p values obtained were used to determine, at least qualitatively, the thermal conductivity (λ_{30}) of the prepared foams (see Section 3.2.3.2).

For PP matrix composites, the specific heat capacity (c_p) was determined using the procedure outlined in the ASTM E-1269 standard. For each composition, three specimens were tested with a single heating run at 20 °C/min in the temperature range from -50 to 200 °C, with a nitrogen flux of 10 ml/min Aside from the heat capacity of the composite materials, the specific heat capacity of the constituents was also measured. For each composition, 10 mg of material was placed inside a 40 µl aluminum crucible. However, a procedure was carried out to achieve a 0.1% weight matching between the specimen, the sapphire standard, and the empty specimen holders, as specified by the standard. After that, the specific heat was calculated using Equation (3-4).

$$c_p(s) = c_p(st) \cdot \frac{D_s \cdot W_{st}}{D_{st} \cdot W_s} \tag{3-4}$$

Where $c_p(s)$ is the specific capacity of the specimens (J/g K), $c_p(st)$ is the specific heat capacity of the sapphire standard, D_s is the vertical displacement between the specimen and the empty crucible DSC curves at a given temperature (mW), D_{st} is the vertical displacement between the sapphire and the empty crucible DSC curves, W_{st} is the sapphire mass, and W_s is the specimen mass. A schematization of the thermogram is reported in Figure 3-13.

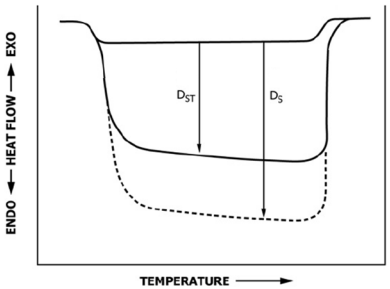

Figure 3-13 Schematization of the DSC thermograms of empty sample holder, of the standard, and of the specimen, utilized in the determination of the c_p values.

3.2.3.2 Thermal conductivity

Light flash analysis (LFA) is a characterization technique that measures the thermal diffusivity of materials by exposing them to a light pulse and monitoring the temperature over time. This test was performed on square specimens (12.7x12.7x4 mm^3) for epoxy matrix samples and small circular samples (12.5 mm diameter and 1 mm thickness) for PP matrix samples. The specimen preparation procedure involved the application of a graphite coating to the surface of both flat sides to improve light pulse absorption. The experiment was conducted using a light flash analyzer LFA 467 (Netzsch Holding, Germany), as shown in Figure 3-14.

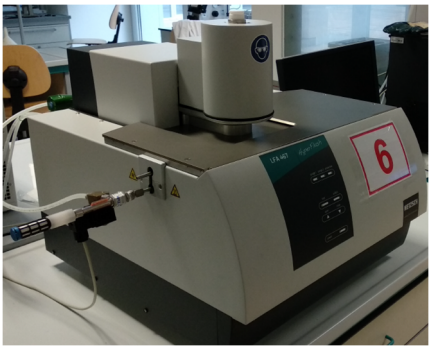

Figure 3-14 Laser flash analyzer Netzsch LFA 467.

For epoxy matrix composites, seven specimens, one for each considered composition, were tested at 30 °C, while PP matrix composites were tested at 20, 45, and 70 °C. A ceramic reference called Pyroceram 9606 was included in the evaluation along with the other specimens to estimate the specific heat of materials directly from LFA. The value of diffusivity was calculated using a fitting procedure of the obtained data through the Netzsch Analyzer software. The transparent materials fitting model was used because it demonstrated the best fitting accuracy. The thermal conductivity (λ(T)) of the prepared foams at a certain temperature was determined by using Equation (3-5).

$$\lambda(T) = \alpha(T) \cdot \rho(T) \cdot c_p(T) \tag{3-5}$$

where ρ(T) is the pycnometer density and α(T) is the thermal diffusivity.

3.2.3.3 Evaluation of TES properties

To understand the potential related to the Thermal Energy Storage capability of the prepared SFs, a specific test was conducted on the most representative compositions by monitoring the evolution of their temperature upon heating/cooling stages. For this purpose, bulk samples (cylindrical and cubic) were prepared with a blind hole reaching their core. Type-K thermocouples, connected to a recording system, were inserted in these holes to monitor the material temperature. The samples were then placed in a preheated oven (60 °C for epoxy/HGM/PCM, and 100 °C for PP/HGM/PCM) and the time required to increase their temperature was recorded (from 26 to 55 °C ($t_{26–55}$) for epoxy/HGM/PCM samples, and from 35 to 80 °C (t_{35-80}) for PP/HGM/PCM samples). After that, the samples were extracted from the oven to cool, and the cooling time was recorded (from 55 to 26 °C (t_{55-26}) for epoxy/HGM/PCM samples, and from 80 to 35 °C (t_{80-35}) for PP/HGM/PCM samples). Figure 3-15 shows a scheme of the developed setup.

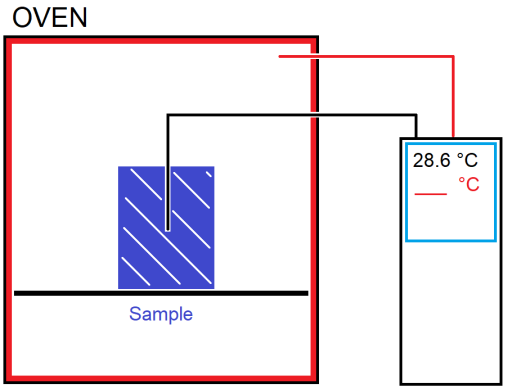

Figure 3-15 Setup used for temperature profiling of the foams

3.2.3.4 Dynamic mechanical thermal analysis (DMTA)

To evaluate the dynamic-mechanical behavior of the prepared foams, dynamic mechanical analysis was carried out. It was helpful to investigate how the PCM and HGM addition affects the viscoelastic properties of the foams, below and above the melting temperature of the PCM. DMTA tests were carried out through a TA Q800 DMA instrument (shown in Figure 3-16) in single cantilever bending mode, with a 17.5 mm distance between the grips. Tests were conducted from 0 °C to 150 °C at 3 °C/min, while the strain amplitude and frequency were set to 0.05 % and 1 Hz, respectively. These experiments made possible to determine the trends of the

storage modulus (E'), loss modulus (E"), and loss tangent (tanδ) at different temperatures. Three distinct ternary plots were developed using the storage modulus E' values at 25 °C, 60 °C, and 130 °C. For the specific storage modulus (E'/ρ), these values of E' were divided by the pycnometer density determined at 23 °C. For these tests, one specimen for each composition was tested.

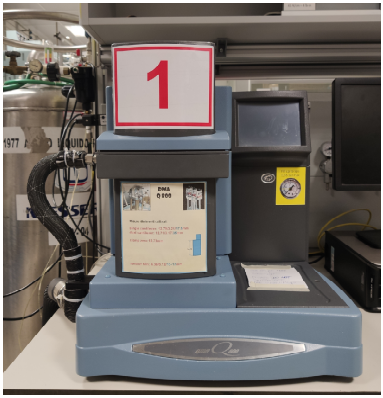

Figure 3-16 Dynamic mechanical thermal analyzer TA Q800 DMA instrument

3.2.4 Mechanical properties

The following section addresses how the mechanical properties of the developed material were evaluated. In particular, five tests were performed: quasi-static tensile tests, quasi-static compression tests, evaluation of the plane-strain fracture toughness (K_{IC}) and of the critical strain energy release rate (G_{IC}), evaluation of the plane-strain fracture toughness (K_{IC}) under impact condition, and Charpy impact tests. These tests were all conducted at 23 °C and with a relative humidity of approximately 50%.

3.2.4.1 Quasi-static tensile tests

For the Epoxy/HGM/PCM samples, an Instron 4502 (Instron, Turin, Italy) universal machine (shown in Figure 3-17a) equipped with a 10 kN load cell was used. Following the ISO-527-2 standard, ten type-1B specimens were tested for each composition to determine the tensile elastic modulus (E_t) and the stress at break (σ_B). The tests for measuring the elastic modulus were all conducted with an extensometer having a gauge length of 50 mm, at a crosshead speed of 0.5 mm/min, until a strain level of 0.8% was reached. The steepest tangent line to the curve was used to determine the elastic modulus. The tests for determining the strain at break

(ε_B) were performed without the extensometer at a crosshead speed of 2 mm/min, setting a gauge length of 115 mm, until the failure of the specimens was reached.

For the PP/HGM/PCM foams, an Instron 5969 (Instron, Turin, Italy) universal machine (shown in Figure 3-17b) equipped with a 1 kN load cell was used. Ten type-1BA specimens having a gage length of 55 mm were tested in accordance with the ISO-527-2 standard. The determination of the elastic modulus (E_t) was performed at a testing speed of 0.25 mm/min, by using an extensometer having a gauge length of 25 mm, and the stress levels associated with deformations of 0.05% and 0.25% were considered to calculate a secant modulus. Tensile properties at break were determined at a crosshead speed of 20 mm/min without the extensometer until failure was reached. In this way, it was possible to determine the stress and the strain at yield (σ_y, ε_y) and at break (σ_B, ε_B).

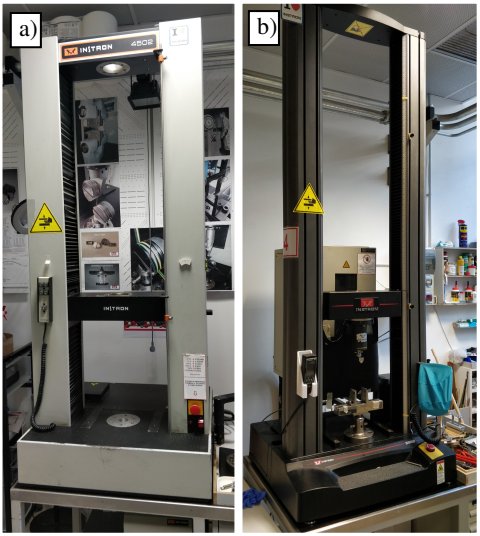

Figure 3-17 Representative images of (a) Instron 4502 and (b) Instron 5969 tensile testing machines.

3.2.4.2 Quasi-static compression tests

All the performed tests were conducted by using an Instron 5969 tensile testing machine (Figure 3-17b), used also for the tensile test of PP/HGM/PCM foams. The tests on the epoxy-based foams were carried out according to the ASTM-D695 standard by using the machine equipped with a 50 kN load cell. The elastic modulus at compression (E_C) and the maximum stress (σ_C) were evaluated by testing

cylindrical specimens (diameter 20 mm, height 40 mm) at a crosshead speed of 1.3 mm/min. The elastic modulus was determined from the slope of the line tangent to the steepest linear part of the stress-strain curve. Ten specimens were tested for each composition.

The tests on the PP-based foams were conducted by using the same machine equipped with a 10 kN load cell. A total of nine cubic specimens (1x1x1 cm^3) were tested for each composition at a crosshead speed of 1.3 mm/min. In this way, the stress at 20% of strain (σ_{20}) and the elastic modulus at compression (E_C), calculated using the tangent approach, were determined.

3.2.4.3 Charpy impact tests

This test was performed only on epoxy-based syntactic foams. Charpy impact tests were carried out following the ISO 179-2 standard with a Ceast 3549/000 impact testing machine (Instron, Turin, Italy), shown in Figure 3-18. The hammer used in this work was an ISO 5J set to a starting angle of 51°, resulting in a maximum potential energy of 1 J and an impact speed of 1.29 m/s. The test was performed on single-notch rectangular specimens with dimensions 80x10x4 mm^3, with a notch depth of 2 mm and a notch tip radius of 0.25 mm. At least 10 specimens, having a span length of 62 mm, were tested for each composition. In this way, it was possible to determine the specific energy absorbed under impact conditions (a_{cN}), by dividing the total absorbed energy for the cross-section of the specimens (J/m^2).

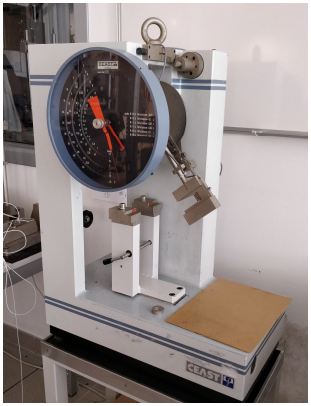

Figure 3-18 Ceast 3549/000 Charpy pendulum.

3.2.4.4 Evaluation of the fracture behavior (K_{IC} and G_{IC})

Because of the different stiffness of the two polymeric matrices investigated, two different procedures were used to evaluate the fracture behavior of the prepared SFs. Epoxy-based syntactic foams ensure plane strain condition allowing the application of the ASTM D5045 standard while PP does not. An Instron 5969 testing machine equipped with a 1 kN load cell was used for this purpose. Ten Single-edge notched specimens having the dimension of 50x12x6 mm^3 were tested for each composition in a three-point bending configuration, at a crosshead speed of 10 mm/min. The support span was four times the width (48 mm) and the notch of the specimens was produced by sawing with a razor blade until reaching their half-width. The detailed procedure for calculating G_{IC} can be found in the ASTM D5045 standard.

For PP-based syntactic foams, K_{IC} was determined under impact conditions, as described in ISO 13586 and ISO 17281 standards. A Ceast 3549/000 impact testing machine (Instron, Turin, Italy) equipped with a 5 J instrumented hammer was used. A three-point bending configuration, with a span length of 62 mm was adopted. A starting impact angle of 39° was set, to hit the specimens with a speed of 1 m/s. For each composition, ten rectangular specimens (10x80x4 mm^3) with a sharp notch having a depth of 5 mm were tested.

In the ASTM D5045 standard, the conditional value (K_Q) of the critical stress intensity factor was determined for each specimen through Equation ((3-6).

$$K_Q = \left(\frac{P_Q}{B\sqrt{W}}\right) f(x) \tag{3-6}$$

Where P_Q is the load value determined as described in the standards, B and W are the specimen thickness and depth, respectively, and f(x) is a geometrical function defined by Equation ((3-7).

$$f(x) = 6\sqrt{x}\frac{1.99 - x(1-x)(2.15 - 3.93x + 2.7x^2)}{(1+2x)(1-x)^{3/2}} \tag{3-7}$$

Where x is the ratio between a and W. The calculated K_Q can be considered as the critical stress intensity factor K_{IC} only when Equation (3-8) is satisfied.

$$B, a, (W-a) > 2.5\left(\frac{K_Q}{\sigma_y}\right)^2 \tag{3-8}$$

Where σ_y is the yield stress, evaluated as the maximum load in the uniaxial tensile tests. The criteria require that B must be sufficient to ensure plane strain and that (W-a) be sufficient to avoid excessive plasticity in the ligament.

In the ISO 17281 standard, the term P_Q is calculated using a computer-aided fitting procedure of the load-time curve. However, in this case, P_{max} was chosen as P_Q. The actual critical stress intensity factor (K_{IC}) could be calculated after the provisional result K_Q was evaluated. This was done following the verification of the criteria for the characteristic length ($\bar{r}$) as reported in Equation ((3-9).

$$\bar{r} = \frac{K_Q^2}{\sigma_y^2} \tag{3-9}$$

3.2.5 Statistical analysis of the experimental data

The analysis of the properties of a ternary system can be a very complex process due to the wide variety of possible compositions. To set up experiments and analyze the results, preliminary and post-production statistical approaches can be very useful. A statistical approach based on a mixture design was used to define the most representative compositions and to represent the results with ternary phase diagrams for both SFs systems [4,45,147,148]. The "mixexp" package in the Rstudio v.1.4.1103 software (Rstudio, Inc., Boston, MA, USA) was used to perform the mixture design, while the "lm" function was used to fit the experimental results using a quadratic linear model called the "Scheffé quadratic model" (see Equation ((3-10)).

$$y = \sum_{i=1}^{q} \beta_i x_i + \sum_{i=1}^{q-1} \sum_{j=i+1}^{q} \beta_{ij} x_i x_j + \epsilon \tag{3-10}$$

where y is the response variable, x_i, and x_j are the binary mixture compositions, β_i represents the expected response at the vertex, and β_{ij} are the coefficients indicating the amount of the quadratic curvature along the edge of the simplex region [147]. After a first fit, the most significant components of the model (x_i, x_j) were evaluated through the analysis of variance (ANOVA). At this point, all non-significant components and combinations were removed from the model and a new fit with the corrected model was performed. This procedure was repeated until only the statistically significant terms remained. At this point, the model could be considered statistically correct and therefore used to represent the analyzed data. The function "ModelPlot" was used to represent the ternary models. Each plot also reported the resulting R^2_{adj} which represents the goodness of the fit reported in Equation ((3-11) and the $S_{y.x}$, which represents the residual standard error of the model shown in

Equation ((3-12). The Pr(>|t|) (which is the upper limit value of the statistical probability of the components from ANOVA procedure) of the less important but still statistically relevant components or combination of components, and the list of the considered components and/or combination of components for the model are also represented in each graph.

$$R^2_{adj} = 1 - \left(\frac{(1 - R^2) \cdot (n - 1)}{n - k - 1}\right) \tag{3-11}$$

$$S_{y.x} = \sqrt{\frac{\sum(residual^2)}{n - k}} \tag{3-12}$$

where n are the experimental values and k is the number of parameters fit by regression, and R^2 is the coefficient of determination that gives information about the goodness of fit of a model.

Chapter 4 - Multifunctional epoxy-based syntactic foams with TES properties

This chapter presents the methods and the experimental results concerning the epoxy/HGM/PCM system.

Part of this Chapter has been published in:

- Galvagnini, F.; Dorigato, A.; Fambri, L.; Fredi, G.; Pegoretti A., ***Thermophysical Properties of Multifunctional Syntactic Foams Containing Phase Change Microcapsules for Thermal Energy Storage.*** Polymers (Basel). 2021, 13.
- Galvagnini, F.; Fredi, G.; Dorigato, A.; Fambri, L.; Pegoretti, A. ***Mechanical Behaviour of Multifunctional Epoxy/Hollow Glass Microspheres/Paraffin Microcapsules Syntactic Foams for Thermal Management.*** Polymers (Basel). 2021, 13.

4.1 Materials and methods

The components needed to prepare these samples and the procedures utilized for sample preparation are presented in this section, together with the list of the experimental techniques applied. A detailed description of the materials and the experimental techniques have been already presented in Chapter 3 - .

4.1.1 Materials

The materials employed for the preparation of these foams are listed in Table 4-1 (please refer to Subchapter 3.1 for the details about the materials).

Table 4-1 List of materials employed for the preparation of epoxy/HGM/PCM syntactic foams.

Constituent	*Label*	*Material*
polymer matrix	EP	epoxy resin
hollow filler	HGMs	hollow glass microspheres (K15)
PCM	PCM	paraffin microcapsules (MPCM43D)

4.1.2 Sample preparation

Epoxy/HGM/PCM syntactic foams were prepared by mixing the epoxy base, PCM, and HGMs in a becker for 5 minutes at 100 rpm with a Dispermat F1 mechanical mixer (VMA-Getzmann GmbH, Reichshof, Germany), and then degassing the mixtures for 5 minutes with a vacuum pump. The hardener was then added, and the mixing and degassing processes were repeated. The mixtures were then cast in silicone molds with different geometries (shown in Figure 4-1(a-b)) and cured at room temperature for 24 hours, before being post-cured in an oven at 80 °C for 6 hours.

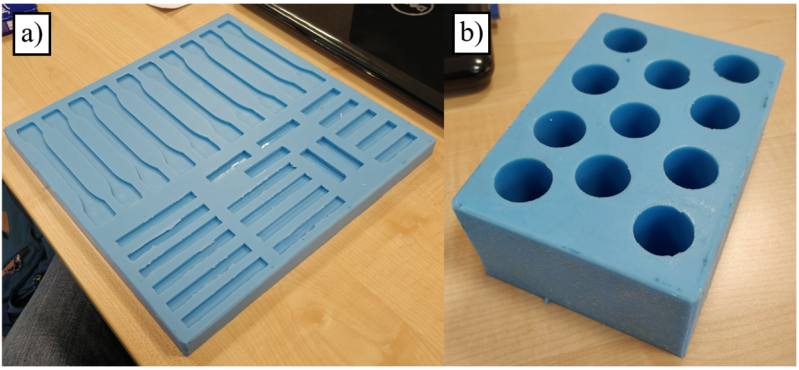

Figure 4-1 Silicon molds utilized to prepare samples for (a) tensile, Charpy, and fracture toughness tests, and (b) compression tests.

The samples were labeled as EPG-x.y, where x represents the PCM volume content and y represents the HGM concentration, both of which ranged between 0 vol% and 40 vol%. The fifteen compositions chosen for this study, with a maximum total filler content (PCM+HGM) of 40 vol%, are listed in Table 4-2 and reported on the ternary diagram shown in Figure 4-2, with the prepared formulations indicated by red dots. Furthermore, Figure 4-2 shows a general example of how to read a ternary phase diagram.

Table 4-2 List and designation of the prepared epoxy-based syntactic foams with their relative composition

#	*Sample*	*Epoxy vol%/wt%*	*PCM vol%/wt%*	*HGM vol%/wt%*
1	EPG-0.0	100.0/100.0	0.0/0.0	0.0/0.0
2	EPG-10.0	90.0/91.6	10.0/8.4	0.0/0.0
3	EPG-20.0	80.0/83.0	20.0/17.0	0.0/0.0
4	EPG-30.0	70.0/74.0	30.0/26.0	0.0/0.0
5	EPG-40.0	60.0/64.6	40.0/35.4	0.0/0.0
6	EPG-0.10	90.0/98.5	0.0/0.0	10.0/1.5
7	EPG-0.20	80.0/96.7	0.0/0.0	20.0/3.3
8	EPG-0.30	70.0/94.5	0.0/0.0	30.0/5.5
9	EPG-0.40	60.0/91.6	0.0/0.0	40.0/8.4
10	EPG-10.10	80.0/89.3	10.0/9.2	10.0/1.5
11	EPG-10.20	70.0/86.5	10.0/10.1	20.0/3.4
12	EPG-10.30	60.0/83.0	10.0/11.3	30.0/5.7
13	EPG-20.10	70.0/79.7	20.0/18.7	10.0/1.6
14	EPG-20.20	60.0/75.8	20.0/20.7	20.0/3.5
15	EPG-30.10	60.0/69.8	30.0/28.6	10.0/1.6

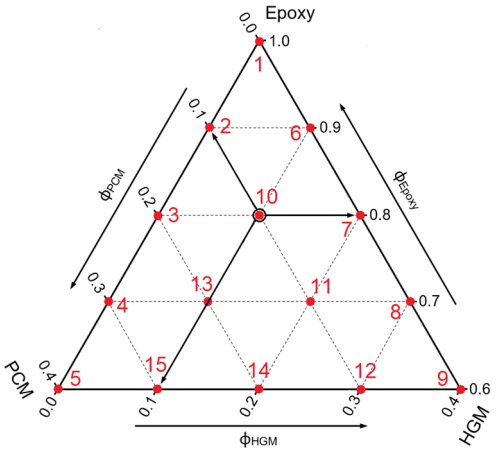

Figure 4-2 Graphical representation on the ternary diagram of the prepared samples (red dots), the number are referred to the compositions reported in Table 4-2. As an example, the black-bordered dot represents the EPG-10.10 foam, which contains 10 vol% of PCM and 10 vol% of HGM.

4.1.3 Characterization techniques

These compositions were studied through the characterization techniques listed in Table 4-3, together with the experimental parameters specifically applied (see Subchapter 3.2 for the detailed description of the experimental techniques).

Table 4-3 Characterization techniques and experimental parameters applied to investigate the properties of the epoxy/HGM/PGM samples.

Technique	*Specific experimental parameters*
Rheometry See section 3.2.1 on page 32	*Flow sweep* shear rate interval = 0.1-1 1/s T = 30 °C *Frequency sweep* maximum shear stress 1 kPa frequency = 1 Hz T = 70/80/90/110 °C
Helium pycnometry See section 3.2.2.1 on page 34	T = 23 °C 1 cm^3 chamber 30 measurements
SEM See section 3.2.2.3 on page 35	potential = 3.5 kV Pt-Pd coating
DSC See section 3.2.3.1 on page 36	T =10-160 °C heating rate = 10 °C/min nitrogen flow = 100 ml/min
LFA See section 3.2.3.2 on page 38	T = 30 °C
Evaluation of TES capability See section 3.2.3.3 on page 39	T = 25-55 °C
DMTA See section 3.2.3.4 on page 39	T = 0-150 °C heating rate =3 °C/min, frequency =1 Hz
Quasi-static tensile tests See section 3.2.4.1 on page 40	for elastic modulus gauge length = 50 mm crosshead speed = 0.5 mm/min for stress at break gauge length = 115 mm crosshead speed = 2.0 mm/min
Quasi-static compression tests See section 3.2.4.2 on page 41	crosshead speed = 1.3 mm/min
Charpy impact tests See section 3.2.4.3 on page 42	starting angle = 51° potential energy = 1 J notch radius = 0.25 mm
Fracture toughness tests See section 3.2.4.4 on page 43	crosshead speed = 10 mm/min

4.2 Results and discussions

4.2.1 Rheological properties

Measuring the rheological features of an uncured thermosetting system after the mixing stage is an efficient way to determine its processability window. Figure 4-3(a,b) shows the results of the dynamic rheological tests that were conducted on the uncured mixtures. For all the compositions under investigation, the viscosity (η) decreases as the applied shear rate ($\dot{\gamma}$) increases (Figure 4-3a). This behavior was expected since the system is still in the liquid state and the very beginning of the curing process is not yet detectable [108]. On the other hand, the addition of solid particles (PCM and/or HGM) results in a considerable rise in η, which is particularly noticeable at higher values of $\dot{\gamma}$, and this aspect could make the system less workable. For example, the value of η at 0.2 s^{-1} for the sample EPG-10.10 is 5.5 Pa·s (+77% compared to EPG-0.0 mixture) and for the sample EPG-40.0 is 21.8 Pa·s (+603% compared to EPG-0.0 sample).

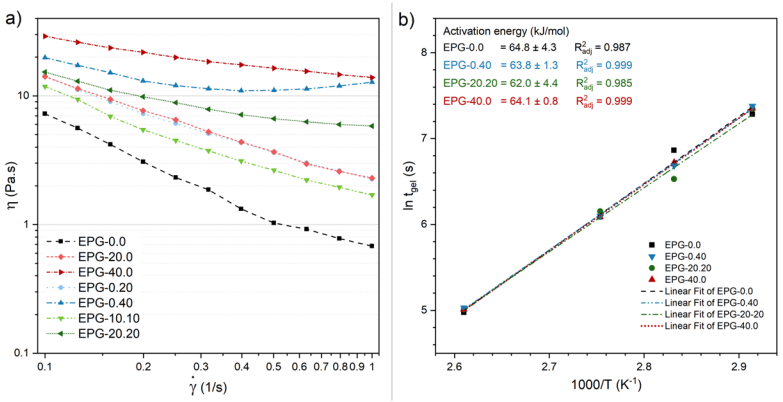

Figure 4-3 Results of dynamic rheological tests on uncured resins. (a) Viscosity (η) as a function of the shear rate ($\dot{\gamma}$) of some selected compositions (T = 30 °C). (b) Gel time (t_{gel}) as a function of the curing temperature (1000/T) of some selected compositions. Experimental data (symbols) were fitted with Equation ((3-1) (dashed lines) to obtain the activation energy of the crosslinking process.

The effect of the type and concentration of solid particles on the viscosity of the liquid resin deserves a deeper insight. Particle type has little impact on viscosity in samples with only one particle type (PCM or HGM) up to a concentration of 20 vol%. In fact, the samples EPG-0.20 and EPG-20.0 show extremely similar

viscosity values over the whole range of shear rates. On the other hand, at larger filler concentrations, the particle type does affect the rheological properties, with the PCM increasing viscosity more than the HGM, particularly at low shear rates. The viscosity of sample EPG-0.40, which contains 40 vol% of PCM, is 13.1 Pa·s at 0.2 s^{-1}, which is 66% greater than the viscosity of sample EPG-40.0, which contains 40 vol% of HGM. This is correlated with the average particle size. Since PCM has a smaller particle size than HGM (approximately 20 µm vs. 60 µm), the matrix-filler contact area is larger, and therefore the tendency to form a percolative network increases, thus leading to a more severe increase in viscosity [149].

In comparison to samples containing a single particle type at the same filler concentration, EPG-10.10 and EPG-20.20 samples have a lower viscosity. Again, the varied particle sizes are to blame for this, since they have an impact on the greatest theoretical particle volume fraction that can be achieved with a random close packing configuration and, consequently, the viscosity. When the size distribution is unimodal, the highest theoretical volume fraction for closely packed spherical particles is 64 vol%. However, this value can increase for bimodal or multimodal distributions, because fine particles can settle within the interstices of coarser particles [108]. This phenomenon, widely described in the literature, helps to explain the lower viscosity of samples containing both PCM and HGM. In fact, the higher the maximum theoretical packing density, the lower the viscosity at a given concentration [149–153].

Rheological tests carried out on the uncured mixtures at a constant shear rate and at four different temperatures (from 70 °C to 110 °C) provide information on the gel time (t_{gel}) and allow the calculation of the activation energy of the crosslinking process for the different compositions (see Equation (3-1)). The results of these tests are illustrated in Figure 4-3b, which reports the natural logarithm of t_{gel} as a function of 1000/T and the values of activation energy of crosslinking determined from the slope of the linear fitting lines. Interestingly, the activation energy is not significantly different in the four analyzed compositions, as was found in previous studies on epoxy/HGM systems [154]. This suggests that the inclusion of PCM and/or HGM does not influence the crosslinking mechanism of the epoxy resin and does not substantially alter the processing window.

4.2.2 Morphological properties

4.2.2.1 Density

The capacity of syntactic foams to achieve a very low density while maintaining excellent stiffness and strength is one of their most significant and interesting features. In order to create the ternary diagram shown in Figure 4-4, the density of

the prepared samples was measured through helium pycnometry, and the resulting data, reported in Table 4-4, were fitted using a linear statistical model (as discussed in Section 3.2.5). The bulk density of neat and cured epoxy is 1.137 g/cm^3. Since the bulk density of HGM (0.150 g/cm^3) is lower than that of PCM (0.955 g/cm^3), it is not surprising that the density decreases more with the HGM introduction. For example, the density of EPG-20.20 is 0.872 g/cm^3 (23% less than neat epoxy), whereas the density of EPG-0.40, which contains only HGM but has the same total filler amount, is 0.735 g/cm^3 (35% less than neat epoxy). Some compositions containing HGMs (like the blue rows) present higher experimental densities than expected from the mixture rule. This can be attributed to two main effects: possible HGMs rupture due to the stirring process and possible heterogeneity in the material. In any case, the discrepancy between the two values is relatively small, less than 5%.

The experimental values of density, thanks to the application of the linear model, can also be applied to evaluate the density for the intermediate compositions. The results of the linear model, obtained with a high R^2_{adj} value (0.988), are in good agreement with the mixture rule, which suggests that most of the HGM and PCM capsules survived the processing step.

Table 4-4 Results of density measurements on the prepared epoxy syntactic foams

Sample	ρ_{th} *g/cm^3*	ρ_{exp} *g/cm^3*
EPG-0.0	1.137±0.002	1.137±0.002
EPG-10.0	1.116±0.002	1.108±0.001
EPG-20.0	1.097±0.002	1.081±0.002
EPG-30.0	1.080±0.001	1.026±0.001
EPG-40.0	1.067±0.001	1.009±0.001
EPG-0.10	1.031±0.002	1.086±0.002
EPG-0.20	0.931±0.001	1.031±0.002
EPG-0.30	0.831±0.001	0.882±0.001
EPG-0.40	0.733±0.001	0.735±0.001
EPG-10.10	1.014±0.001	1.037±0.002
EPG-10.20	0.913±0.001	0.935±0.001
EPG-10.30	0.813±0.001	0.826±0.001
EPG-20.10	0.995±0.001	0.962±0.002
EPG-20.20	0.895±0.001	0.872±0.001
EPG-30.10	0.978±0.001	0.937±0.001

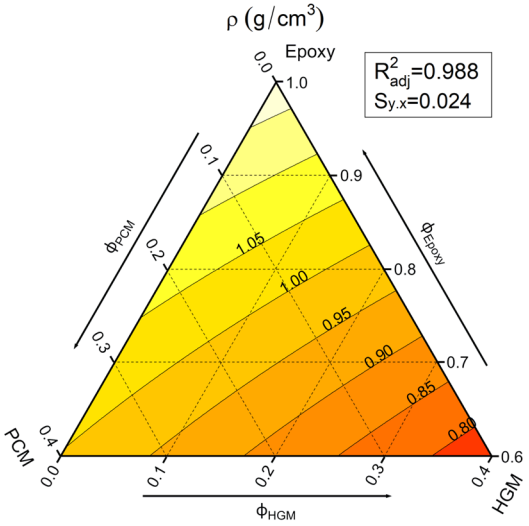

Figure 4-4 Fit-model of the pycnometer density of the prepared epoxy syntactic foams.

4.2.2.2 Scanning electron microscopy (SEM)

SEM was used to study the microstructure of the cured samples, and Figure 4-5(a-d) displays SEM micrographs of the fracture surface of some representative compositions (i.e., EPG-0.0, EPG-0.40, EPG-40.0, and EPG-20.20).

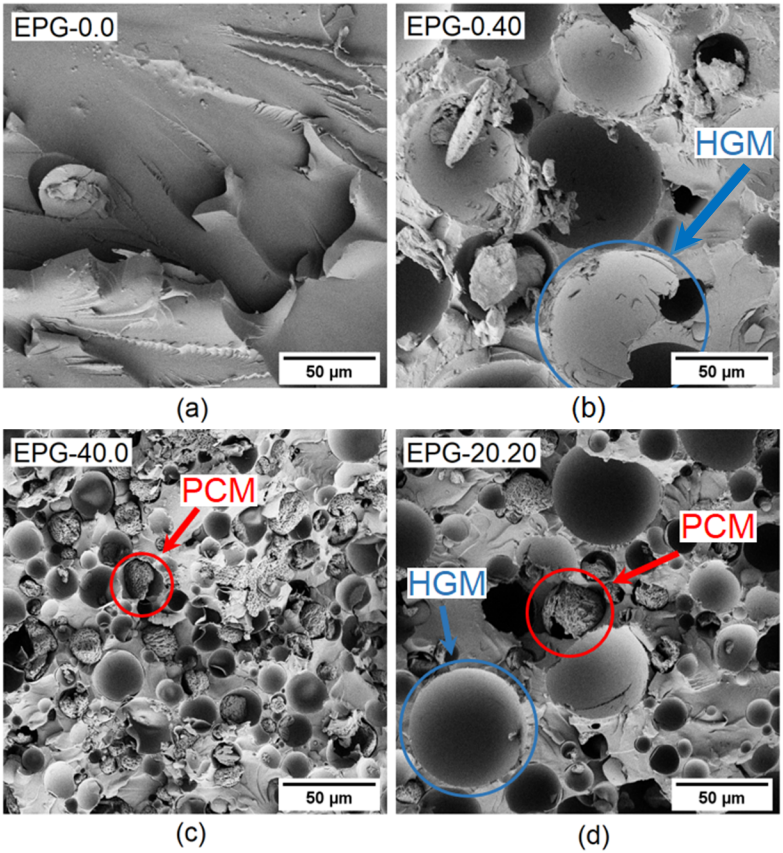

Figure 4-5 SEM micrographs of the fracture surface of some selected compositions: (a) EPG-0.0, (b) EPG-0.40, (c) EPG-40.0, and (d) EPG-20.20 (the blue arrow in figure (b) indicates a cracked HGM).

Figure 4-5a shows the typical brittle fracture surface of epoxy matrix similar to what has been already found in literature [108,155,156]. All samples exhibit a brittle fracture, as evidenced by the flat fracture surface. HGMs are homogeneously dispersed within the epoxy matrix (Figure 4-5b) and with good interfacial adhesion, as evidenced by the absence of gaps between the outer shell surface and the epoxy matrix. HGMs show a brittle behavior, observable from the cracks on some shell fragments (see Figure 4-5b). Additionally, the fact that the majority of HGMs are empty with clean inner surfaces suggests that the breakage happened during the

fracture process rather than during the mixing phase, confirming that the adopted processing conditions are suitable to maintain the integrity of the HGMs.

Figure 4-5c depicts the microstructure of the sample EPG-40.0, which contains 40% PCM. The PCM is made up of core-shell spherical microcapsules with an average diameter of about 20 μm, which is consistent with previous literature evidences [108] and the manufacturer's datasheet. The adhesion between the outer PCM shell and the epoxy matrix is rather poor, as it can be seen in higher magnification micrographs (not reported for brevity). However, the fact that the majority of PCM microcapsules are broken suggests that the fracture propagates across the microcapsules rather than at the interface with the epoxy matrix [120,157].

In any case, the low interfacial adhesion evidenced in these samples could be a drawback, which will be addressed in future research works. Moreover, most PCM capsules still show a rough and irregular paraffinic core, while the core of the smooth empty capsules has probably remained on the other side of the fracture surface. This suggests that the integrity of the PCM is preserved during processing, thereby excluding any possibility for the paraffinic core to leak out of the composite. A comparison between Figure 4-5b and c evidences the size difference between PCM and HGM, and this is confirmed by the micrograph of the sample EPG-20.20 (Figure 4-5d), which also highlights the different size distributions of the fillers. The smaller PCM capsules are located in the interstices of the bigger HGMs, in good agreement with the results of the rheological measurements (see Figure 4-3a).

4.2.3 Thermal and Thermo-mechanical properties

4.2.3.1 Differential scanning calorimetry (DSC)

The addition of PCM to epoxy/HGM syntactic foams imparts TES properties to these systems. DSC is one of the most widely used techniques for measuring TES properties because it requires a small amount of sample and allows the measurement of latent heat stored and released through the evaluation of the total phase change enthalpy. In this work, DSC was employed to measure not only the melting/crystallization enthalpy of the PCM (ΔH_m, ΔH_c) and the corresponding phase change temperatures (T_m, T_c) but also the glass transition temperature of the epoxy matrix (T_g) and the specific heat of the foams at 30 °C (c_{p30}). All these results were obtained by performing heating/cooling/heating DSC scans, but only the data from the first heating scan are shown in Figure 4-6a and b, while Table 4-5 reports also the results collected in the cooling scan. Table 4-5 also includes the DSC results for neat PCM. As already observed in previous works on this PCM [158,159], neat PCM exhibits a prominent endothermic peak between 35 °C and 60 °C, associated

with the melting of the paraffinic core. Figure 4-6a shows this signal in all PCM-containing samples in the same temperature range. Table 4-5 reports the melting temperature and enthalpy values respectively denoted as T_m and ΔH_m. T_m values increase slightly with PCM concentration, which is likely due to increased thermal inertia, as previously observed in other works in which the same PCM was utilized [108]. In any case, the temperature interval over which heat is exchanged is very similar for all the samples studied. It is evident that T_c is generally lower than T_m. This phenomenon, which is due to thermal inertia and undercooling, is already visible for neat microcapsules, with T_m and T_c of 45.9 °C and 27.9 °C, respectively, and is even more visible for all the other samples. In fact, while T_m ranges from 47 to 53 ° C, T_c ranges from 19 to 24 ° C.

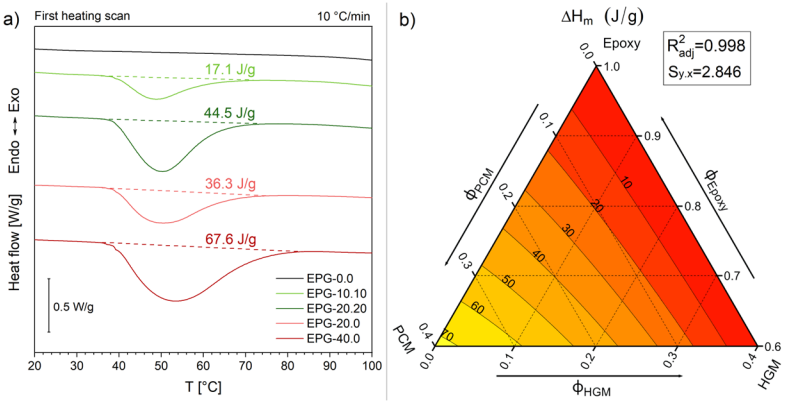

Figure 4-6 (a) DSC thermograms of some prepared foams (first heating scan); (b) fit-model of the melting enthalpy values (first heating scan) of the prepared foams.

Moreover, the values of ΔH_m increase with the PCM content and are nearly proportional to the PCM weight fraction. The values of ΔH_c are very close to those of ΔH_m, which highlights the reversibility of the process. The melting enthalpy can be also graphically evaluated from Figure 4-6b, which shows the results of the fitting of the melting enthalpy data with the linear ternary model (as reported in Section 3.2.5), obtained with a R^2_{adj} value of 0.998. Some interesting compositions can be EPG-20.20 and EPG-30.20, which are capable of storing and releasing approximately 45 J/g and 68 J/g of thermal energy, respectively.

As reported in the work of Fredi et.al [108], repeated heating-cooling cycles do not have big effects on the shape and position of the two peaks. For that reason, this cyclic analysis was not performed.

DSC tests also allowed the determination of the T_g of the epoxy phase and of the c_{p30} of the samples, which are reported in Table 4-5. The T_g of the neat epoxy in the first heating scan is approximately 92 °C, and it does not follow a specific trend with the filler concentration, confirming that the fillers do not substantially affect the curing process, as already shown by rheological tests. However, because the T_g signal is weaker at elevated filler loading, it is very challenging to detect the inflection point in DSC thermograms. The incorporation of PCM has the greatest impact on the values of c_{p30} listed in Table 4-5. Even though these values have not been measured by following the ASTM E-1269 standard, they are comparable with those found in the literature [160,161] and were thus used to calculate thermal conductivity (see Section 3.2.3.2).

Table 4-5 Main results of DSC tests on the prepared foams (first heating and cooling scans).

Sample	C_{p30} *J/(g·K)*	T_m *°C*	ΔH_m *J/g*	T_g *°C*	T_c *°C*	ΔH_c *J/g*
EPG-0.0	1.34	-	0.0	91.8	-	0.0
EPG-10.0	1.45	48.2	16.5	91.6	22.7	16.5
EPG-20.0	1.46	50.5	36.3	88.3	21.4	34.7
EPG-30.0	1.47	51.2	55.6	89.1	20.8	56.5
EPG-40.0	1.53	53.0	67.6	89.3	19.3	69.7
EPG-0.10	1.36	-	0.0	92.1	-	0.0
EPG-0.20	1.29	-	0.0	89.2	-	0.0
EPG-0.30	1.34	-	0.0	89.3	-	0.0
EPG-0.40	1.28	-	0.0	85.3	-	0.0
EPG-10.10	1.47	49.1	17.8	92.8	22.0	16.2
EPG-10.20	1.40	47.6	18.4	87.9	23.5	17.6
EPG-10.30	1.39	47.8	24.2	91.1	23.2	21.4
EPG-20.10	1.48	52.7	46.6	89.0	19.7	41.8
EPG-20.20	1.45	50.4	44.5	89.4	21.2	42.1
EPG-30.10	1.53	52.0	60.4	85.9	19.7	58.5
PCM	1.86	45.9	218.1	-	27.9	217.0

c_{p30} = specific heat at 30 °C; T_m = melting temperature of the PCM (first heating scan); ΔH_m = melting enthalpy of the PCM (first heating scan); T_g = glass transition temperature of the epoxy matrix (first heating scan); T_c = crystallization temperature of the PCM (cooling scan); ΔH_c = crystallization enthalpy of the PCM (cooling scan).

4.2.3.2 Thermal conductivity

The thermal conductivity and diffusivity of the prepared foams were quantitatively evaluated using Light Flash Analysis (LFA). By using the expression reported in Equation (3-5), it is possible to calculate the thermal conductivity (λ_{30}) and thermal

resistivity (R_λ) at 30 °C. All the numerical results are reported in Table 4-6. Moreover, the obtained values of thermal conductivity were fitted with a ternary model, resulting in the plot of Figure 4-7.

Table 4-6 Thermal conductivity and resistivity at 30 °Cof the prepared foams.

Sample	λ_{30} *W/(m·K)*	R_λ *(m·K)/W*
EPG-0.0	0.199±0.014	5.02±0.36
EPG-20.0	0.203±0.029	4.94±0.68
EPG-40.0	0.196±0.021	5.10±0.56
EPG-0.20	0.169±0.046	5.97±1.53
EPG-0.40	0.116±0.013	8.61±0.93
EPG-10.10	0.196±0.034	5.14±0.87
EPG-20.20	0.169±0.012	5.91±0.42

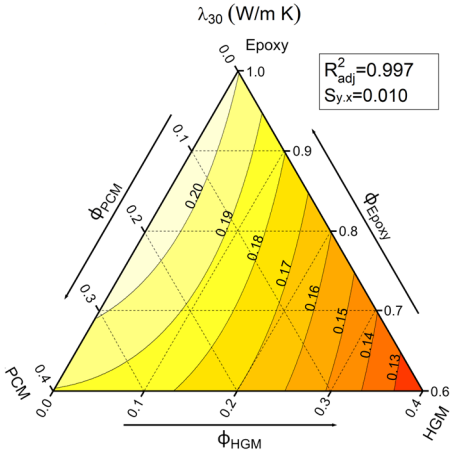

Figure 4-7 Fit-model of thermal conductivity of the prepared foams at 30 °C.

As expected, an increase in HGM content significantly decreases the thermal conductivity, which agrees with the results found in previous literature [162]. On the other hand, the PCM promotes only a modest decrease in thermal conductivity. For example, the value of λ_{30} for the sample EPG-40.0 is only 5% lower than that of neat epoxy, while for EPG-0.40 the reduction in λ_{30} is close to 40% (from 0.199 to 0.116 W/(m·K)). Therefore, the optimal composition must be chosen according to the intended application of the foam to maximize the TES properties or the

thermal insulation capability. Maximizing TES capability could be important when the aim is to manage and smooth temperature peaks of limited duration, while a low value of thermal conductivity could be preferable when the temperature conditions are stationary. Intermediate compositions, such as EPG-20.20, could be a good compromise to match both requirements.

4.2.3.3 Evaluation of TES capability

A temperature profiling test was performed under heating and cooling conditions to investigate the TES properties of the prepared samples on a larger scale. In this experiment, cylindric samples with a volume of about 10 cm^3 were heated in an oven at 60 °C and then allowed to cool at 25 °C, while their inner temperature was measured with a K-type thermocouple. Figure 4-8(a-d) show the results of these tests.

These profiles clearly show the influence of PCM, because samples containing PCM exhibit a plateau-like region at the PCM phase change temperature (43 °C), which is especially noticeable at higher PCM concentrations. This behavior, which has been already observed in literature [163], delays the heating (Figure 4-8a) and cooling (Figure 4-8c) processes and increases $t_{26\text{-}55}$ and $t_{55\text{-}26}$ values i.e., the time required for the specimens to reach a target temperature during the heating and cooling transients. In the heating test, for example, the sample EPG-20.20 takes 19.8 minutes to reach 55 °C (63% slower than neat epoxy), whereas the sample EPG-40-0 takes 25.6 minutes (111% slower than neat epoxy). These findings suggest that samples with higher PCM loadings are more promising for thermal management applications.

The values of $t_{26\text{-}55}$ and $t_{55\text{-}26}$ (Figure 4-8(b,d)) show the effect played by PCM in decreasing the heating and cooling rates. On the other hand, the influence of HGM is unexpected. An increasing HGM content seems to decrease both $t_{26\text{-}55}$ and $t_{55\text{-}26}$, i.e., to accelerate the heating and cooling processes. The fit-model correctly interprets the experimental data since the temperature profiles of the samples containing only HGM are indeed steeper than that of the neat epoxy. Given their low thermal conductivity, this suggests that HGM favors thermal exchange, whereas the opposite effect could be expected. These effects may be caused by the fact that HGMs are introducing voids that reduce the available volume of matrix capable of storing sensible heat. In addition, thermal diffusivity also plays a role in this, as shown by Equation (3-5). As reported in a technical paper produced by 3M™ [164], syntactic foams show at the same time reduced thermal conductivity and increased thermal diffusivity, due to the presence of HGMs that reduce the final density.

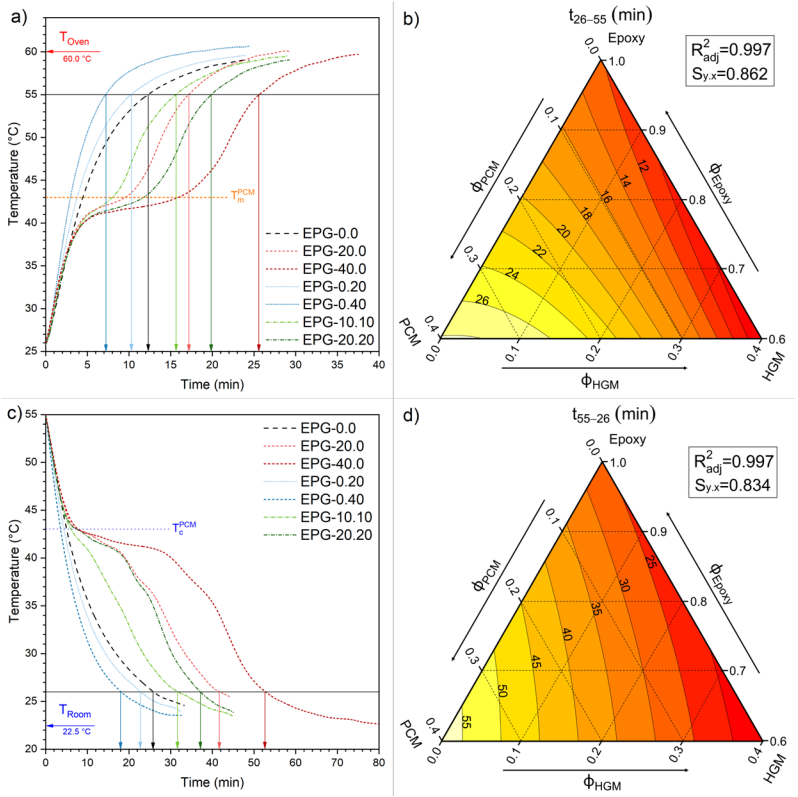

Figure 4-8 (a) Temperature evolution of the prepared epoxy-based syntactic foams during the heating stage, (b) fit-model of t_{26-55} values, (c) temperature evolution of the prepared syntactic foams during the cooling stage, and (d) fit-model of t_{55-26} values.

4.2.3.4 Dynamic mechanical thermal analysis (DMTA)

Figure 4-9(a,b) and Figure 4-10(a-c) summarize DMTA results, where Figure 4-9 shows the trends of the storage modulus (E') and the loss tangent (tanδ) of the prepared foams as a function of temperature, and Figure 4-10 represents E' values at three different temperatures (i.e, 25, 60, and 130 °C).

As it can be noticed in Figure 4-9a, neat epoxy E' decreases with temperature in the entire temperature range but the decrease is faster at approximately 90–100 °C, the temperature interval at which the matrix undergoes glass transition. This decreasing step in E' corresponds to a peak in tanδ. The introduction of HGM does not

substantially modify the dynamic behavior of the epoxy matrix, since the samples EPG-0.30 and EPG-0.40 also show a single relaxation event at 90-100 °C. However, the values of E' below the glass transition slightly decrease by increasing the HGM fraction, while the opposite is true above 70 °C. Furthermore, when HGM is added, the E' inflection point and tanδ peak temperature are slightly shifted to higher temperatures, implying that HGM may restrict the mobility of the polymer chains, delaying the glass transition. The height of the tanδ peak is also reduced by HGM introduction. These effects are comparable to those reported in the literature for other epoxy/HGM systems [165,166], implying that the effect played by HGM on the viscoelastic behavior of the epoxy resin is relatively weak.

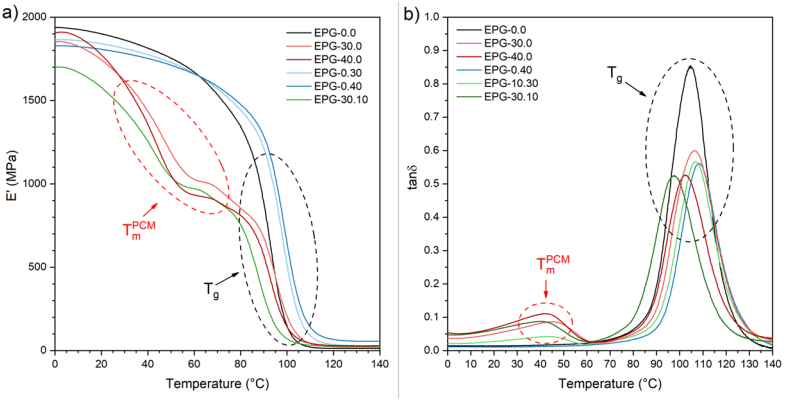

Figure 4-9 DMTA thermograms of the prepared epoxy-based foams. (a) Storage modulus (E′) and (b) loss tangent (tanδ) as a function of the temperature.

The effect played by PCM introduction is more evident. The samples containing PCM exhibit an additional transition in the temperature range 20-60 °C, with a relative maximum at around 40 °C, related to PCM melting. This transition is accompanied by a significant decrease in E' and by a small tanδ peak, which has been already observed in composites containing the same PCM type [108,155]. Furthermore, the relative composition of these foams has only a minor effect on the T_g of the epoxy, and there is no clear trend with PCM fraction, which is consistent with DSC results. This demonstrates that the PCM and HGM do not interfere with the crosslinking process of epoxy and that the addition of a microencapsulated PCM retains the thermal properties of the epoxy resin. In fact, the literature reports some examples in which an epoxy matrix was filled with other types of PCMs, namely shape-stabilized paraffins, and in those cases, the PCM domains did influence the mobility of the matrix chains and the value of T_g [167,168].

The effect of PCM and HGM on the values of E' is better illustrated in Figure 4-10(a–c), which show the fitted models of E' at 25 °C, 60 °C, and 130 °C. At 25 °C (Figure 4-10a) E' decreases by increasing filler concentration and is more influenced by PCM than by HGM. The effect of PCM is much more visible at 60 °C (Figure 4-10b), between the T_m of the PCM and the T_g of the epoxy matrix. E' decreases noticeably as the PCM fraction increases, but it remains nearly constant when only the HGM content is varied. On the other hand, above the T_g of the epoxy (at 130 °C, see Figure 4-10c), the filler content has an opposite effect on E'. In fact, E' increases with the HGMs concentration since these stiff particles help in retaining the mechanical properties also above the T_g of the epoxy.

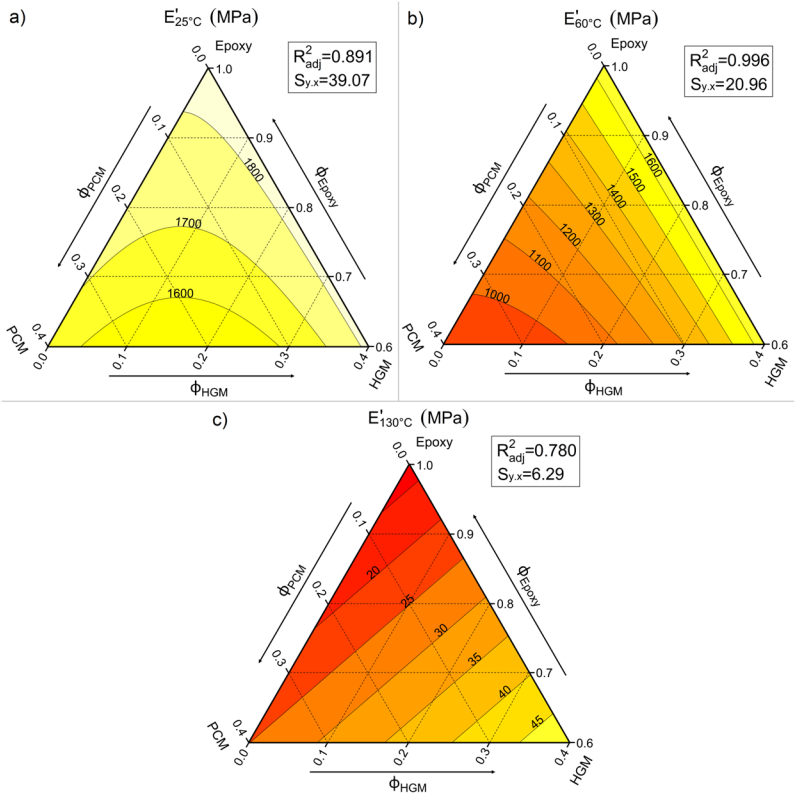

Figure 4-10 Fit-model of storage modulus (E') values at (a) 25 °C, (b) at 60 °C, and (c) at 130 °C from DMTA tests on the prepared epoxy-based syntactic foams.

Although both PCM and HGM reduce the E' values, it is important to determine whether this decrease is solely due to a decrease in density. Parameters such as stiffness and strength normalized by density provide a more accurate evaluation of material performances, and they are more commonly used for structural design [169]. The resulting specific storage moduli (E'/ρ) (Table 4-7) show that HGM has a positive contribution at all temperatures studied, and this effect increases with temperature. For example, the E'/ρ value of the sample EPG-0.40 at 25 °C is 2444 MPa/(g/cm^3) (+48% higher than neat epoxy), 2256 MPa/(g/cm^3) at 60 °C (+54%), and 77 MPa/(g/cm^3) at 130 °C (+600%).

Table 4-7 Specific storage modulus values (E'/ρ) at different temperatures from DMTA tests on the prepared epoxy-based foams

Sample	*E'/ρ MPa/(g/cm^3) T=25 °C*	*E'/ρ MPa/(g/cm^3) T=60 °C*	*E'/ρ MPa/(g/cm^3) T=130 °C*
EPG-0.0	1655	1469	11
EPG-30.0	1642	100	20
EPG-40.0	1680	925	29
EPG-0.10	1646	1499	24
EPG-0.30	2073	1886	34
EPG-0.40	2444	2256	77
EPG-10.30	1982	1551	51
EPG-30.10	1618	1035	28

The PCM contribution is even more temperature dependent. At 25 °C, the PCM slightly raises the value of E'/ρ since the sample EPG-40.0 has an E'/ρ of 1680 MPa/(g/cm^3) (+1.5% higher than neat epoxy). PCM, on the other hand, strongly reduces E'/ρ at 60 °C because the paraffinic core is completely molten but the epoxy matrix is still in a glassy state. EPG-40.0 foam, for example, has an E'/ρ value of 925 MPa/(g/cm^3) (-37% than neat epoxy). Finally, at 130 °C, the PCM raises E'/ρ to 29 MPa/(g/cm^3) for the EPG-40.0 sample (+163% than neat epoxy).

In conclusion, even though none of the fillers increases the absolute value of E', the reduction in density provided by the combination of PCM and HGM results in a significant increase in E'/ρ, particularly at high temperatures. As a result, such materials could be used as lightweight materials with high specific stiffness in a wide variety of structural applications.

4.2.4 Mechanical properties

4.2.4.1 Quasi-static tensile tests

The uniaxial quasi-static tensile test is one of the most widely used methods for evaluating the mechanical properties of polymeric materials. Figure 4-11 reports representative stress-strain curves of some selected compositions, whereas Figure 4-12 summarizes the trends of tensile elastic modulus (E_t), specific elastic modulus (E_t/ρ), stress at break (σ_B), and specific stress at break (σ_B/ρ) in ternary diagrams. Table 4-8 Results of the quasi-static tensile tests performed on the produced epoxy-based syntactic foams. summarizes these results in numerical form.

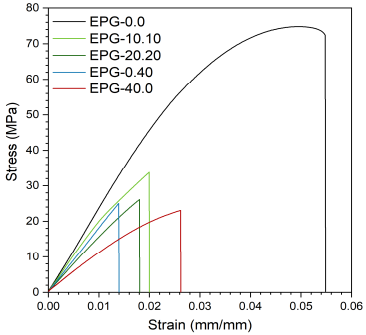

Figure 4-11 Representative stress–strain curves from quasi-static tensile tests on some compositions of the prepared epoxy-based syntactic foams.

Table 4-8 Results of the quasi-static tensile tests performed on the produced epoxy-based syntactic foams.

Sample	E_t *MPa*	E_t/ρ *MPa/ (g/cm³)*	σ_B *MPa*	σ_B/ρ *MPa/ (g/cm³)*	ε_B *%*	ε_B/ρ *%/ (g/cm³)*
EPG-0.0	3121±113	2746±100	73.7±1.8	64.8±1.6	5.65±0.46	4.97±0.40
EPG-10.0	2586±92	2333±83	48.4±4.6	43.6±4.1	3.24±0.59	2.92±0.54
EPG-20.0	2145±83	1983±77	39.0±4.0	36.1±3.7	2.83±0.36	2.62±0.33
EPG-30.0	1564±69	1521±67	31.6±0.9	30.8±0.9	3.01±0.26	2.93±0.25
EPG-40.0	1282±29	1271±29	22.4±0.8	22.2±0.8	2.54±0.29	2.52±0.28
EPG-0.10	3040±85	2798±79	42.2±3.2	38.8±3.0	2.04±0.43	1.88±0.40
EPG-0.20	2762±100	2680±97	33.7±2.4	32.7±2.3	1.57±0.23	1.52±0.22
EPG-0.30	2450±94	2779±107	31.3±1.2	35.5±1.3	1.55±0.14	1.76±0.15
EPG-0.40	2123±55	2890±75	24.0±1.6	32.7±2.1	1.31±0.21	1.78±0.28
EPG-10.10	2238±67	2158±65	34.1±1.4	32.9±1.4	1.85±0.18	1.78±0.17
EPG-10.20	2160±52	2309±56	29.1±2.9	31.1±3.1	1.63±0.24	1.75±0.26
EPG-10.30	1979±61	2395±74	26.1±1.9	31.5±2.3	1.54±0.20	1.86±0.25
EPG-20.10	2052±76	2132±79	29.8±0.9	31.0±1.0	2.02±0.15	2.10±0.15
EPG-20.20	1806±34	2072±39	25.5±2.3	29.2±2.6	1.81±0.36	2.08±0.41
EPG-30.10	1569±34	1675±36	26.1±0.9	27.9±0.9	2.28±0.16	2.43±0.17

Figure 4-11 and Figure 4-12 evidence the role played by both filler types (i.e., PCM and HGM) on the tensile properties. Compared to neat epoxy resin, the elastic modulus, strength, and strain at break of all composites are considerably lower. As reported in Table 4-8, the elastic modulus, which is reduced especially by the PCM introduction, decreases from 3121 MPa down to 1282 MPa for the EPG-40.0 sample (−60%), while the strain at break decreases from 5.6 % down to 2.5 % (−56%). These results are in good agreement with previous findings on epoxy/PCM composites [108]. These trends are also evidenced by the application of the linear model (see Figure 4-12(a–d)). The elastic modulus (Figure 4-12a) decreases especially upon PCM addition, while a less evident effect can be observed with HGMs, as the stiffness of the sample containing 40 vol% of HGMs is 2123 MPa (−32% than neat epoxy). Considering the compositions with both HGMs and PCM at constant total volumetric concentration, moving horizontally on the ternary diagram, it can be concluded that the gradual substitution of PCM with HGMs increases the elastic modulus, due to the higher stiffness of HGMs compared to the PCM capsules. For example, considering the compositions with a total filler concentration of 30 vol%, EPG-30.0 foam shows an elastic modulus of 1564 MPa, the EPG-20.10 foam of 2052 MPa, the sample EPG-10.20 of 2160 MPa, and EPG-0.30 of 2450 MPa. This effect is even more pronounced when the specific modulus (E_t/ρ) is considered, as shown in Figure 4-12b. Moving horizontally from left to right on the diagram, the increase in specific modulus at constant filer volume fraction is still visible. Furthermore, the specific modulus is strongly dependent on the amount of PCM. In fact, by keeping the PCM concentration constant, the specific modulus remains nearly constant as the HGM content increases. This is because HGMs reduce the elastic modulus while also significantly lowering the density, allowing the E_t/ρ ratio to remain nearly constant. This result is significant from the perspective of design because it clearly shows that the HGMs reduce the foam density without compromising the specific stiffness.

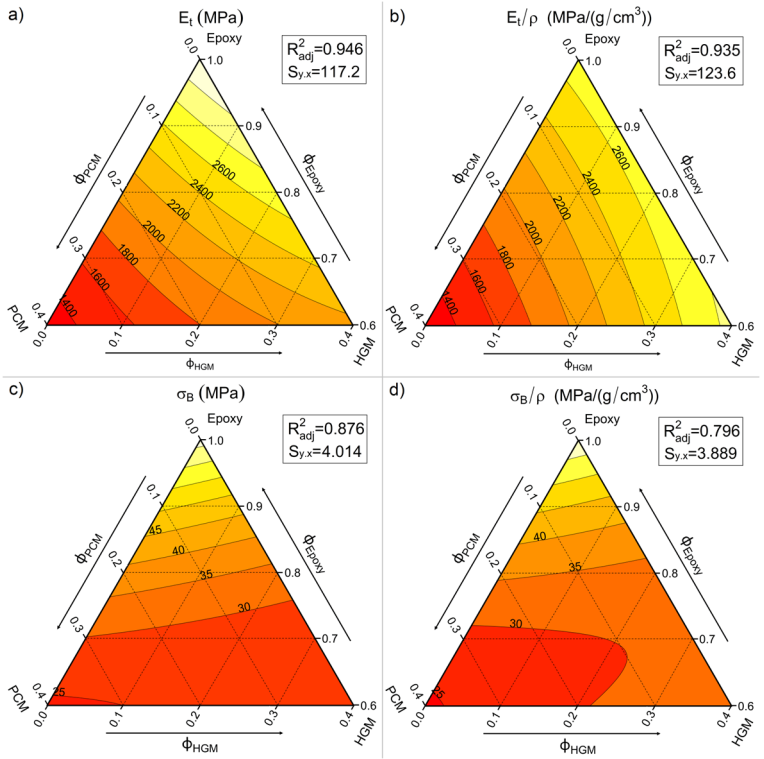

Figure 4-12 Fit-models of the main results of quasi-static tensile tests on the prepared epoxy-based syntactic foams. (a) Young's modulus (E_t); (b) specific Young's modulus (E_t/ρ); (c) tensile stress at break (σ_B); and (d) specific stress at break (σ_B/ρ).

In terms of mechanical strength, Table 4-8 reports that the stress at break is reduced from 73.7 MPa of EPG-0.0 down to 22.4 MPa (–70%) of EPG-40.0. This trend can be seen also in Figure 4-12c where the incorporation of PCM or HGMs reduces the stress at break. In compositions containing only PCM, the strength decreases as the PCM fraction increases, and for the sample EPG-40.0, the strength drop is close to -65%, when compared with neat epoxy resin. A similar trend can be seen in samples containing only HGMs. As shown in Figure 4-12d, normalization by density has no significant effect on the strength. This decrease in mechanical strength can be attributed to porosity formation caused by HGM insertion [45], as well as by the limited HGM/epoxy interfacial adhesion [170–173]. A possible way to overcome this issue could be the surface functionalization of the HGMs by silanization [146].

4.2.4.2 *Quasi-static compression tests*

The compression test is another widely used mechanical test to analyze the properties of syntactic foams, as their compressive resistance has great importance in many practical applications [174–176]. Figure 4-13 depicts the compressive stress-strain curves of some selected compositions, whereas Figure 4-14(a-d) show the trends of the compression modulus (E_C), specific compression modulus (E_C/ρ), maximum stress (σ_C) and specific maximum stress (σ_C/ρ) in ternary diagrams. Table 4-9 collects all the results from the tests performed on all the considered compositions, also including the strain at maximum stress (ε_C).

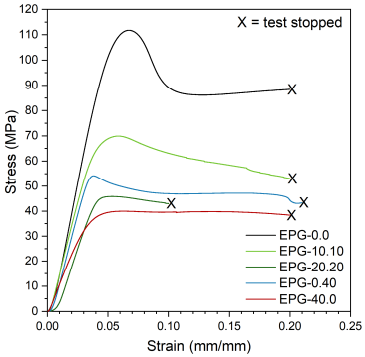

Figure 4-13 Representative stress–strain curves from quasi-static compressive tests on the prepared epoxy-based syntactic foams.

Table 4-9 Results of the quasi-static compression tests performed on the produced epoxy-based foams.

Sample	E_C *MPa*	E_C/ρ *MPa/ (g/cm³)*	σ_C *MPa*	σ_C/ρ *MPa/ (g/cm³)*	ε_C *%*	ε_C/ρ *%/ (g/cm³)*
EPG-0.0	2461±39	2165±34	109.9±1.7	96.7±1.5	6.50±0.20	5.72±0.18
EPG-10.0	2180±26	1967±24	84.0±0.8	73.9±0.7	5.90±0.10	5.19±0.09
EPG-20.0	1824±18	1687±17	65.2±0.8	57.3±0.7	5.90±0.30	5.19±0.26
EPG-30.0	1445±15	1408±15	50.8±0.6	44.6±0.5	6.60±0.60	5.81±0.53
EPG-40.0	1172±18	1162±18	40.0±0.6	35.2±0.6	7.20±0.60	6.33±0.53
EPG-0.10	2339±61	2154±56	89.4±1.1	78.7±1.0	5.20±0.20	4.57±0.18
EPG-0.20	2049±77	1988±74	71.7±1.4	63.0±1.2	5.30±0.40	4.66±0.35
EPG-0.30	2043±60	2317±68	62.6±2.4	55.1±2.1	4.10±0.30	3.61±0.26
EPG-0.40	1868±27	2542±37	54.1±1.3	47.6±1.1	3.70±0.10	3.25±0.09
EPG-10.10	1933±16	1864±15	69.2±0.9	60.9±0.7	5.70±0.10	5.01±0.09
EPG-10.20	1791±13	1914±14	56.5±0.7	49.7±0.6	4.60±0.30	4.05±0.26
EPG-10.30	1647±6	1994±7	49.4±0.2	43.4±0.2	3.90±0.10	3.43±0.09
EPG-20.10	1588±43	1650±45	51.9±2.7	45.7±2.4	5.10±0.20	4.49±0.18
EPG-20.20	1457±7	1671±8	45.5±0.6	40.0±0.5	4.70±0.30	4.13±0.26
EPG-30.10	1309±13	1397±14	43.3±0.9	38.1±0.8	5.80±0.30	5.10±0.26

The representative stress–strain curves (Figure 4-13) evidence that the compressive properties decrease upon the addition of both PCM and HGMs. The compressive modulus (E_C) decreases from 2461 MPa of neat epoxy down to 1172 MPa of the sample EPG-40.0 (−53%), while σ_C is reduced from 109.9 MPa of neat epoxy down to 40.0 MPa of the sample EPG-40.0 (−63%). If the compressive curves with the same filler amount are considered, e.g., EPG-20.20, EPG-0.40, and EPG-40.0, a similar trend can be detected, especially after the yield point.

Figure 4-14(a-d) show the quantitative trends of the investigated mechanical properties. The compressive modulus (E_C), like the tensile one, decreases more dramatically with PCM insertion rather than with HGMs addition. In fact, in compositions containing only PCM, as already said, the E_C drops by 53% with the incorporation of 40 vol% of PCM, while in compositions containing only HGM, the E_C drops by only 24%, from 2461 MPa of neat epoxy to 1868 MPa of EPG-0.40 foam. Moreover, the progressive substitution of PCM with HGMs increases the stiffness of the system. Conversely, the shape of E_C level lines slightly differs from that observed in tensile tests. For compositions containing only HGMs, the elastic modulus decreases with the HGM amount, but E_C is less affected than E_t. This difference is even more evident by looking at the trends of specific compressive modulus (Figure 4-14b), where the maximum value is not shown by the neat epoxy, as in tensile tests, but by the EPG-0.40 sample. This is one of the most important reasons why syntactic foams are mainly used in applications where a compression state is applied, as the combination of low density and good compressive stiffness results in a very high specific compressive modulus.

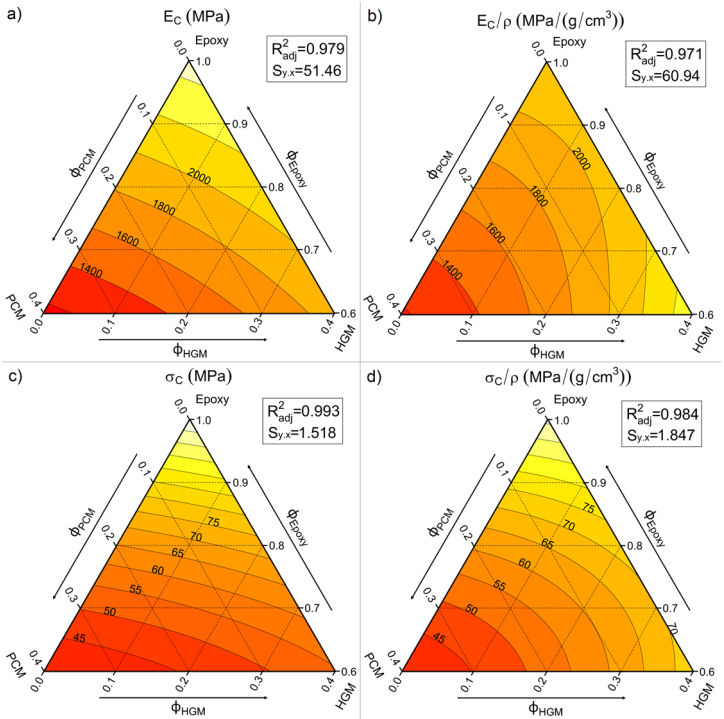

Figure 4-14 Fit-models of the main results of quasi-static compressive tests on the prepared epoxy-based syntactic foams. (a) compressive modulus (E_C); (b) specific compressive modulus (E_C/ρ); (c) maximum compressive stress (σ_C); and (d) specific maximum compressive stress (σ_C/ρ).

The maximum stress σ_C (Figure 4-14c) decreases as the total filler amount increases. In the PCM-filled samples, the reduction in σ_C is approximately 65%, from 109.9 MPa of the neat epoxy resin to 40.0 MPa of the EPG-40.0 foam. This reduction is slightly less pronounced in HGM-filled samples (approximately 50% for EPG-0.40). Normalization by density, on the other hand, bends the level curves (Figure 4-14d), and σ_C/ρ values are also interesting for compositions with a rather elevated concentration of fillers.

In conclusion, the better compressive properties of HGMs compared to the PCM [171,177] and the lower effect played by the poor epoxy/HGMs adhesion in compression [178] result in higher E_C and σ_C performance of HGM-filled samples

compared to those containing also PCM. When normalized properties are considered, this effect becomes even more pronounced.

4.2.4.3 Charpy impact tests

Figure 4-15 shows ternary diagrams representing the linear model fitting of the Charpy impact strength values of the prepared foams, while Table 4-10 reports the numerical values.

Table 4-10 Impact strength a_{cN} values from Charpy impact tests of the prepared foams

Sample	a_{cN} *kJ/m²*
EPG-0.0	9.32±1.66
EPG-20.0	5.20±0.76
EPG-30.0	5.30±0.70
EPG-40.0	4.03±1.18
EPG-0.10	3.59±0.69
EPG-0.20	3.91±1.25
EPG-0.30	3.15±0.65
EPG-0.40	3.04±0.55
EPG-10.10	3.76±0.74
EPG-10.20	4.55±0.61
EPG-10.30	4.98±0.30
EPG-20.10	4.11±0.68
EPG-20.20	3.39±0.62
EPG-30.10	5.38±0.80

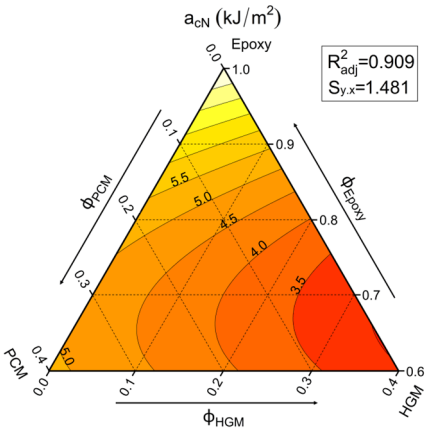

Figure 4-15 Fit-models of the Charpy impact strength (a_{cN}) of the prepared epoxy-based syntactic foams.

The high $S_{y.x}$ value (1.481), which represents the residual standard error of the model fitting the experimental data, is typical in Charpy impact tests [179]. Figure 4-15 shows that HGM-filled composites have a lower impact strength due to the brittle nature of HGM and to the presence of voids within the material, whereas PCM has a lower impact strength due to its plastic nature. In particular, by looking at the compositions with the same total filler amount (i.e., moving horizontally on the graph) it is evident that the substitution of HGMs with PCM increases noticeably the impact strength (from 3.15 kJ/m^2 of EPG-0.30 sample up to 5.30 kJ/m^2 of the EPG-30.0 foam, as reported in Table 4-10). The samples containing only PCM show a decreasing trend, which is consistent with our previous work on epoxy/PCM composites [108]. HGMs, on the other hand, reduce the impact strength more at lower HGM contents (up to 30%) than at higher HGM loadings. The impact strength decreases from 9.32 kJ/m^2 of neat epoxy to 3.91 kJ/m^2 of EPG-0.20 foam, and to 3.04 kJ/m^2 of EPG-0.40. These findings show that incorporating both fillers result in a general decrease in impact strength, but the extent of the observed a_{cN} drop is dependent on the filler type. In any case, it is reasonable to believe that increasing the adhesion between HGMs and the epoxy matrix could significantly improve the impact properties of these foams.

4.2.4.4 Evaluation of the fracture behavior

It is well known that both the critical stress intensity factor (K_{IC}) and critical strain energy release rate (G_{IC}) describe the capability of the material to resist crack propagation. Both properties were investigated, and the results are represented by ternary graphs in Figure 4-16, while Table 4-11 reports the numerical values.

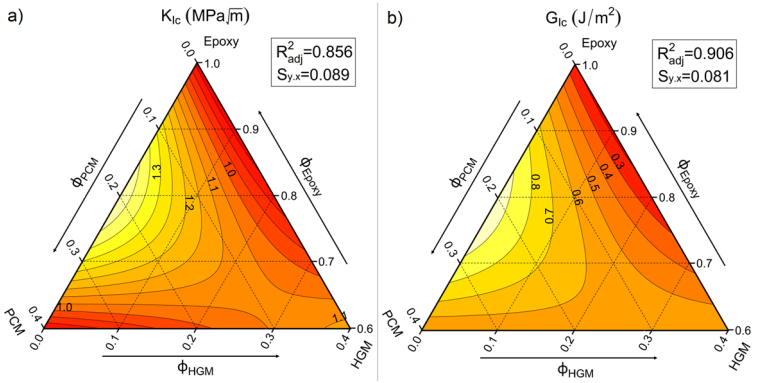

Figure 4-16 Fit-models of the main results from fracture toughness tests on the prepared epoxy-based syntactic foams. (a) Mode I fracture toughness (K_{IC}) and (b) critical strain energy release rate (G_{IC}).

Table 4-11 Critical stress intensity factor K_{IC} and critical energy release rate G_{IC} values of the prepared syntactic foams.

Sample	K_{IC} $MPa\sqrt{m}$	G_{IC} J/m^2
EPG-0.0	0.83±0.05	0.21±0.04
EPG-20.0	1.42±0.05	0.96±0.06
EPG-40.0	0.85±0.06	0.50±0.08
EPG-0.20	0.85±0.10	0.24±0.05
EPG-0.40	1.13±0.08	0.60±0.10
EPG-10.10	1.19±0.09	0.58±0.08
EPG-20.20	0.97±0.06	0.54±0.07

For the sample containing 20 vol% PCM, both K_{IC} and G_{IC} are maximized (EPG-20.0). The results obtained for PCM-only filled compositions agree with those obtained in a previous work of our group [108], where the incorporation of PCM microcapsules increased both K_{IC} and G_{IC} up to a PCM content of 20 wt% and decreased both properties at higher microcapsule contents. HGM introduction, on the other hand, has a weak influence on K_{IC} and G_{IC}, with a slight increase occurring only at high HGM contents. K_{IC} and G_{IC} for neat epoxy result 0.83 $MPa \cdot m^{0.5}$ and 0.21 kJ/m^2, respectively, while EPG-20.0 reaches 1.42 $MPa \cdot m^{0.5}$ and 0.96 kJ/m^2 (+80% and +370% with respect to the neat matrix). On the other hand, EPG-40.0 shows values close to that of the unfilled epoxy resin. As shown by SEM micrographs reported in Section 4.2.2.2 [45], this behavior could be explained by the introduction of new toughening mechanisms due to the presence of PCM, such as crack pinning, debonding, and microcracking.

4.2.5 General comparison of the properties of epoxy/HGM/PCM syntactic foams

Figure 4-17 shows a radar graph that was used to compare and rank the various compositions of these new ternary systems in terms of thermal and mechanical properties. It compares seven representative compositions over ten selected properties, i.e., specific tensile modulus (E_t/ρ), specific tensile stress at break (σ_B/ρ), specific compression modulus (E_C/ρ), specific compression stress at 10% of strain (σ_{10}/ρ), impact strength (a_{cN}), mode I fracture toughness (K_{IC}), critical strain energy release rate (G_{IC}), specific volume ($\upsilon = 1/\rho$ [45]), specific melting enthalpy (ΔH_m), and thermal resistivity ($R_\lambda = 1/\lambda$ [45]). Below each axis label, the maximum measured values for each property are reported [4].

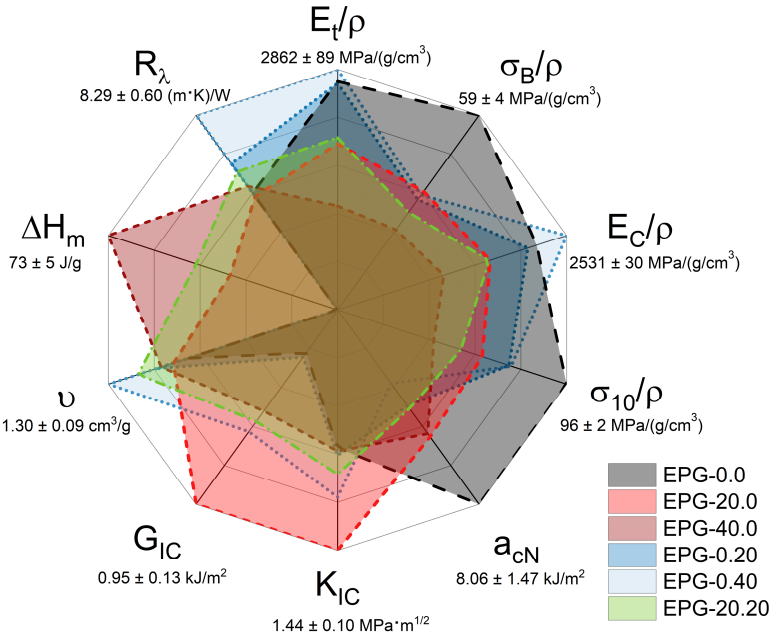

Figure 4-17 Graphical comparison of the properties of some representative compositions analyzed.

As expected, neat epoxy resin (EPG-0.0) has the best tensile, compressive, and impact properties but the worst general performance. It combines the highest impact strength with the lowest K_{IC} and G_{IC} values. This sample also has the lowest specific volume, thermal resistance, and no TES capability. When compared to unfilled resin, the PCM-only filled samples (EPG-0.20, EPG-0.40, blue area) cover vastly different areas. They cover lower areas in the tensile, compression, and impact properties than EPG-0.0, indicating a general decrease in mechanical performances. These compositions, on the other hand, have higher K_{IC}, G_{IC}, υ, and R_λ values than neat epoxy.

In tensile, compression, and impact properties, the area covered by PCM-only filled samples (i.e., EPG-20.0 and EPG-40.0 foams) is even smaller than that of HGM-only filled samples, with EPG-40.0 being the worst composition. In contrast, EPG-20.0 has the best K_{IC} and G_{IC} values, and EPG-40.0 also outperforms EPG-0.0. As expected, the presence of PCM provides TES capability to these compositions, with high ΔH_m values. Because the property set of these compositions prioritizes TES

properties rather than mechanical ones. For this reason, they are recommended for cavity filling where TES capabilities are required.

The use of PCM and HGMs in the EPG-10.10 and EPG-20.20 samples allows for a good balance of mechanical and TES properties. These samples have a more circular and centered area than the others, indicating a more balanced property distribution. While the mechanical properties of EPG-10.10 are slightly better, the TES performance of EPG-20.20 is superior. These compositions represent a good compromise between HGM-only and PCM-only formulations, making them the most promising ones in terms of multifunctionality.

4.3 Conclusions

Incorporating HGMs and PCM microcapsules into an epoxy resin produced syntactic foams with a peculiar combination of properties.

Both PCM and HGM significantly increased the viscosity of the uncured mixtures at elevated filler amounts (up to +630% for EPG-40.0 at $\dot{\gamma}$= 0.2 s^{-1}) in dynamic rheological tests, and the effect of PCM was more pronounced than that of HGM due to its smaller size (20 um vs 60 um). Moreover, systems containing both PCM and HGM always showed a lower viscosity than foams with a single filler type at the same total filler volume fraction, because of the higher maximum packing factors of bimodal filler distributions. Furthermore, none of the fillers had a significant effect on the gel time or activation energy of the curing process.

HGM significantly reduced the density, which ranged from 1.137g/cm^3 of neat epoxy to 0.733 g/cm^3 of EPG-0.40 sample. Furthermore, as evidenced by LFA, HGM decreased thermal diffusivity and conductivity, whereas PCM only marginally decreased thermal conductivity. PCM addition, on the other hand, increased the TES properties. Indeed, DSC demonstrated an increase in melting enthalpy with the PCM content, up to 68 J/g with a PCM amount of 40 vol%. The temperature profiling tests also revealed interesting thermal management properties in the transient regime of this foam composition.

DMTA tests showed that E' was generally decreased by both HGM and PCM addition below the T_g of the epoxy matrix, while above T_g the presence of stiff particles (especially HGM) promoted an increase in E' when compared to unfilled epoxy. On the other hand, the values of specific storage modulus (E'/ρ) increased with the HGM concentration and this was more evident at higher temperatures. The PCM generally decreased E'/ρ, especially below the T_g of the epoxy matrix.

HGMs reduced density significantly, resulting in higher specific mechanical properties. Indeed, HGMs contributed to the retention of the specific tensile elastic modulus, while the specific compressive modulus was higher than that of neat epoxy resin for HGM contents greater than 20 vol%. The PCM, on the other hand, reduced all specific tensile and compressive properties. In Charpy impact tests, the presence of brittle HGMs significantly reduced the impact properties, whereas the PCM microcapsules were able to restrain this reduction, likely due to their better deformability. K_{IC} and G_{IC} showed interesting trends as well. Both K_{IC} and G_{IC} showed a maximum at a PCM content of 20 vol% in samples containing only PCM, indicating that PCM played a relevant toughening effect. HGMs also increased K_{IC} and G_{IC}, but only at concentrations greater than 20 vol%.

The selection of the best composition could be facilitated by the proposed linear ternary fitting models, which further allowed the evaluation of properties of intermediate compositions between those experimentally investigated. The radar plot allowed the direct comparison between some analyzed compositions. For instance, the composition showing balanced properties could be EPG-20.20. In fact, EPG-20.20 had a density of 0.872 g/cm^3, a heat storage capacity of 45 J/g, and a thermal conductivity of 0.17 W/(m·K).

The present findings can be viewed as a general and useful guide for the development of epoxy/HGM syntactic foams containing microencapsulated PCMs, which is promising in applications requiring high specific mechanical properties, low thermal conductivity, and thermal management properties. The resulting property set can be finely tuned simply by changing the relative concentration of the constituents, demonstrating elevated versatility for different applications like in electronic, automotive, refrigeration, and aerospace industries. The mechanical performance of these foams and their applicability could be significantly enhanced by improving the interfacial adhesion between the HGMs and the matrix, which will be the subject of future research on these materials.

Chapter 5 - PP-based syntactic foams with TES properties

This Chapter presents the methods and results concerning the PP/HGM/PCM system.

Part of this Chapter has been published in:

- Galvagnini, F.; Dorigato, A.; Fambri, L.; Pegoretti, A.
  Development of Novel Polypropylene Syntactic Foams Containing Paraffin Microcapsules for Thermal Energy Storage Applications.
  Molecules 2022, 27 (23)

5.1 Materials and methods

The materials utilized to prepare these samples and the procedures adopted for sample preparation are described in this Section, together with the list of the experimental techniques applied. A detailed description of the materials and the experimental techniques have been already presented in Chapter 3 - .

5.1.1 Materials

The materials employed for the preparation of these foams are listed in Table 5-1 (please refer to Section 3.1 for the details about the materials).

Table 5-1 List of materials employed for the preparation of PP/HGM/PCM syntactic foams.

Constituent	*Label*	*Material*
polymer matrix	PP	Polypropylene (Moplen HP456J)
compatibilizer	-	Compoline PP/H60
silane	APTES	γ-Aminopropyl-Triethoxysilane
hollow filler	HGMs	hollow glass microspheres (iM16K)
PCM	PCM	Paraffin microcapsules (MPCM57D)

5.1.2 Sample preparation

5.1.2.1 Silanization of HGMs

Silanization is a chemical process that aims to improve adhesion between two incompatible surfaces by joining them with specific molecules known as silanes (see Section 3.1.5) [180]. Typically, this process is used on glass fibers to improve their adhesion to the matrix. This procedure was used on HGMs for the same reason,

and the main operative steps are listed below. This procedure is the result of an optimization based on information taken from the literature [25,145,146,181,182].

- Hydroxylation
  - 12 g of HGMs were added in a 0.5 M solution of NaOH.
  - The solution was stirred using a magnetic anchor at 90 °C for 1 h.
  - After the solution reached room temperature it was filtered and washed with distilled water until a pH = 7 was reached.
  - The filter with the washed HGMs was then dried in a vacuum oven at 80 °C for 12 h.
- Silanization
  - 10 g of HGMs were mixed with a preheated solution (200 mL, 70 °C) of 50/50 mass of ethanol and distilled water plus 2 g of APTES.
  - After the mixture was mixed for 1.5 h the solution was cooled and filtered again as in the hydroxylation step.
  - The silanized HGMs were filtered and then dried in a vacuum oven for 12 h at 80 °C.

5.1.2.2 Preparation of the foams

The constituents (PP, compatibilizer, silanized HGMs, and PCM) were mixed in different relative contents for 5 minutes using a Thermo Haake Rheomix 600 internal mixer with counter-rotating rotors (shown in Figure 5-1a) at 30 rpm and 200 °C. The prepared mixtures were placed in steel plates and hot pressed at 200 °C for 5 minutes at a pressure of 550 kPa with a hot plate Carver laboratory press (shown in Figure 5-1b). Different steel plates with specific dimensions were used to prepare specimens for different tests (see Figure 5-2).

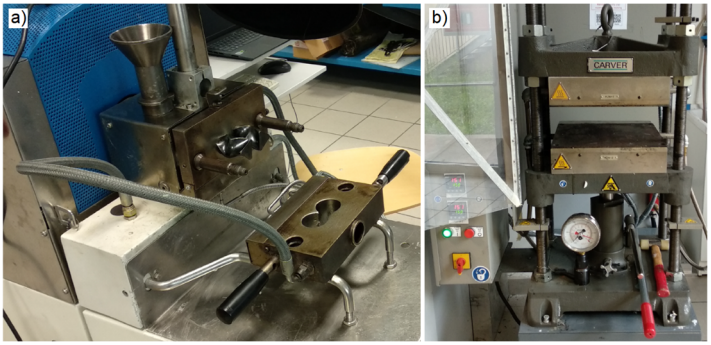

Figure 5-1 Processing equipments for themoplastics. (a) Thermo Haake Rheomix 600 internal mixer, and (b) Hot plate Carver laboratory press.

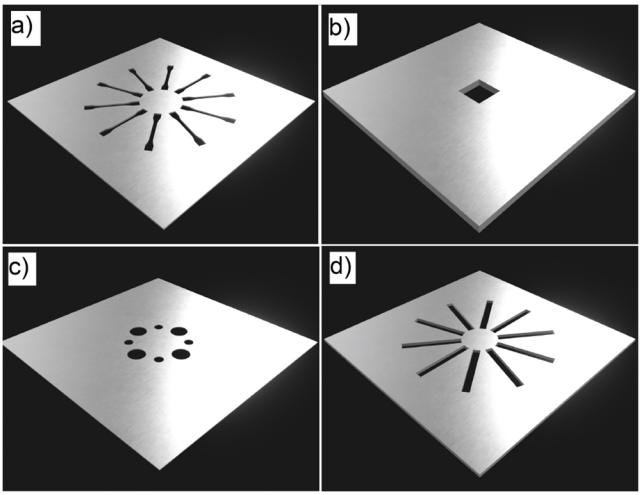

Figure 5-2 Representative images of steel molds used for the preparation of different specimens. (a) 1BA sample mold, used for producing ten quasi-static tensile test specimens, (b) single hole plate, used for producing quasi-static compressive test specimens, (c) mold used to produce specimens for both rheometry and light flash analysis,(d) mold used to produce ten specimens for K_{IC} determination under impact conditions.

To characterize this new ternary system (PP/HGM/PCM), ten compositions were analyzed as represented in Table 5-2 and Figure 5-3. In Figure 5-3, PP is the matrix, composed of 95 vol% of polypropylene and 5 vol% of compatibilizer. The optimal concentration of compatibilizer was selected through preliminary tests.

Table 5-2 List of the prepared samples with their desination and nominal composition.

#	*Sample*	*Compatibilizer vol%*	*PP vol%*	*HGM vol%*	*PCM vol%*
1	H0-P0	5.00	95.00	0.00	0.00
2	H0-P20	4.00	76.00	0.00	20.00
3	H0-P30	3.50	66.50	0.00	30.00
4	H20-P0	4.00	76.00	20.00	0.00
5	H40-P0	3.00	57.00	40.00	0.00
6	H7-P7	4.33	82.33	6.70	6.70
7	H13-P13	3.67	69.67	13.33	13.33
8	H7-P27	3.33	63.33	6.67	26.67
9	H27-P7	3.33	63.33	26.67	6.67
10	H20-P20	3.00	57.00	20.00	20.00

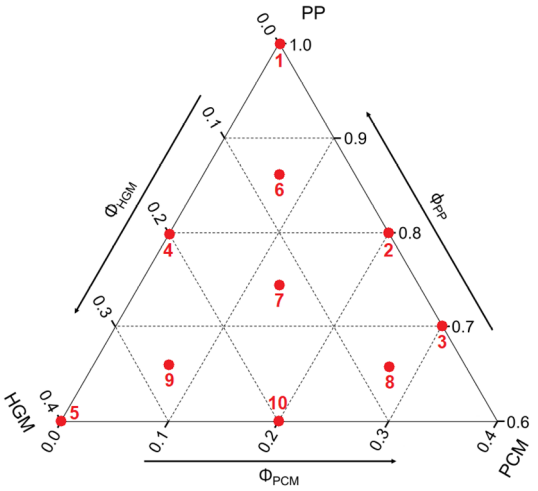

Figure 5-3 Graphical representation of the selected compositions (highlighted by the red dots) on the ternary diagram. The numbers (1–10) on each dot correspond to the sample numbers indicated in Table 5-2.

5.1.3 Experimental techniques

These compositions were studied through the characterization techniques listed in Table 5-3, together with the experimental parameters specifically applied (see Subchapter 3.2 for the full description of the characterization parameter and specimen preparation).

Table 5-3 Characterization techniques and experimental parameters applied to the preparedPP/HGM/PCMsyntactic foams.

Technique	*Specific experimental parameters*
Rheometry See section 3.2.1 on page 32	*Flow sweep* shear rate interval = 0.01-200 1/s, T = 200 °C *Frequency sweep* maximum shear strain 1% T = 200 °C frequency = 0.1-600 rad/s
Helium pycnometer See section 3.2.2.1 on page 34	T = 23 °C 1 cm^3 chamber 30 measurements

Light microscopy (LM) See section 3.2.2.2 on page 35	magnifications = 20X, 50X
SEM See section 3.2.2.3 on page 35	potential = 3.5 kV Pt-Pd coating
DSC See section 3.2.3.1 on page 36	T = -50/220 °C heating rate = 10 °C/min nitrogen flow = 100 ml/min *For C_p* T = -50/200 °C heating rate = 20 °C/min
LFA See section 3.2.3.2 on page 38	T = 25,45, and 70 °C
Evaluation of TES capability See section 3.2.3.3 on page 39	T = 35-80 °C
Quasi-static tensile test See section 3.2.4.1 on page 40	*For elastic modulus* gauge length = 25 mm crosshead speed = 0.25 mm/min *For properties at break* gauge length = 55 mm crosshead speed = 20 mm/min
Quasi-static compression test See section 3.2.4.2 on page 41	crosshead speed = 1.3 mm/min
K_{IC} See section 3.2.4.4 on page 43	starting angle = 39° potential energy = 0.6 J

5.2 Results and discussions

5.2.1 Rheological properties

A simple way to investigate the processability of thermoplastics is to measure their rheological properties. Two different tests were performed for this purpose: frequency sweep tests, to determine G' and G" trends as a function of angular frequency (ω), and flow sweep tests, to detect the dependence of viscosity (η) on applied shear rate ($\dot{\gamma}$). The frequency sweep analysis results for the prepared foams are shown in Figure 5-4 and Table 5-4. Figure 5-4 depicts the G' and G" trends of four representative compositions, H0-P0, H20-P20, H20-P0, and H0-P20, whereas Table 5-4 displays the crossover point coordinates of all analyzed samples.

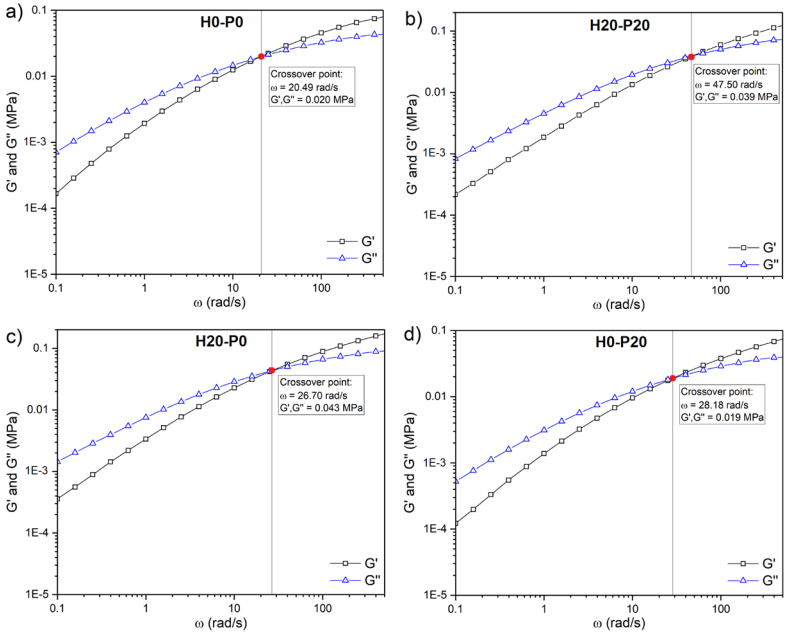

Figure 5-4 Results of frequency sweep tests on the prepared syntactic foams with the indication of the crossover point. (a) H0-P0, (b) H20-P20, (c) H20-P0, and (d) H0-P20 samples.

Table 5-4 Crossover point coordinates from frequency sweep analysis on the prepared PP-based syntactic foams.

Sample	*Crossover Point*	
	ω *rad/s*	*G', G" MPa*
H0-P0	20.5	0.020
H0-P20	28.2	0.019
H0-P30	35.0	0.024
H20-P0	26.7	0.043
H40-P0	21.6	0.098
H7-P7	36.0	0.027
H13-P13	34.4	0.034
H7-P27	39.2	0.023
H27-P7	42.7	0.031
H20-P20	47.5	0.039

Figure 5-4 shows that for all of the compositions under consideration, G" is greater than G' below the crossover frequency, indicating that viscous behavior dominates over the elastic one. At frequencies higher than the crossover point, G" < G' because the molten polymer macromolecules do not have enough time to relax the stress [180]. In the case of compositions containing only PCM, Table 5-4 shows that the presence of PCM capsules tends to shift the crossover point to higher frequencies in comparison to the PP matrix (H0-P0). In compositions containing only HGM, on the other hand, the crossover point is shifted to higher values of G' and G". As expected, the effect of the two fillers is combined when they are both present in the composites. For example, the frequency of the H20-P20 crossover point is 47.5 rad/s, which is higher than the crossover frequency of the H20-P0 (26.7 rad/s) and H0-P20 (28.2 rad/s) samples. Even when compared to mono-filler compositions with the same amount of filler, such as the H40-P0 sample (21.6 rad/s), the crossover frequency of H20-P20 (47.5 rad/s) is the highest. These trends are well illustrated in Figure 5-5, which depicts the crossover frequency ($\omega_{crossover}$) of the prepared foams in a ternary diagram.

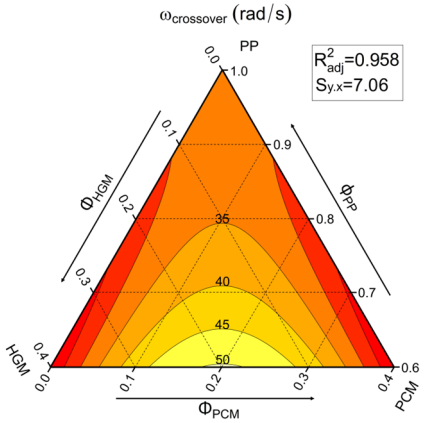

Figure 5-5 Ternary diagram representing the crossover frequency derived from rheological (frequency sweep) tests on the prepared PP-based foams.

Figure 5-6 shows the results of flow sweep rheological tests on seven representative compositions.

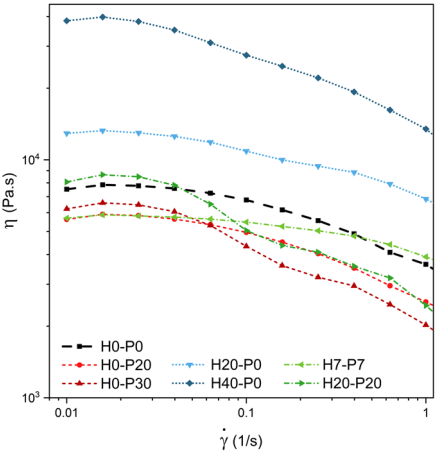

Figure 5-6 Viscosity (η) as a function of the shear rate ($\dot{\gamma}$) from flow sweep rheological tests on the prepared PP-based foams.

Figure 5-6 highlights the non-Newtonian behavior of the analyzed foams, which is typical of the rheological behavior of polymeric materials [169]. It can be seen that samples containing HGMs have higher viscosity values than the PP matrix proportionally to their concentration, whereas the presence of PCM capsules shifts the curves at lower viscosity levels. This could be due to the partial breakage of the PCM capsules during the manufacturing process, which implies extremely high shear stresses. Furthermore, during the mixing step, the PCM core is molten, allowing it to leak from the broken capsules and act as a lubricant. The two effects tend to balance out when both fillers are present [148].

5.2.2 Morphological properties

5.2.2.1 Density

One of the most attractive properties of syntactic foams is their tailorable density, combined with high specific strength, stiffness, and buoyancy. In this sense, the density (ρ) of the prepared syntactic foams was determined using a helium pycnometer. The numerical results are reported in Table 5-5, while the ternary diagrams shown in Figure 5-7(a,b) represent the trends of the density and of the void content.

Table 5-5 Experimental and theoretical density, and void content of the prepared PP-based foams.

Sample	ρ_{exp} g/cm^3	ρ_{th} g/cm^3	*Void content* %
H0-P0	0.90	0.90	0.0
H0-P20	0.83	0.90	8.1
H0-P30	0.86	0.91	5.0
H20-P0	0.81	0.81	0.0
H40-P0	0.70	0.72	1.8
H7-P7	0.80	0.87	7.4
H13-P13	0.77	0.84	9.1
H7-P27	0.83	0.89	5.8
H27-P7	0.74	0.78	5.0
H20-P20	0.73	0.82	10.2

The addition of HGMs to polypropylene results in a decrease in density, as expected. According to literature results [22,45,180], the density ranges from 0.90 g/cm^3 for the neat matrix to 0.70 g/cm^3 for the H40-P0 foam (-22%). Quite surprisingly, the PCM capsules also lead to a density decrease. The density of PCM capsules is 0.94 g/cm^3, which is higher than that of the matrix, therefore in principle, the density of the resulting composites should be increased. This behavior could be explained by the void development during the mixing stage generated by the partial evaporation of the PCM leaking from the broken capsules, acting as a sort of foaming agent, with a consequent density decrease. The worst situation can be observed in the H20-P20 foam (Figure 5-7b), where the porosity reaches 10.2%, due to the additional tribological effect provided by the HGMs introduction (like diamonds powder in diamond paste), as already found in Section 5.2.1, which increases the PCM capsule breakage.

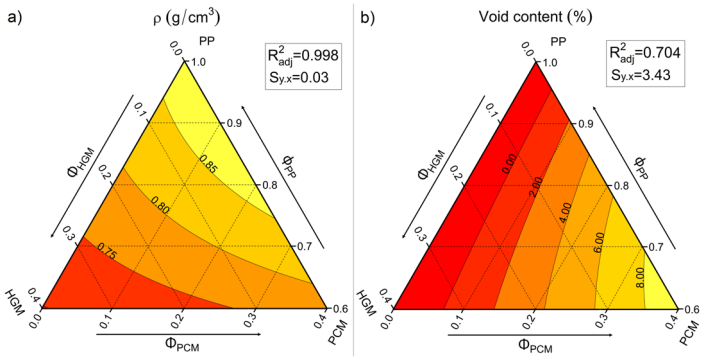

Figure 5-7 Ternary diagram of (a) the experimental density and (b) the void content of the prepared PP-based foams.

5.2.2.2 Light microscopy (LM)

The polished surface of some selected compositions was observed via optical microscopy to get qualitative information regarding the shape and distribution of the fillers within the PP matrix. Figure 5-8(a,b) represent the micrographs of the H0-P20 sample. In particular, Figure 5-8a shows the good dispersion of PCMs inside the matrix without aggregation, while in Figure 5-8b the shape and morphology of a single PCM microcapsule can be observed.

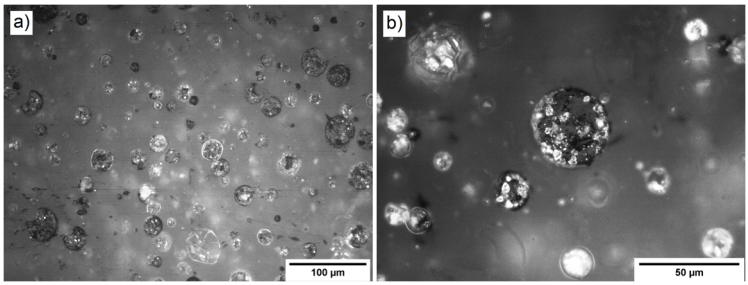

Figure 5-8 Light microscope images of the H0-P20 sample at (a) 20X and (b) 50X magnification.

Figure 5-9(a,b) reports two images of the composition H20-P0 at two different magnification levels. Figure 5-9a shows the typical morphology of syntactic foams in agreement with the literature [26], while Figure 5-9b gives an image at the capsules at elevated magnification. Adjusting the depth of focus it was possible to obtain a visualization of the HGMs present just below the surface, exploiting the

transparency of the glass and of the polypropylene. The spherical hollow shape and the refractive nature of glass particularly stand out. Also in this case, a good dispersion of the filler seems to be achieved without any sign of agglomeration.

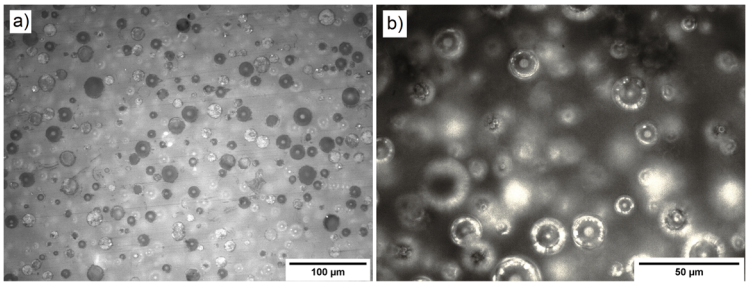

Figure 5-9 Light microscope images of the H20-P0 sample at (a) 20X and (b) 50X magnification.

Finally, Figure 5-10 shows the composition H20-P20 at 50X magnification. Also in this case, both fillers appear homogeneously distributed, meaning that the selected processing parameters were appropriate in terms of filler dispersion. In particular, PCM microcapsules can be easily distinguished from HGMs because of their white core.

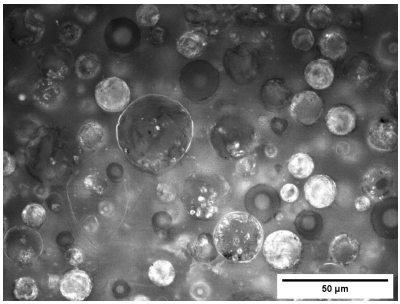

Figure 5-10 Light microscope image of the H20-P20 sample at 50X magnification.

5.2.2.3 Scanning electron microscopy (SEM)

To confirm the PCM capsule partial breakage during the compounding operations and to study the microstructure of the prepared foams, SEM analysis was conducted on the cryo-fractured surfaces of four selected compositions (H0-P0, H20-P20, H40-P0, and H0-P30), as shown in Figure 5-12(a-d)

Prior to that, the cryo-fractured surfaces of a composition (H20-P0, shown in Figure 5-11a) with untreated HGM and un-compatibilized PP were compared to those of a composition (H40-P0, shown in Figure 5-11b) with compatibilized matrix and silanized microspheres.

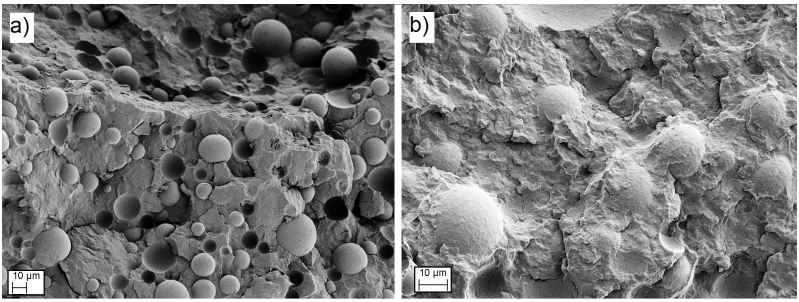

Figure 5-11 Comparison between SEM micrographs of (a) H20-P0 with untreated PP and HGM and (b) H40-P0 with treated HGM and PP.

Differently to what can be seen in Figure 5-11a, Figure 5-11b shows the good adhesion between HGMs and the surrounding matrix thanks to the silanization treatment and the use of compatibilizer. The difference in the interface is clearly visible between the two pictures. Figure 5-11a shows lots of HGMs capsules embedded in the matrix without adhesion with it, as noticeable from the gaps surrounding them. Some craters left from the detached HGMs, sign of bad adhesion, can also be noticed. This situation creates a material, from a mechanical point of view, more similar to a foam where the porosity is made by foaming, taking less advantage from the mechanical strength of HGMs. In addition, the voids produced by HGMs facilitate the crack propagation. On the other hands, Figure 5-11b highlights a completely different situation, where HGMs seem to be under the fracture surface and no gaps between capsules and matrix can be seen. This figure denotes two important aspects. First, the crack propagates through the matrix surrounding the capsules without connecting gaps, and second, HGMs possess enough strength to sustain the crack load without breaking. In practice, this foam acts as a bulk material without voids from a mechanical point of view, because of the good adhesion and strength of HGMs.

Concerning the foam produced with compatibilizer and with silanized HGMs, Figure 5-12a shows the typical fracture surface morphology of polypropylene, while the breakage of the PCM capsules can be clearly seen in Figure 5-12b, showing the H0-P30 foam.

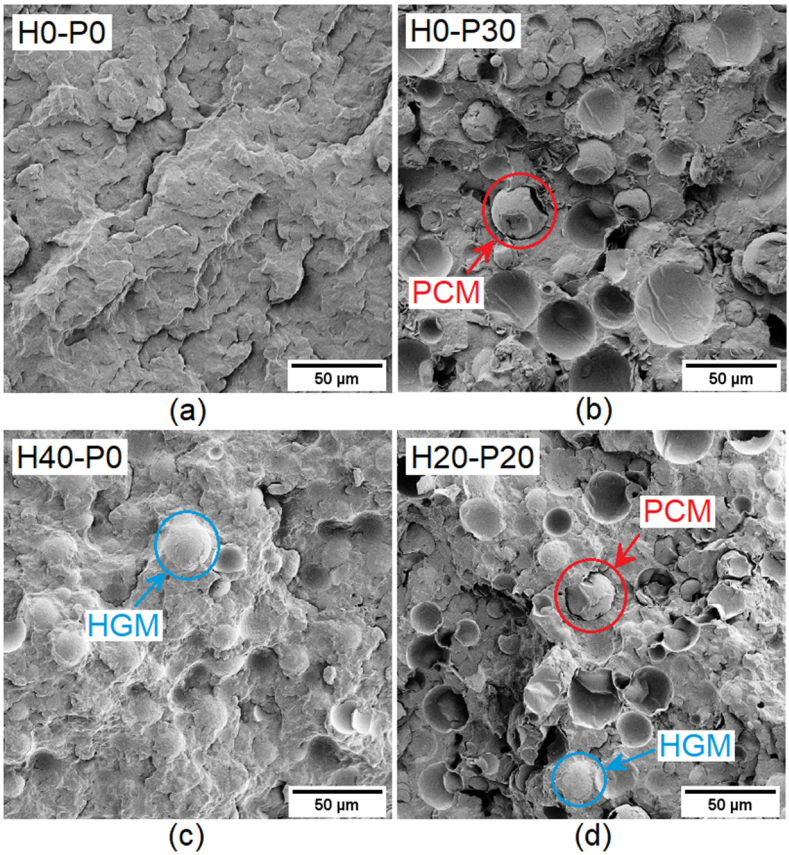

Figure 5-12 SEM micrographs of the cryo-fractured surfaces of four selected compositions. (a) H0-P0, (b) H0-P30, (c) H40-P0, and (d) H20-P20.

The majority of the capsules in Figure 5-12b results damaged or deformed, supporting the hypothesis of void generation caused by the molten PCM leakage (see Table 5-5). Even if they are partially broken, this does not imply that the PCM has completely left the composite. Indeed, this image demonstrates that the matrix can work as a second shell, preventing further PCM loss. DSC results will confirm this evidence. Furthermore, Figure 5-12b demonstrates a poor interfacial adhesion between the PCM capsules and the PP matrix, whereas Figure 5-12c demonstrates that the silanization of HGMs and the presence of a compatibilizer in the matrix result in a good PP/HGM interfacial adhesion. This finding may have a positive

impact on the elastic modulus and strength of the material, particularly under compression. Figure 5-12d displays the fracture surface of the composition containing both HGM and PCM capsules, and it is confirmed that the presence of HGM beads further increases the breakage tendency of PCM capsules, due to the higher shear stresses developed during the compounding stage. Moreover, this result agrees with the fact that this composition is also the most porous one, as demonstrated by density measurements.

5.2.3 Thermal properties

5.2.3.1 Differential scanning calorimetry (DSC)

Differential scanning calorimetry (DSC) is one of the simplest methods for measuring the TES capability of materials because it quantifies phase change temperatures (T_m and T_c), enthalpy of fusion and crystallization (ΔH_m and ΔH_c), and specific heat capacity (c_p).

Figure 5-13(a,b) shows the thermogram of the first DSC scan of five representative compositions and the ternary diagram representing the enthalpy of fusion evaluated in the first heating scan (ΔH_m), while Table 5-6 summarizes the results of the first heating and cooling DSC scan of all the compositions and the reduction in PCM content for cycle 2 and 5.

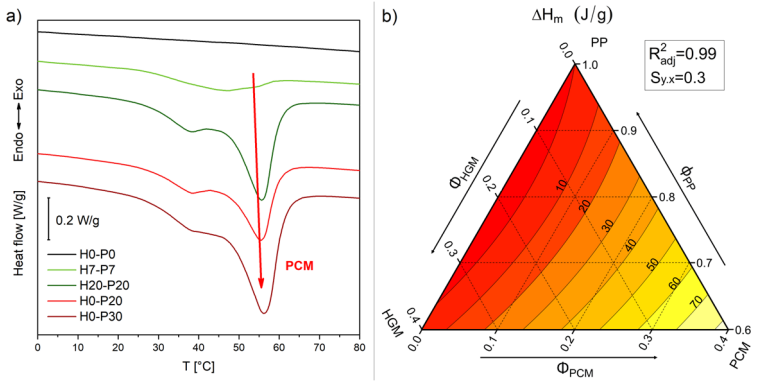

Figure 5-13 (a) DSC thermograms of five prepared PP-based foams (first heating scan), (b) ternary diagram of the measured ΔH_m values.

Table 5-6 DSC results of the first heating and cooling scans of the prepared PP-based foams. The final column shows the theoretical melting enthalpy ($\Delta H_{m,th}$), referred to the nominal PCM content in the foams.

Sample	T_m °C	ΔH_m J/g	T_c °C	ΔH_c J/g	$\Delta H_{m,th}$ J/g	*PCM loss after 2 cycles*	*PCM loss after 5 cycles*
H0-P0	-	0.0	-	0.0	0.0	-	-
H0-P20	55.6	36.5	37.2	36.5	43.1	-38.9%	-39.4%
H0-P30	55.7	58.4	37.3	58.2	64.3	-18.0%	-18.5%
H20-P0	-	0.0	-	0.0	0.0	-	-
H40-P0	-	0.0	-	0.0	0.0	-	-
H7-P7	46.9	8.2	35.1	8.2	14.9	-	-
H13-P13	54.6	22.4	36.6	22.3	30.8	-	-
H7-P27	55.3	53.0	37.6	51.5	59.1	-	-
H27-P7	54.6	11.4	36.4	11.3	16.6	-	-
H20-P20	55.2	43.9	37.5	43.4	47.7	-22.0%	-22.7%

Some compositions do not show phase transitions due to the absence of PCM capsules, as reported in Table 5-6. For all the compositions containing PCM, Figure 5-13a shows an increase in the heat stored as the volume fraction of PCM increases. This proportionality can also be clearly seen in the ternary diagram in Figure 5-13b. The presence of two melting peaks in Figure 5-13a is due to the presence of paraffin fractions with different molecular weight. Moreover, these results also demonstrate that the PP matrix acts as a second shell, because most of the samples possess enthalpy of fusion close to the theoretical one ($\Delta H_{m,th}$), evaluated considering the PCM content in the foams. For example, H0-P30 has a melting enthalpy of 58.4 J/g, close to the $\Delta H_{m,th}$ value of 64.3 J/g. In the sample characterized by the highest porosity degree (i.e., H20-P20) the enthalpy of fusion differs only by 8% from the theoretical one. The last two column of the table report the loss of PCM in percentage of three compositions. As can be noticed, the loss is significant due to the interconnection created by the molten PCM during the mixing stage, which allows higher amounts of it to evacuate the subsurface. On the other hand, after two cycles, the trend stabilized, reaching a plateau. The discrepancy between melting and crystallization temperatures is due to the thermal inertia of the system and the undercooling phenomena [183].

Specific heat measurement

Figure 5-14 reports the c_p measurements of the foam components, while Table 5-7 shows the c_p results at 20, 45, and 70 °C, and Figure 5-15 the c_p ternary diagram at 20 °C. The c_p of HGMs appears to be fairly constant in the temperature interval considered (Figure 5-14), while it increases slightly for H0-P0. The c_p of PCM

varies greatly over the temperature range chosen, reaching a maximum value around 60 °C. This increase in specific heat is related to the PCM phase transition. The melting transition is endothermic, and heat absorption increases the c_p at this temperature.

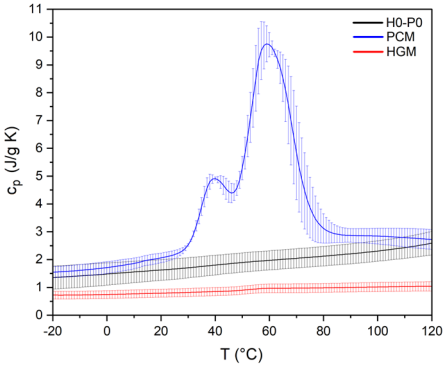

Figure 5-14 Specific heat capacity of the constituents as a function of the temperature from DSC analysis.

Table 5-7 Specific heat capacity of the prepared PP-based foams at 20, 45, and 70 °C from DSC tests.

Sample	***c_p** 20 °C J/(g·K)*	*c_p 45 °C J/(g·K)*	*c_p 70 °C J/(g·K)*
H0-P0	1.63±0.37	1.85±0.35	2.05±0.35
H0-P20	1.76±0.33	2.47±0.31	2.63±0.37
H0-P30	1.83±0.39	2.94±0.42	2.69±0.25
H20-P0	1.51±0.35	1.72±0.29	1.95±0.26
H40-P0	1.56±0.16	1.74±0.15	1.95±0.16
H7-P7	1.78±0.23	2.22±0.36	2.23±0.39
H13-P13	1.62±0.17	2.22±0.19	2.16±0.28
H7-P27	1.84±0.36	2.88±0.36	2.62±0.32
H27-P7	1.58±0.28	2.00±0.25	2.04±0.27
H20-P20	1.80±0.80	2.72±0.97	2.53±0.96

From Table 5-7, it can be noticed that compositions containing only HGMs do not show significant variations in the specific heat other than a slight reduction, while in compositions containing PCM this effect is much more evident. An increase of the amount of PCM produces an increase in the value of c_p proportional to the PCMs amount, as also evidenced by Figure 5-15 which shows the ternary diagram of c_p values at 20 °C.

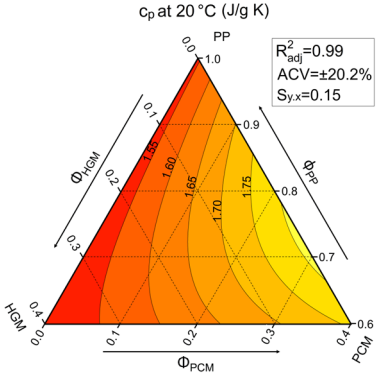

Figure 5-15 Ternary diagram of the specific heat capacity at 20 °C of the prepared PP-based foams.

As can be seen, HGMs do not play any role in changing the c_p of the materials, while PCMs increase it at any temperature.

5.2.3.2 Thermal conductivity

As reported in Equation (3-5), thermal conductivity is related to the density (ρ), to the thermal diffusivity (α), and to the specific heat capacity (c_p). This relationship was applied to the thermal diffusivity results from the Laser Flash Analysis (LFA) to determine the thermal conductivity of the analyzed samples. The tests were carried out at three different temperatures: 20, 45, and 70 °C, with the resulting thermal diffusivity values reported in Table 5-8, and the conductivity values shown in Table 5-9, in Figure 5-16 and in Figure 5-17(a-c).

Table 5-8 Thermal diffusivity (α) values at 20, 45, and 70 °C of the PP-based foams.

Sample	$\alpha_{20°C}$ *mm²/s*	$\alpha_{45°C}$ *mm²/s*	$\alpha_{70°C}$ *mm²/s*
H0-P0	0.181±0.013	0.166±0.012	0.148±0.011
H0-P20	0.148±0.021	0.114±0.021	0.124±0.016
H0-P30	0.116±0.008	0.082±0.006	0.098±0.008
H20-P0	0.161±0.026	0.148±0.024	0134±0.020
H40-P0	0.173±0.005	0.161±0.003	0.149±0.003
H7-P7	0.150±0.045	0.131±0.040	0.127±0.042
H13-P13	0.128±0.015	0.106±0.015	0.110±0.011
H7-P27	0.118±0.010	0.085±0.010	0.101±0.008
H27-P7	0.116±0.005	0.095±0.003	0.103±0.003
H20-P20	0.123±0.011	0.095±0.011	0.111±0.005

When all PCM-containing compositions (H0-P20 and H0-P30) are considered, the value of thermal diffusivity at 45 °C is lower than the values at 20 and 70 °C. The reason for this is due to the specific heat capacity dependence on temperature. Being that α is inversely proportional to c_p, the strong increase that occurs in this temperature interval translates in a decrease in thermal diffusivity. The same concept is valid also for the thermal diffusivity values at 20 and 70 °C, which are lower with respect to the non-containing PCM compositions. HGMs addition to the mixture produces a slight reduction in thermal diffusivity. This could be related to the expected reduction in thermal conductivity produced by this filler. However, composition H40-P0 shows values of α very similar to those of H0-P0. This can be explained once again by looking at the definition of thermal diffusivity. While thermal conductivity decreases with the addition of HGM, density and specific heat behave in the same way.

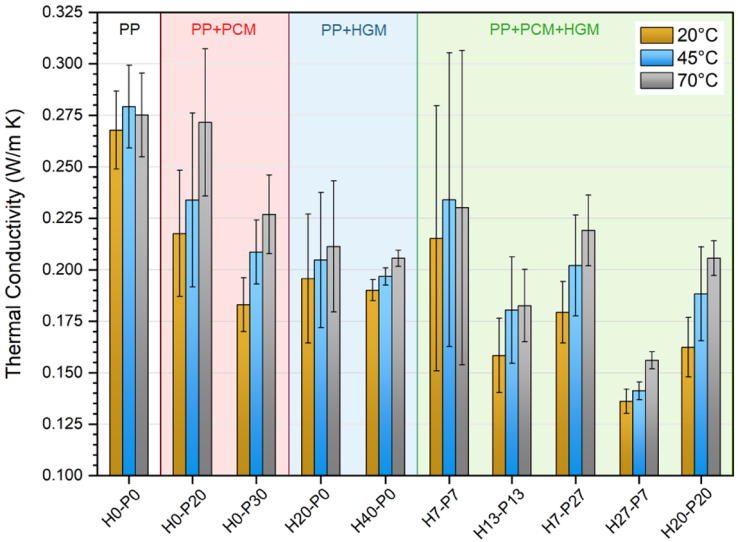

Figure 5-16 Thermal conductivity values of the prepared PP-based foams from LFA analysis.

Table 5-9 Values of thermal conductivity at 20, 45, and 70 °C of the PP-based foams

Sample	$\lambda_{20°C}$ *W/(m·K)*	$\lambda_{45°C}$ *W/(m·K)*	$\lambda_{70°C}$ *W/(m·K)*
H0-P0	0.268±0.019	0.279±0.020	0.275±0.020
H0-P20	0.218±0.031	0.234±0.042	0.272±0.036
H0-P30	0.183±0.013	0.209±0.016	0.227±0.019
H20-P0	0.196±0.031	0.205±0.033	0.211±0.032
H40-P0	0.190±0.005	0.197±0.004	0.206±0.004
H7-P7	0.215±0.064	0.234±0.071	0.230±0.076
H13-P13	0.158±0.018	0.180±0.026	0.183±0.018
H7-P27	0.179±0.015	0.202±0.024	0.219±0.017
H27-P7	0.136±0.006	0.141±0.004	0.156±0.004
H20-P20	0.162±0.014	0.188±0.023	0.206±0.008

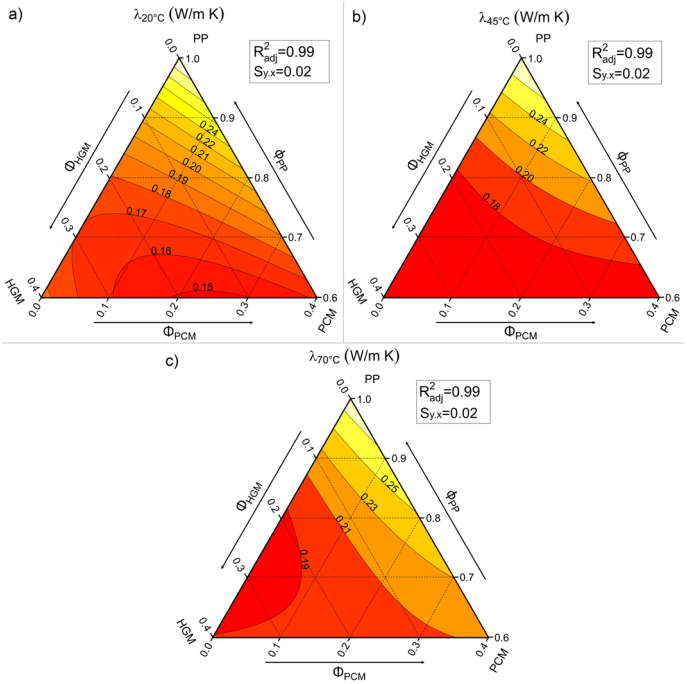

Figure 5-17 Ternary diagram of the thermal conductivity at (a) 20 °C, (b) 45 °C, and (c) 70 °C of the prepared PP-based foams.

The addition of HGMs to the polymeric matrix produces a significant reduction in thermal conductivity. This is in agreement with the results previously found in literature [45,184]. Differently from these works, in which the thermal conductivity was correlated only to the HGMs content, in this work the PCM concentration also plays an important role. In fact, the compositions that show the lowest values of thermal conductivity are those containing both HGM and PCM, i.e., H20-P20 and H27-P7 foams. For example, H40-P0, which contains only HGMs, shows a thermal conductivity at 20 °C of 0.190 W/m·K, which is 29% lower than that of the neat matrix. When half of the HGMs are replaced with PCMs, like in H20-P20 foam, the thermal conductivity drops down to 0.162 W/m·K (-15% than H40-P0, and -40% than the PP matrix). This behavior can be explained by the development of voids in the mixed compositions (containing both PCM and HGMs), that decrease the thermal conductivity and the density of the foams.

5.2.3.3 Evaluation of TES capability

Temperature profiling during heating and cooling stages is another method used in this study to investigate TES properties. The temperature of seven compositions was monitored using K-type thermocouples while they were heated from room temperature to 100 °C and then cooled from 100 °C to room temperature. In each step, the time required for the samples to reach 80 or 35 °C was recorded ($t_{35\text{-}80}$ and $t_{80\text{-}35}$). Figure 5-18(a,b) depict the temperature profiles obtained during the heating and cooling stages, while Table 5-10 Results of thermal profiling tests on the prepared PP-based foams. summarizes the results of these tests in terms of $t_{35\text{-}80}$ and $t_{80\text{-}35}$ values. Finally, Figure 5-19(a,b) show the same results in ternary diagrams.

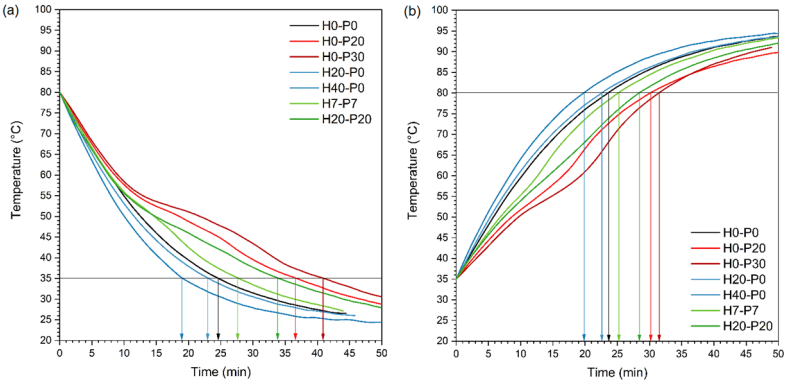

Figure 5-18 Temperature profiles of the prepared PP-based foams in (a) cooling and (b) heating stages.

Table 5-10 Results of thermal profiling tests on the prepared PP-based foams.

Sample	$t_{35\text{-}80}$ *min*	$t_{80\text{-}35}$ *min*
H0-P0	23.5	24.6
H0-P20	30.1	36.7
H0-P30	31.4	41.0
H20-P0	22.6	23.1
H40-P0	19.8	19.1
H7-P7	25.1	27.8
H13-P13	28.4	34.0
H7-P27	23.5	24.6
H27-P7	30.1	36.7
H20-P20	31.4	41.0

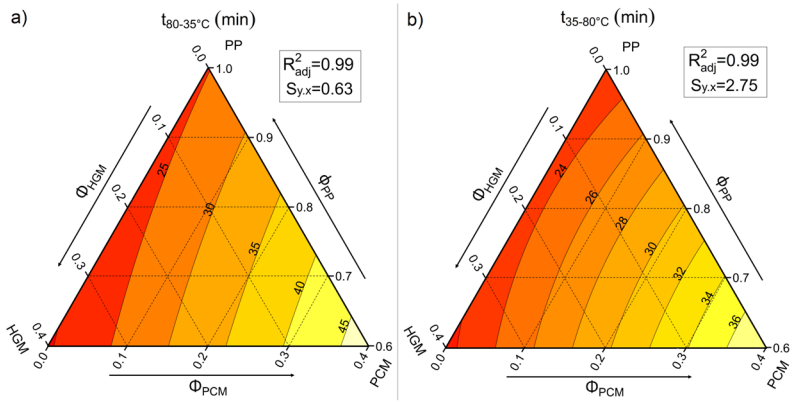

Figure 5-19 Ternary diagram of (a) $t_{35\text{-}80}$ and (b) $t_{80\text{-}35}$ °C values of the prepared PP-based foams.

As shown in Figure 5-18(a,b), the presence of PCM clearly influences the temperature profiles, with an inflection at the melting point of PCM. Moreover, Figure 5-19(a,b) report a direct proportionality between PCM content and transient time. This results in a longer time needed to reach the target temperature with respect to the PP matrix, as reported in Table 5-10. In this sense, PCM is capable of giving TES properties to the material since it can store and release heat during temperature transients. Another intriguing feature highlighted by Figure 5-18(a,b), Table 5-10, and Figure 5-19(a,b) is that the use of HGMs shortens the heating and cooling times. According to a 3M™ technical paper [164], syntactic foams exhibit

both reduced thermal conductivity and increased thermal diffusivity due to the presence of HGMs, which reduces the final density (see Equation (3-5). This reduces the transient time, a feature that can be useful in injection molding technology to increase productivity.

5.2.4 Mechanical properties

5.2.4.1 Quasi-static tensile tests

To evaluate the elastic modulus (E_t), stress and strain at yield (σ_y and ε_y), and stress and strain at break (σ_B and ε_B) of the prepared foams, quasi-static tensile tests were performed. The elastic modulus and stress at break values were also normalized by the density (E_t/ρ and σ_B/ρ). Figure 5-20 shows representative stress-strain curves of seven selected compositions, while Table 5-11 lists the most important tensile properties. Figure 5-21(a-d) shows ternary diagrams of the elastic modulus, stress at break, and their normalized values.

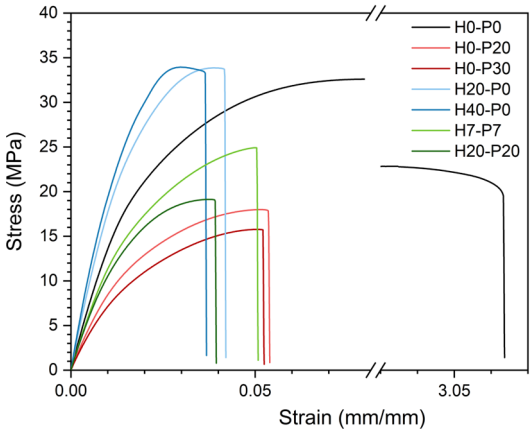

Figure 5-20 Representative tensile stress–strain curves for some representative compositions.

Figure 5-20 shows a significant decrease in the tensile strain at break for all compositions containing both fillers (PCM and/or HGMs) when compared to the neat matrix. The compositions that better perform in this sense, as reported in Table 5-11, are those incorporating only PCM capsules, where H0-P30 shows a strain at break "only" 80% lower than the PP matrix. Similarly, samples containing only HGMs exhibit the worst situation, with an 84% decrease in strain at break compared to the neat PP matrix.

Table 5-11 Tensile properties of all the prepared PP-based syntactic foams.

Sample	E_t *MPa*	E_t/ρ *MPa/(g/cm³)*	σ_B *MPa*	σ_B/ρ *MPa/(g/cm³)*	ε_B *%*
H0-P0	1509±19	1677±21	33.5±0.5	37.2±0.5	232.0±197.0
H0-P20	845±55	1018±66	17.4±0.8	21.0±1.0	4.8±0.4
H0-P30	758±15	881±17	15.5±0.4	18.0±0.5	4.8±0.3
H20-P0	1873±61	2312±75	31.8±1.3	39.3±1.6	4.2±0.7
H40-P0	2480±66	3543±94	33.8±0.8	48.3±1.1	3.7±0.6
H7-P7	1183±65	1479±81	23.6±2.3	29.5±2.9	4.4±1.0
H13-P13	1159±31	1505±39	20.9±0.5	27.1±0.7	4.1±0.2
H7-P27	751±15	905±18	14.6±0.8	17.6±1.0	3.8±0.3
H27-P7	1649±37	2228±50	24.5±0.9	33.1±1.2	3.0±0.3
H20-P20	1117±39	1530±53	17.9±0.8	24.5±1.1	3.5±0.3

Figure 5-20 also shows the benefits provided by HGMs in terms of elastic modulus, by increasing the stiffness from 1509 MPa of the PP matrix to 2480 MPa of the H30-P0 foam (+64%), due to the stiff nature of HGMs and to the good adhesion between HGMs and the matrix. On the other hand, because of the limited stiffness of the PCM capsules and their post-production integrity (see Figure 5-12b and d), PCMs reduce the elastic modulus from 1509 MPa down to 758 MPa of H0-P30 (−50%). Mixed compositions, on the other hand, show intermediate stiffness values, because HGMs counterbalance the decrease caused by PCMs introduction. These trends are better represented in the ternary diagram of Figure 5-21a, which also shows the proportionality of the elastic modulus when the PCMs are gradually substituted by an equivalent volumetric amount of HGMs (by moving horizontally from right to left in the graph). This trend is even more evident when the normalized elastic modulus, shown in Figure 5-21b, is considered.

As for the elastic modulus, the stress at break is also similarly influenced. While the presence of HGMs results in a significant σ_B retention, the presence of PCMs reduces σ_B from 33.5 MPa of the PP matrix to 15.5 MPa of the H0-P30 (-54%). Figure 5-21c shows that the stress at break is linearly related to the PCM content, whereas HGMs have no effect. When σ_B is normalized with density, as shown in Figure 5-21d, the resulting trend resembles that of the elastic modulus, leading to similar conclusions.

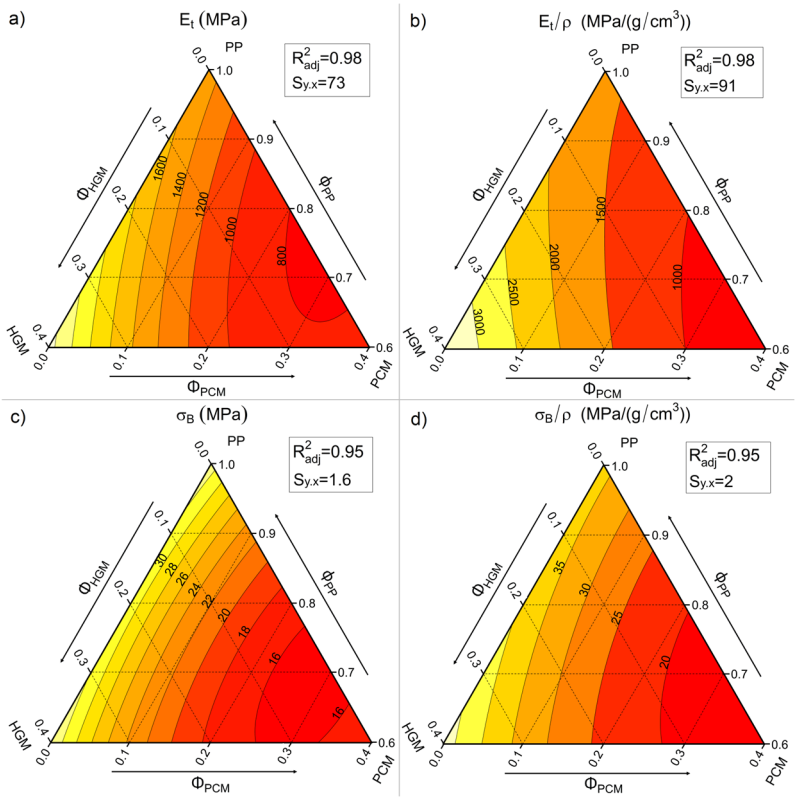

Figure 5-21 Ternary diagrams of the quasi-static tensile properties of the prepared PP-based syntactic foams. (a) Elastic modulus (E_t), (b) specific elastic modulus (E_t/ρ), (c) tensile stress at break (σ_B), and (d) specific stress at break (σ_B/ρ).

5.2.4.2 Quasi-static compression tests

The high compression strength of syntactic foams is an important feature that enables their widespread use in the marine environment [174,185–187]. Therefore, quasi-static compression tests were conducted on the prepared foams, to study the trends of the compressive elastic modulus (E_C), the specific elastic modulus (E_C/ρ), the stress at 20% of strain (σ_{20}), and the specific stress at 20% of strain (σ_{20}/ρ) with the amount of PCM and HGMs. Figure 5-22 depicts representative stress-strain curves obtained during compression tests for seven compositions, while Table 5-12 and Figure 5-23(a-d) report these results numerically and graphically.

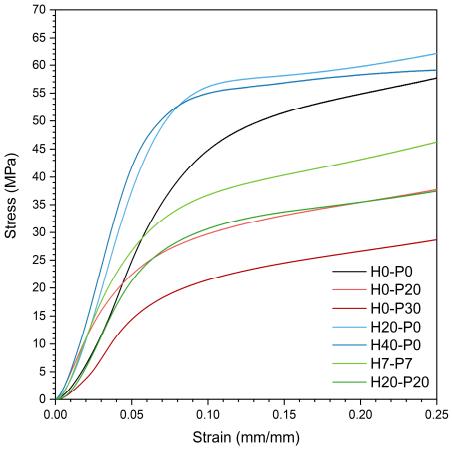

Figure 5-22 Representative compressive stress–strain curves for some selected representative compositions.

Table 5-12 Compressive properties of the prepared PP-based foams.

Sample	E_C *MPa*	E_C/ρ *MPa/(g/cm³)*	σ_{20} *MPa*	σ_{20}/ρ *MPa/(g/cm³)*
H0-P0	685±120	761±133	54.3±3.3	60.3±3.7
H0-P20	602±40	725±48	33.9±1.9	40.8±2.3
H0-P30	421±39	490±45	27.5±1.3	32.0±1.5
H20-P0	937±116	1157±143	58.4±3.0	72.1±3.7
H40-P0	1011±82	1444±117	56.7±3.6	81.0±5.1
H7-P7	714±43	893±54	45.3±2.5	56.6±3.1
H13-P13	617±65	801±84	39.8±1.9	51.7±2.5
H7-P27	543±55	654±66	31.2±1.4	37.6±1.7
H27-P7	793±83	1072±112	41.4±3.6	56.0±4.9
H20-P20	582±42	797±58	35.7±2.4	48.9±3.3

According to tensile test results, Figure 5-22 shows that the compressive performances improve with the addition of HGMs, while they decrease with the addition of PCM. The elastic modulus increases from 685 MPa in the neat PP matrix to 1011 MPa in the H40-P0 sample (+49%) and decreases to 421 MPa in the H0-P30 sample (-39%), as shown in Table 5-12. Furthermore, the stress–strain curves of the compositions containing both HGM and PCM (Figure 5-22) lie in the middle, with lower values of elastic modulus than the matrix (−15% for H20-P20).

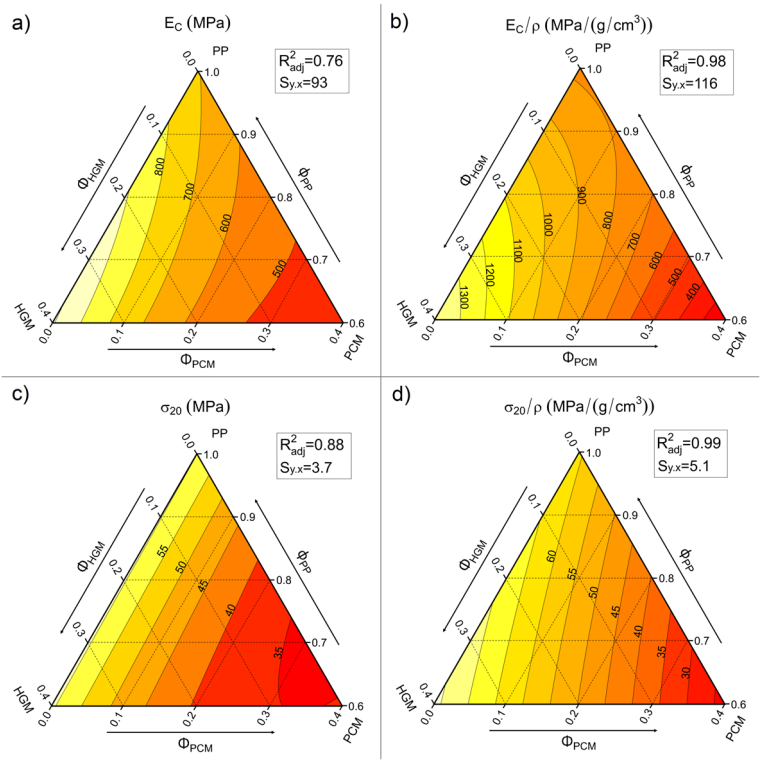

Figure 5-23 Ternary diagrams of the quasi-static compressive properties of the prepared PP-based syntactic foams. (a) Compressive modulus (E_C), (b) specific compressive modulus (E_C/ρ), (c) compressive stress at 20% (σ_{20}), and (d) specific compressive stress at 20% (σ_{20}/ρ).

Figure 5-23a better represents the trends of the compressive modulus, which are similar to those observed in tensile mode. As shown in tensile tests (Figure 5-21a), the elastic modulus is proportional to the degree of substitution of PCMs with HGMs (moving horizontally from right to left). This trend is even more pronounced in Figure 5-23b, which shows the specific compressive modulus. The increase in stiffness, as in tensile tests, can be attributed to the excellent adhesion between the HGM and the PP matrix due to the silanization process and the compatibilizing agent. Considering the results of stress at 20% of strain (σ_{20}), reported in Table 5-12, it is clear that the introduction of HGMs leads to a retention of the σ_{20} values, while the addition of PCMs decreases it. This trend is even better represented in Figure 5-23c. The σ_{20} decreases from 54.3 MPa of the matrix down to 27.5 MPa for

the H0-P30 foam (–49%), while it remains stable with the addition of HGMs. This trend becomes much more similar to that of the compressive elastic modulus when specific values (σ_{20}/ρ) are considered (Figure 5-23d).

In conclusion, these findings support the positive compressive properties of traditional syntactic foams (i.e., those containing only HGMs), whereas the addition of PCMs reduces compressive performance. A good adhesion between HGMs and the PP matrix is critical in increasing mechanical performances, especially when normalized properties are considered.

5.2.4.3 Evaluation of the fracture behavior under impact conditions

The stress intensity factor (K_{IC}) is a fundamental property in structural design, which describes the resistance of materials to crack propagation. Because of the ductility of PP, measuring this property under quasi-static conditions in accordance with the ASTM D5045 standard is extremely difficult. Therefore, these tests were carried out under impact conditions at a testing speed of 1.5 m/s, as recommended by ISO 13586 standard. Table 5-13 contains the results of these tests, and Figure 5-24 depicts the ternary diagram with the K_{IC} values.

It is clearly shown that PCM content has the greatest influence on K_{IC} values. In fact, HGM incorporation has no significant effect on the fracture toughness of the foams, whereas PCM incorporation reduces K_{IC} from 2.12 $MPa \cdot m^{0.5}$ of the PP matrix to 1.24 $MPa \cdot m^{0.5}$ of the H0-P30 sample (41%). The correlation between K_{IC} and PCM content is even more pronounced in compositions containing HGMs. This behavior can be attributed to the poor mechanical properties of PCM and to the poor adhesion to the PP matrix. HGMs, on the other hand, can retain the pristine fracture toughness of the PP, also reducing the overall weight of the material.

Table 5-13 Critical stress intensity factor K_{IC} results of the prepared PP-based foams

Sample	K_{IC} $MPa \cdot \sqrt{m}$
H0-P0	2.12±0.07
H0-P20	1.51±0.06
H0-P30	1.24±0.06
H20-P0	1.96±0.06
H40-P0	2.06±0.14
H7-P7	1.88±0.14
H13-P13	1.61±0.09
H7-P27	1.25±0.05
H27-P7	1.65±0.10
H20-P20	1.38±0.07

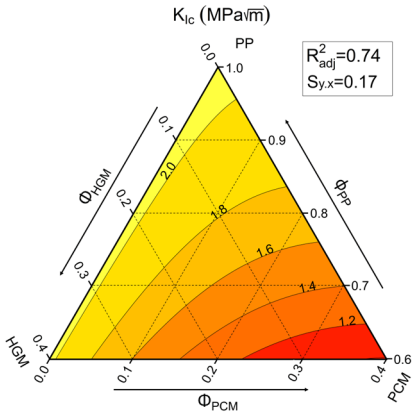

Figure 5-24 Ternary diagram of the critical stress intensity factor (K_{IC}) under impact conditions of the prepared PP-based foams.

5.2.5 General comparison of the properties of PP/HGM/PCM syntactic foams

To perform a general comparison between the most important properties of the prepared foams, Figure 5-25 reports in a single radar plot a direct comparison of the performances of the six most representative compositions. This comparative analysis has been conducted in terms of specific tensile modulus (E_t/ρ), specific tensile stress at break (σ_B/ρ), specific compressive elastic modulus (E_C/ρ), specific compressive stress at 20% of strain (σ_{20}/ρ), stress intensity factor (K_{IC}), specific volume (v, that is $1/\rho$), melting enthalpy (ΔH_m), and thermal resistance at 45 °C (R_λ).

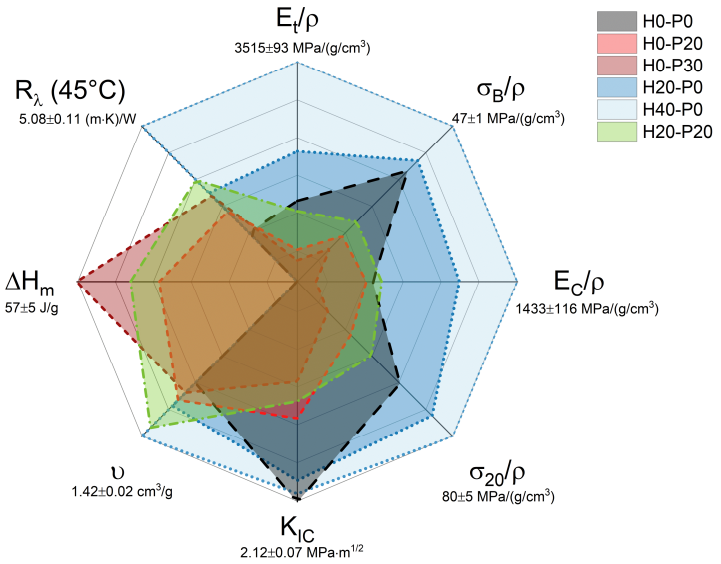

Figure 5-25 Radar diagram showing a graphical comparison of the most important properties of the prepared PP-based foams.

The color code in Figure 5-25 allows to distinguish between three types of composites: samples containing only HGMs (blue area), samples containing only PCMs (red area), and samples containing both (green area), as well as the neat matrix (black area). This graph demonstrates the clear dominance of compositions containing only HGMs in mechanical properties, lightness, and thermal resistivity (blue area). On the other hand, as expected, they lack TES capability. On the contrary, compositions containing only PCMs (red area) exhibit the best TES properties, but the same cannot be said for mechanical properties. Mixed compositions containing both fillers provide a good compromise (green area). The presence of HGMs improves the mechanical properties of these samples, while TES properties remain interesting for many applications, making these compositions very appealing for their multi-functionality.

In conclusion, if mechanical performance is the primary goal and TES properties are not required, H40-P0 may be the best choice because it exhibits interesting mechanical performances, particularly when component weight is a factor to be considered. If the primary goal is TES properties and the material is not subjected to severe mechanical stresses, H0-P30 may be the best choice. Combining the two fillers allows for the creation of very different types of composites that can meet a

variety of needs, resulting in versatile materials, with properties that can be tuned for specific applications.

5.3 Conclusions

In this study, HGMs and PCMs were incorporated at different relative ratios into a compatibilized polypropylene matrix to create novel multifunctional syntactic foams with thermal energy storage capability.

Rheological tests revealed that HGMs increased the viscosity of the molten material at 200 °C, while PCM decreased it slightly due to the capsule breakage during the manufacturing process. SEM micrographs confirmed the partial breakage of the PCM microcapsules and revealed good adhesion between the matrix and HGMs due to the silanization process performed on the surface of the glass beads and the presence of the compatibilizer.

As expected, the density of these syntactic foams was diminished by addition of HGMs, but also the introduction of PCMs led to a density drop, probably because of the increased porosity generated by the partial evaporation of the PCM that leaked out from the broken capsules.

The ability of PCMs to impart TES properties to the foams was confirmed by DSC and temperature profiling analyses, with the H0-P30 sample storing 57 J/g in the first DSC heating scan. The thermal conductivity of the foams was reduced by both HGMs and PCMs, from 0.268 W/(m·K) of the PP matrix to 0.190 W/(m·K) of the H40-P0 sample (30%) and 0.183 W/(m·K) of the H0-P30 foam (33%). Thermal conductivity was reduced further in compositions containing both fillers, reaching 0.136 W/(m·K) in the H27-P7 sample (50%), due to the voids generated by PCM introduction. HGMs introduction, on the other hand, increases thermal diffusivity, making it easier to heat and cool the material.

From a mechanical point of view, the compositions containing only HGMs proved to be the best choice. Quasi-static tensile tests revealed that the addition of HGMs increased mechanical performances (particularly the elastic modulus), whereas PCMs decreased them. A similar trend was observed in compression, where the addition of HGMs increased the elastic modulus and compressive strength significantly. HGM had no effect on K_{IC}, while PCM capsules affected the fracture toughness, due to their low strength and limited interfacial addition with the PP matrix.

As a result, the incorporation of PCMs into these PP syntactic foams resulted in a material with a set of properties that could be finely tuned, depending on the final purpose, by simply adjusting the filler amount. This feature opens up new

possibilities for these systems in applications where TES properties are critical, such as electronics, automotive, refrigeration, and aerospace. In the future, by modifying the manufacturing process, the failure of PCMs could be significantly reduced, improving the final performances of these materials.

Chapter 6 - General conclusions

This work aimed to develop novel polymeric syntactic foams for thermal energy storage (TES) applications and to characterize their properties as a function of their compositions. The goal was to create materials with both elevated mechanical properties, required for structural/semi-structural applications, and heat storage/management capabilities. Because there is little literature on this topic, the experimental work considered and compared two polymer/PCM/reinforcement systems to highlight their respective advantages and disadvantages.

Chapter 4 reported the results of the characterization of the epoxy-based syntactic foams incorporating PCM capsules. Because of their larger mean diameter, HGMs proved to be more suitable for incorporation into epoxy resin than PCM capsules. However, the PCM capsules resulted undamaged by the stirring process, as highlighted by SEM and DSC analysis. HGMs sensibly reduced the overall density of the system as predicted by the mixture law and also reduced the thermal conductivity of the system. At temperatures above the T_g of the epoxy, only HGMs gave strength to the material, while at room temperature both fillers limited the mechanical properties, with PCM capsules that greatly influenced the performance and HGMs to a lesser extent. When the mechanical properties were normalized, the beneficial effect of HGMs was evident. As expected, the compositions containing PCM capsules showed the best TES and impact properties at the expenses of the other properties. The combination of HGM and PCM capsules produced the most versatile compositions capable of satisfying the most diverse needs.

Chapter 5 illustrated the results of the thermo-mechanical characterization of PP-based syntactic foams incorporating PCM capsules. Due to the severity of the compounding process lots of capsules were damaged, causing partial paraffin leakage with consequent voids generation into the matrix, as shown by pycnometric analysis. On the other hand, HGMs survived the production steps as reported by SEM micrography, which also highlighted the good level of adhesion achieved between the matrix and HGMs. Although some of the PCM capsules were broken, most of them were still surrounded by the matrix that acted as a second shell. In fact, DSC showed how the compositions containing PCM capsules were in any case capable of storing a significant amount of heat, not too far from the theoretical one. HGMs improved all the mechanical properties, especially if normalized values are considered. On the contrary, PCM capsules sensibly reduced them. By combining HGMs and PCM capsules it was possible to retain the mechanical properties while adding TES capabilities.

To perform a general comparison between the most important properties of these two systems, five radar plots, similar to those shown in Figure 4-17 and Figure 5-25, were produced. Each plot compares the general performance of similar compositions of the two systems. Figure 6-1 shows the comparison between the two matrices used in this Thesis, Figure 6-2 reports the results of the compositions containing 20 vol% of PCM capsules, Figure 6-3 and Figure 6-4 report the results of the compositions containing respectively 20 and 40 vol% of HGMs. Finally, Figure 6-5 shows the comparison between the compositions of the two systems containing 20 vol% of HGMs and PCM capsules. This comparative analysis has been conducted in terms of specific tensile modulus (E_t/ρ), specific tensile stress at break (σ_B/ρ), specific compressive elastic modulus (E_C/ρ), specific volume (ν, that is $1/\rho$), melting enthalpy (ΔH_m), and thermal resistance at 30 °C (R_λ).

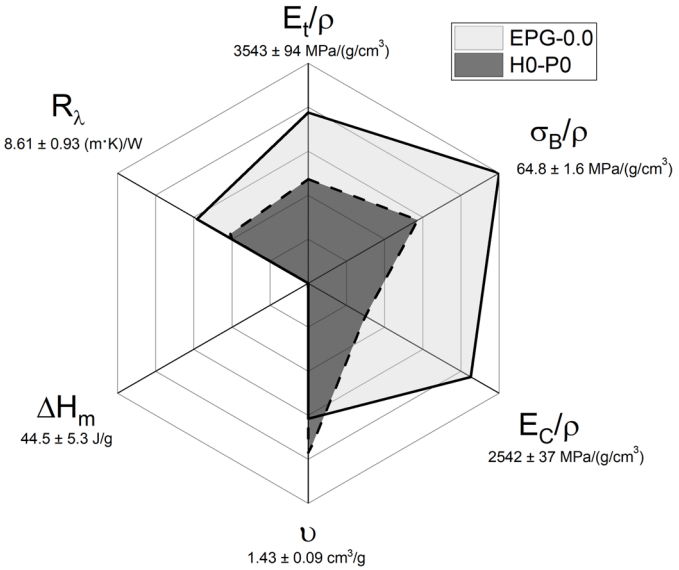

Figure 6-1 Radar diagram showing a graphical comparison of the physical properties of the polymer matrices of the two considered systems (epoxy and PP).

Figure 6-1 clearly shows the difference between the two matrices used, where epoxy resin possesses higher stiffness in both tensile and compression tests, and polypropylene (with compatibilizer) shows higher impact properties and specific volume.

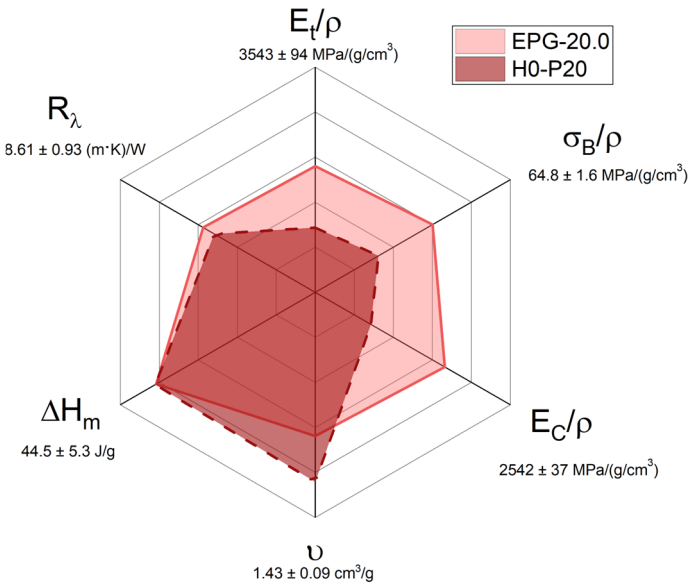

Figure 6-2 Radar diagram showing a graphical comparison of the properties of the compositions of the two systems containing 20 vol% of PCM (EPG-20.0 and H0-P20).

The properties of compositions containing 20% PCM are shown in Figure 6-2. The matrix, as expected, played an important role in these types of composites. Indeed, the stronger epoxy resin can withstand higher stresses in tensile and compression tests. Furthermore, the mechanical properties of the PP-based syntactic foams were reduced due to the breakage of the PCM capsules. Because both systems contained the same amount of PCM capsules, the heat stored in both systems was the same, as expected. In general, these systems should be considered in all those applications where TES properties are required. For example, the epoxy system can be used in aeronautical composite materials to manage temperature fluctuations or in electronics to limit the maximum temperature, increasing the performance and lifetime span of components. On the other hand, the PP systems with PCM also find different applications, like in thermoregulating buildings, car components (battery applications), food packaging, smart textiles, and pharmaceutical packaging. All these applications will increase their performance and durability with the incorporation of PCM technology. These features will not only improve the component's performance, but will also make it more efficient and, as a result, more environmentally friendly. Unfortunately, in this work, not all went smoothly.

A better compounding step with a low PCM capsule braking rate should be used to improve the mechanical performance of the PP-based system. While epoxy-based composites have better mechanical properties and, due to their castability, they showed a reduced number of defects. Although technically viable, there is insufficient data and preferred approaches addressing the recyclability of such materials. This would offer us the chance to investigate this topic, which is still up for debate and needs to be defined in more detail in subsequent work.

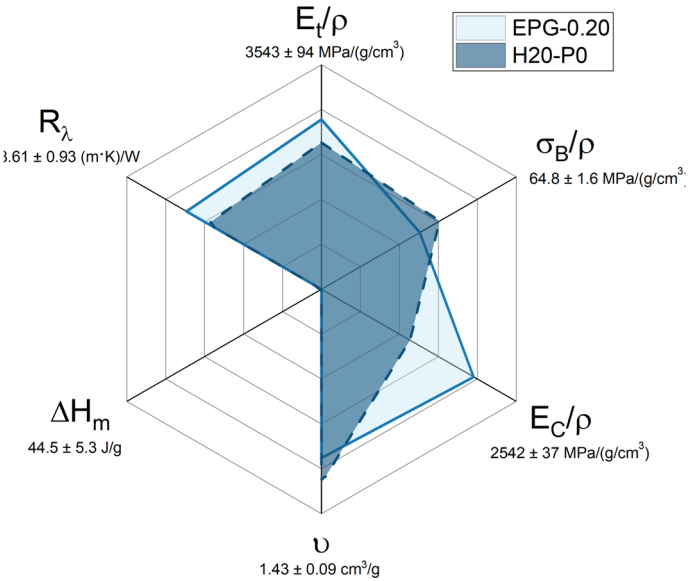

Figure 6-3 Radar diagram showing a graphical comparison of the properties of the compositions of the two systems containing 20 vol% of HGMs (EPG-0.20 and H20-P0).

Figure 6-3 depicts an equilibrate situation between the two systems in terms of thermal resistivity and tensile properties. Even though the HGMs incorporated in PP-based foams are stronger and have better adhesion than the other system, the epoxy-based foam performs better in compression. It should be noted that the two HGMs used differ in density (0.15 vs. 0.43 g/cm^3), implying that the epoxy system benefits from a greater decrease in density, which further increases the specific properties. Even though the two HGMs are different, the tough nature of PP clearly improves the fracture toughness of the composite over the less ductile epoxy matrix. Again, the reduction in specific volume is the result of a combination of different matrix and HGMs. In comparison to their respective matrices (Figure 4-17 and

Figure 5-25), the PP-based system is the one that benefits the most from HGM incorporation. The potentiality of syntactic foams is better expressed with higher amounts of HGMs, as shown in Figure 6-4.

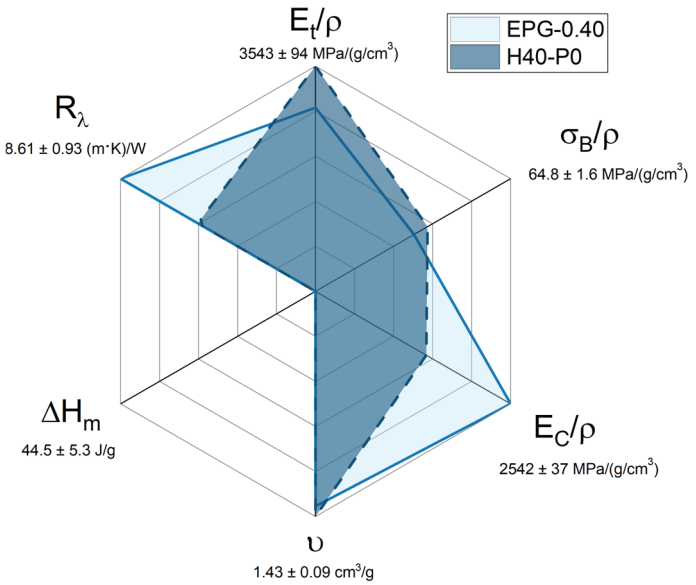

Figure 6-4 Radar diagram showing a graphical comparison of the properties of the compositions of the two systems containing 40 vol% of HGMs (EPG-0.40 and H40-P0).

Figure 6-4 depicts a comparison of two compositions containing only HGMs with a filler content of 40 vol%. With a few exceptions, the figure is very similar to Figure 6-3. The thermal resistivity is primarily affected by the HGMs type, while the specific volume appears to be balanced by the density difference between the two matrices. The higher adhesion between HGMs and the PP matrix, as well as the stronger nature of the HGMs used in this system, produced a composite material that sometimes outperforms the epoxy-based mechanical performances. The only property where the epoxy system outperforms a PP matrix is in compression testing, where the strong nature of epoxy produced a stiffer composite. As previously stated, PP-based composites benefit more from HGM incorporation than their epoxy counterparts. This is because of the stronger HGMs used in this system, as well as

the high level of adhesion achieved. Epoxy systems could benefit more from HGM incorporation with different HGMs and better surface treatments.

Epoxy-based syntactic foams, as already indicated, have numerous uses in marine applications as a result of their buoyancy and chemical characteristics, but they also have uses in other industries. These composites can be employed, for instance, in aeronautics to lighten the composite or in particular situations that call for a low thermal dilatation coefficient, such as the mirror of telescopes or scientific equipment in general. The usage of PP-based syntactic foams in injection-molded components, such as those for the automotive industry where they are utilized in parts with high dimensional stability and low weight, is already widespread. They could also be used for food containers to limit the thermal conductivity and increase the life-span of food, or in all injection-molded components to increase dimensional stability, reduce weight, and reduce shrinkage with a faster cycling time thanks to the reduced thermal inertia of the system. The outcomes of all these advancements also take environmental considerations into account. The efficiency of the overall system is improved by lightening components mounted on moving machinery, which lowers fuel consumption and greenhouse gas emissions. Another benefit to the environment is that the component is produced with less energy because of the shorter injection mold cycle time. The recycling of these systems seems more feasible than that of those containing PCMs. In an epoxy-based system, the glass bubbles can be recycled and some of the polymeric material recovered by pyrolyzing the component, whereas PP systems should be simple to reshape. The grinding stage, where HGMs may be fractured, is the primary problem with recycling PP-based foams.

By combining both fillers, also their properties will be combined as reported in Figure 6-5 where the properties of epoxy and PP-based systems containing both PCM and HGMs are compared.

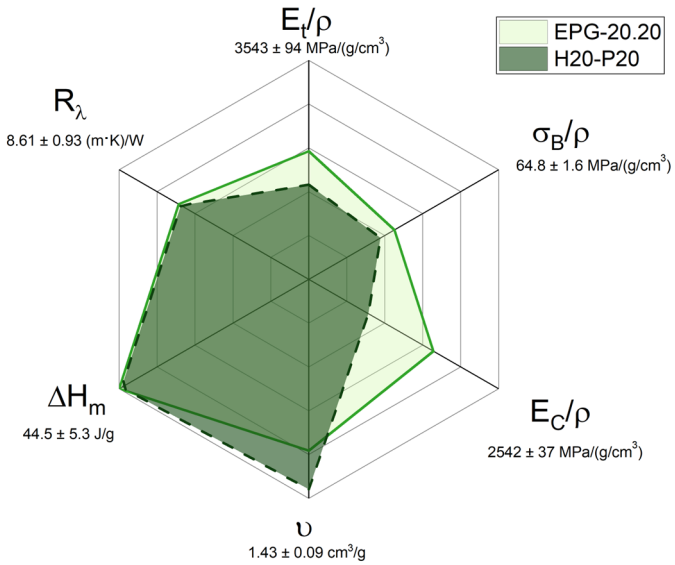

Figure 6-5 Radar diagram showing a graphical comparison of the properties of the compositions of the two systems containing 20 vol% of HGMs and PCM (EPG-20.20 and H20-P20).

As it can be seen in Figure 6-5, the shape of the two areas resulted similar to that of Figure 6-2, where PCM capsules showed a significant influence on the performance of the composites. The epoxy-based system revealed better tensile and compression properties, due to the stronger matrix utilized. PP-based composite, on the other hand, had higher fracture toughness due to the ductile nature of PP. Both systems, as expected, exhibited comparable TES capability. The decrease in mechanical performances for epoxy systems was even more pronounced when compared to its matrix (Figure 4-17). From Figure 6-2 it can be concluded that PP-based syntactic foams can be mechanically improved by limiting PCM rupture during the manufacturing step. On the other hand, increasing the adhesion between HGMs and the epoxy resin can improve their mechanical properties.

Concerning their possible applications, they could find several different uses thanks to their interesting combination of properties. For instance, in applications where heat management and lightness are required, like in the batteries of electric vehicles (EVs) or in aeronautics, but also in the marine field to build lighter, stronger, and more insulated ships. These kinds of materials, which enable lighter containers with lesser heat dispersion, could potentially be advantageous to the food packaging

business for food preservation. For similar reasons, pharmaceutical packaging may also consider using this type of materials.

In all matrixes, the combination of these two fillers creates materials with balanced qualities that strike a compromise between them. As a result, the materials do not excel in just one area but rather respond to a variety of demands. These will have a positive impact on the environment thanks to their improved efficiency and decreased mass, which can consequently cut their lifetime emissions of greenhouse gases. The end of life will encounter the same opportunities and problems as those systems already mentioned.

At the end of this thesis, some recommendations for future research in this area should be made.

Epoxy/PCM/HGMs systems

- Epoxy-based syntactic foams consider the use of very light and brittle HGMs to produce the foams. Incorporating low-density HGMs result in lighter composites, but in some cases, the reduction in mechanical performance may be an overly harsh compromise, limiting the possible fields of application. Stronger HGMs (such as those used in the PP system) should be used to improve the mechanical properties and the multifunctionality of this system. A silanization process could also be considered to improve adhesion to the matrix.
- By using stronger and denser HGMs it is possible to limit also another problem encountered during the casting process, where the light HGMs were more concentrated near the surface.
- A possible future research topic could be focused on incorporating PCM capsules with different melting temperature, to enlarge the melting peak and satisfy different needs in terms of TES capability.

PP/PCM/HGMs systems

- This system used very strong HGMs that easily survived the melt compounding stage. They also show very good adhesion with the matrix thanks to the silanization process and the presence of the compatibilizer. On the other hand, PCM capsules hardly survived the severe compounding stage. inducing a partial drop in mechanical performances. The combination of the two fillers partially restored the mechanical properties. An important topic that should be studied is the development of less severe manufacturing processes to avoid, or at least limit, PCM capsule breakage. By solving this problem, this material could become very attractive for designers thanks to the peculiar combination of thermal and mechanical properties.

In conclusion, the incorporation of PCMs and HGMs into these syntactic foams resulted in materials with a set of properties that could be properly tuned, depending on the final purpose, by simply adjusting the filler amount. This feature opens up new opportunities for these systems in applications requiring TES properties together with low weight, thermal conductivity, and thermal expansion. The recyclability of these materials could be technically feasible, but the economic aspects often limit their further development. For this reason, when a clear market interest in this class of material is expressed, further studies must be conducted to properly explore their recyclability. On the other hand, since they could produce less polluting and more effective products, manufacturers of cars, airplanes, and ships ought to think about the possibility of using these novel materials in their products.

Bibliography

1. Salleh, Z.; Islam, M.M.; Ku, H. Study on Compressive Properties of Syntactic Foams for Marine Applications. *J. Multifunct. Compos.* **2014**, *2*, 21–27, doi:10.12783/issn.2168-4286/2.1/salleh.

2. Rubel, R.I.; Yusuf, S.S. A review on syntactic foams processing, preparation and applications Controlled release fertilizer View project Smart Hybrid Grid Simulation View project. In Proceedings of the ICMERE2019; **2019**.

3. Afolabi, L.O.; Ariff, Z.M.; Hashim, S.F.S.; Alomayri, T.; Mahzan, S.; Kamarudin, K.A.; Muhammad, I.D. Syntactic foams formulations, production techniques, and industry applications: A review. *J. Mater. Res. Technol.* **2020**, *9*, 10698–10718, doi:10.1016/j.jmrt.2020.07.074.

4. Galvagnini, F.; Fredi, G.; Dorigato, A.; Fambri, L.; Pegoretti, A. Mechanical Behaviour of Multifunctional Epoxy/Hollow Glass Microspheres/Paraffin Microcapsules Syntactic Foams for Thermal Management. *Polymers (Basel).* **2021**, *13*, 2896, doi:10.3390/polym13172896.

5. Nguyen, Q.B.; Nai, M.L.S.; Nguyen, A.S.; Seetharaman, S.; Leong, E.W.W.; Gupta, M. Synthesis and properties of light weight magnesium–cenosphere composite. *Mater. Sci. Technol.* **2016**, *32*, 923–929, doi:10.1080/02670836.2015.1104017.

6. Szlancsik, A.; Katona, B.; Károly, D.; Orbulov, I.N. Notch (in)sensitivity of aluminum matrix syntactic foams. *Materials (Basel).* **2019**, *12*, 56–59, doi:10.3390/ma12040574.

7. Imran, M.; Rahaman, A.; Pal, S. Thermo-Mechanical and Mechanical properties of Epoxy/CNT Composite modified by Hollow Glass Microspheres. In Proceedings of the Materials Today: Proceedings; **2019**; Vol. 22, pp. 2469–2474. doi.org/10.1016/j.matpr.2020.03.374

8. Porfiri, M.; Gupta, N. Effect of volume fraction and wall thickness on the elastic properties of hollow particle filled composites. *Compos. Part B Eng.* **2009**, *40*, 166–173, doi:10.1016/j.compositesb.2008.09.002.

9. Paul, D.; Velmurugan, R. Analysis of the specific properties of glass microballoon-epoxy syntactic foams under tensile and flexural loads. In Proceedings of the Materials Today: Proceedings; **2018**; Vol. 5, pp. 16956–16962.

10. Gupta, N.; Woldesenbet, E. Microballoon wall thickness effects on properties of syntactic foams. *J. Cell. Plast.* **2004**, *40*, 461–480,

doi:10.1177/0021955X04048421.

11. Tagliavia, G.; Porfiri, M.; Gupta, N. Influence of moisture absorption on flexural properties of syntactic foams. *Compos. Part B Eng.* **2012**, *43*, 115–123, doi:10.1016/j.compositesb.2011.06.016.

12. Yousaf, Z.; Smith, M.; Potluri, P.; Parnell, W. Compression properties of polymeric syntactic foam composites under cyclic loading. *Compos. Part B Eng.* **2020**, *186*, doi:10.1016/j.compositesb.2020.107764.

13. Engineered syntactic systems Available online: https://esyntactic.com/products-solutions/syntactic-buoyancy-materials/. Last access April 1, **2023**

14. Im, H.; Roh, S.C.; Kim, C.K. Fabrication of Novel Polyurethane Elastomer Composites Containing Hollow Glass Microspheres and Their Underwater Applications. *Ind. Eng. Chem. Res.* **2011**, *50*, 7305–7312, doi:10.1021/ie102600q.

15. Lammers, M.O.; Brainard, R.E.; Au, W.W.L.; Mooney, T.A.; Wong, K.B. An ecological acoustic recorder (EAR) for long-term monitoring of biological and anthropogenic sounds on coral reefs and other marine habitats. *J. Acoust. Soc. Am.* **2008**, *123*, 1720–1728, doi:10.1121/1.2836780.

16. Gupta, N.; Zeltmann, S.E.; Shunmugasamy, V.C.; Pinisetty, D. Applications of polymer matrix syntactic foams. *Jom* **2014**, *66*, 245–254, doi:10.1007/s11837-013-0796-8.

17. Boeing Boeing Patent Donation to the University of Pennsylvania Could Help Treat Bone Disease and Injuries Available online: https://boeing.mediaroom.com/2001-10-15-Boeing-Patent-Donation-to-the-University-of-Pennsylvania-Could-Help-Treat-Bone-Disease-and-Injuries#:~:text=Boeing's Converted Freighters%3A 20 More Years of Life&text=Material used in the antenna,to the University.

18. Pont, D.; Tegeler, A.F.; Fallon, O.; Tracy, L. Loaded syntactic foam-core material (US, patent N. 5665787) **1997**.

19. Hohe, J.; Hardenacke, V.; Fascio, V.; Girard, Y.; Baumeister, J.; Stöbener, K.; Weise, J.; Lehmhus, D.; Pattofatto, S.; Zeng, H.; et al. Numerical and experimental design of graded cellular sandwich cores for multi-functional aerospace applications. *Mater. Des.* **2012**, *39*, 20–32, doi:10.1016/j.matdes.2012.01.043.

20. Mae, H.; Omiya, M.; Kishimoto, K. Effects of strain rate and density on tensile behavior of polypropylene syntactic foam with polymer

microballoons. *Mater. Sci. Eng. A* **2008**, *477*, 168–178, doi:10.1016/j.msea.2007.05.028.

21. Yang, X.; Xia, Y.; Zhou, Q. Influence of stress softening on energy-absorption capability of polymeric foams. *Mater. Des.* **2011**, *32*, 1167–1176, doi:10.1016/j.matdes.2010.10.024.

22. Ozkutlu, M.; Dilek, C.; Bayram, G. Effects of hollow glass microsphere density and surface modification on the mechanical and thermal properties of poly(methyl methacrylate) syntactic foams. *Compos. Struct.* **2018**, *202*, 545–550, doi:10.1016/j.compstruct.2018.02.088.

23. Kumar, B.R.B.; Zeltmann, S.; Doddamani, M.; Gupta, N.; Uzma; Gurupadu, S.; Rrn, S. Effect of cenosphere surface treatment and blending method on the tensile properties of thermoplastic matrix syntactic foams. *J. Appl. Polym. Sci.* **2016**, *133*, doi:10.1002/app.43881.

24. Taherishargh, M.; Belova, I. V; Murch, G.; Fiedler, T. On the effect of infiltration pressure on structural and mechanical properties of EP/A356 Al syntactic foam. In Proceedings of the 3rd Biennial Conference of Australian Combined Material Societies; **2014**.

25. Bharath Kumar, B.R.; Doddamani, M.; Zeltmann, S.E.; Gupta, N.; Uzma; Gurupadu, S.; Sailaja, R.R.N. Effect of particle surface treatment and blending method on flexural properties of injection-molded cenosphere/HDPE syntactic foams. *J. Mater. Sci.* **2016**, *51*, 3793–3805, doi:10.1007/s10853-015-9697-2.

26. Amos, S.E.; Yalcin, B. Hollow Glass Microspheres for Plastics, Elastomers, and Adhesives Compounds; William Andrew, **2015**; ISBN 9781455774432.

27. Carlisle, K.B.; Chawla, K.K.; Gladysz, G.M.; Koopman, M. Structure and mechanical properties of micro and macro balloons: An overview of test techniques. *J. Mater. Sci.* **2006**, *41*, 3961–3972, doi:10.1007/s10853-006-7571-y.

28. Dillinger, B.; Clark, D.; Suchicital, C.; Wicks, G. Crush strength analysis of hollow glass microspheres, **2018**, Vol. 38. 220-225, doi.org/10.1002/9781119474678.ch2

29. Jayavardhan, M.L.; Bharath Kumar, B.R.; Doddamani, M.; Singh, A.K.; Zeltmann, S.E.; Gupta, N. Development of glass microballoon/HDPE syntactic foams by compression molding. *Compos. Part B Eng.* **2017**, *130*, 119–131, doi:10.1016/j.compositesb.2017.07.037.

30. Koopman, M.; Gouadec, G.; Carlisle, K.; Chawla, K.K.; Gladysz, G.

Compression testing of hollow microspheres (microballoons) to obtain mechanical properties. *Scr. Mater.* **2004**, *50*, 593–596, doi:10.1016/j.scriptamat.2003.11.031.

31. Garza-Cruz, T. V.; Nakagawa, M. On a hybrid method to characterize the mechanical behavior of thin hollow glass microspheres. *Granul. Matter* **2012**, *14*, 309–318, doi:10.1007/s10035-012-0315-6.

32. Dhanumalayan, E.; Joshi, G. M.; Performance properties and applications of polytetrafluoroethylene (PTFE)—a review. *Adv. Compos. Hybrid Mater.* **2018**, *1*, 247–268, doi:10.1007/s42114-018-0023-8.

33. Yalcin, B.; Amos, S.E. Hollow Glass Microspheres in Thermoplastics. In *Hollow Glass Microspheres for Plastics, Elastomers, and Adhesives Compounds* ; Elsevier, **2015**; pp. 35–105 ISBN 9781455775507.

34. Liang, J.Z. Estimation of thermal conductivity for polypropylene/hollow glass bead composites. *Compos. Part B Eng.* **2014**, *56*, 431–434, doi:10.1016/j.compositesb.2013.08.072.

35. Liang, J.Z.; Li, F.H. Heat transfer in polymer composites filled with inorganic hollow micro-spheres: A theoretical model. *Polym. Test.* **2007**, *26*, 1025–1030, doi:10.1016/j.polymertesting.2007.07.002.

36. Agari, Y.; Ueda, A.; Tanaka, M.; Nagai, S. Thermal conductivity of a polymer filled with particles in the wide range from low to super-high volume content. *J. Appl. Polym. Sci.* **1990**, *40*, 929–941, doi.org/10.1002/app.1990.070400526.

37. Pal, R. On the Lewis-Nielsen model for thermal/electrical conductivity of composites. *Compos. Part A Appl. Sci. Manuf.* **2008**, *39*, 718–726, doi:10.1016/j.compositesa.2008.02.008.

38. Danish, A.; Mosaberpanah, M.A. Formation mechanism and applications of cenospheres: a review. *J. Mater. Sci.* **2020**, *55*, 4539–4557, doi:10.1007/s10853-019-04341-7.

39. Bertling, J.; Blömer, J.; Kümmel, R. Hollow Microsperes. *Chem. Eng. Technol.* **2004**, *27*, 829–837, doi.org/10.1002/ceat.200406138.

40. Swetha, C.; Kumar, R. Quasi-static uni-axial compression behaviour of hollow glass microspheres/epoxy based syntactic foams. *Mater. Des.* **2011**, *32*, 4152–4163, doi:10.1016/j.matdes.2011.04.058.

41. Yousaf, Z.; Morrison, N.F.; Parnell, W.J. Tensile properties of all-polymeric syntactic foam composites: Experimental characterization and mathematical modelling. *Compos. Part B Eng.* **2022**, *231*, 109556, doi.org/10.1016/j.compositesb.2021.109556.

42. Gupta, N.; Zeltmann, S.E.; Shunmugasamy, V.C.; Pinisetty, D. Applications of polymer matrix syntactic foams. *JOM* **2014**, *66*, 245–254, doi:10.1007/s11837-013-0796-8.

43. John, M.; Li, G. Self-healing of sandwich structures with a grid stiffened shape memory polymer syntactic foam core. *Smart Mater. Struct.* **2010**, *19*, 75013, doi:10.1088/0964-1726/19/7/075013.

44. Fredi, G.; Dorigato, A.; Fambri, L.; Unterberger, S.H.; Pegoretti, A. Effect of phase change microcapsules on the thermo-mechanical, fracture and heat storage properties of unidirectional carbon/epoxy laminates. *Polym. Test.* **2020**, *91*, 106747, doi:10.1016/j.polymertesting.2020.106747.

45. Galvagnini, F.; Dorigato, A.; Fambri, L.; Fredi, G.; Pegoretti, A. Thermophysical Properties of Multifunctional Syntactic Foams Containing Phase Change Microcapsules for Thermal Energy Storage. *Polymers (Basel).* **2021**, *13*, 20, doi:10.3390/polym13111790.

46. Huang, R.; Li, P. Elastic behaviour and failure mechanism in epoxy syntactic foams: The effect of glass microballoon volume fractions. *Compos. Part B Eng.* **2015**, *78*, 401–408, doi.org/10.1016/j.compositesb.2015.04.002.

47. Jin, F.L.; Li, X.; Park, S.J. Synthesis and application of epoxy resins: A review. *J. Ind. Eng. Chem.* **2015**, *29*, 1–11, doi:10.1016/j.jiec.2015.03.026.

48. Campbell, F.C. *Structural Composite Materials*. ASM Technical Books, ASM International, **2010**, doi:10.31399/asm.tb.scm.9781627083140.

49. Olabisi, O.; Adewale, K. *Handbook of Thermoplastics, Second Edition*; CRC Press,Taylor & Francis Group, 2015; ISBN 13: 978-1-4665-7722 & 10: 1466577223.

50. Jayavardhan, M.L.; Doddamani, M. Quasi-static compressive response of compression molded glass microballoon/HDPE syntactic foam. *Compos. Part B Eng.* **2018**, *149*, 165–177, doi:10.1016/j.compositesb.2018.04.039.

51. Doumbia, A.; Bourmaud, A.; Jouannet, D.; Falher, T.; Orange, F.; Retoux, R.; Pluart, L.; Laurent, C. Hollow microspheres – Poly-(Propylene) blends: relationship between microspheres degradation and composite properties. *Polym. Degrad. Stab.* **2015**, *114*, doi:10.1016/j.polymdegradstab.2014.12.024.

52. Awaja, F.; Pavel, D. Recycling of PET. *Eur. Polym. J.* **2005**, *41*, 1453–1477, doi:10.1016/j.eurpolymj.2005.02.005.

53. Xie, L.; Gao, M.; Zhao, S.; Ma, J.; Sun, Z.; Li, T. 118 - Trialkysiloxy-ethers as New External Donors in the Ziegler-Natta Catalyst. In *Science*

and Technology in Catalysis 2006; Eguchi, K., Machida, M., Yamanaka, I.B.T.-S. in S.S. and C., Eds.; Elsevier, **2007**; Vol. 172, pp. 517–518 ISBN 0167-2991.

54. Ariff, Z.; Ariffin, A.; Jikan, S.; Abdul Rahim, N. Rheological Behaviour of Polypropylene Through Extrusion and Capillary Rheometry. In *Polypropylene*; Intechopen, Croatia, **2012**; pp. 29–48.ISBN 978-953-51-0636-4

55. Busico, V.; Cipullo, R. Microstructure of polypropylene. *Prog. Polym. Sci.* **2001**, *26*, 443–533, doi:10.1016/S0079-6700(00)00046-0.

56. Wypych, G. *Handbook of Polymers*; 3rd ed.; ChemTec Publishing, **2022**; ISBN 9781927885956.

57. Thiyagarajan, R.; Senthil kumar, M. A Review on Closed Cell Metal Matrix Syntactic Foams: A Green Initiative towards Eco-Sustainability. *Mater. Manuf. Process.* **2021**, *36*, 1333–1351, doi:10.1080/10426914.2021.1928696.

58. Szlancsik, A.; Norbert Orbulov, I. Compressive properties of metal matrix syntactic foams in uni- and triaxial compression. *Mater. Sci. Eng. A* **2021**, *827*, 142081, doi.org/10.1016/j.msea.2021.142081.

59. Pan, L.; Yang, Y.; Ahsan, M.U.; Luong, D.D.; Gupta, N.; Kumar, A.; Rohatgi, P.K. Zn-matrix syntactic foams: Effect of heat treatment on microstructure and compressive properties. *Mater. Sci. Eng. A* **2018**, *731*, 413–422, doi.org/10.1016/j.msea.2018.06.072.

60. Fiedler, T.; Öchsner, A.; Belova, I.V.; Murch, G.E. Recent Advances in the Prediction of the Thermal Properties of Syntactic Metallic Hollow Sphere Structures. *Adv. Eng. Mater.* **2008**, *10*, 361–365, doi.org/10.1002/adem.200700335.

61. Vogiatzis, C.A.; Tsouknidas, A.; Kountouras, D.T.; Skolianos, S. Aluminum–ceramic cenospheres syntactic foams produced by powder metallurgy route. *Mater. Des.* **2015**, *85*, 444–454, doi.org/10.1016/j.matdes.2015.06.154.

62. Gupta, N.; Rohatgi, P.K. *Metal matrix syntactic foams: processing, microstructure, properties and applications*; DEStech Publications, Inc, **2014**; ISBN 978-1-932078-83-1

63. Lin, Y.; Zhang, Q.; Ma, X.; Wu, G. Mechanical behavior of pure Al and Al–Mg syntactic foam composites containing glass cenospheres. **2016**, *87*, 194–202.

64. Katona, B.; Szebényi, G.; Orbulov, I.N. Fatigue properties of ceramic

hollow sphere filled aluminium matrix syntactic foams. *Mater. Sci. Eng. A* **2017**, *679*, 350–357, doi.org/10.1016/j.msea.2016.10.061.

65. Zhang, Q.; Lin, Y.; Chi, H.; Chang, J.; Wu, G. Quasi-static and dynamic compression behavior of glass cenospheres/5A03 syntactic foam and its sandwich structure. *Compos. Struct.* **2018**, *183*, 499–509, doi.org/10.1016/j.compstruct.2017.05.024.

66. Sánchez de la Muela, A.M.; García Cambronero, L.E.; Malheiros, L.F.; Ruiz-Román, J.M. New Aluminum Syntactic Foam: Synthesis and Mechanical Characterization. *Materials (Basel).* **2022**, *15*, 5320 doi:10.3390/ma15155320.

67. Dave, H.; Samvatsar, K. A comprehensive review on aluminium syntactic foams obtained by dispersion fabrication methods. *Mater. Today Proc.* **2021**, *47*, 4243–4248, doi.org/10.1016/j.matpr.2021.04.501.

68. Kemény, A.; Katona, B.; Movahedi, N.; Fiedler, T. Fatigue tests of zinc aluminium matrix syntactic foams filled with expanded perlite. *IOP Conf. Ser. Mater. Sci. Eng.* **2020**, *903*, 12050, doi:10.1088/1757-899X/903/1/012050.

69. Castro, G.; Nutt, S.R. Synthesis of syntactic steel foam using gravity-fed infiltration. *Mater. Sci. Eng. A* **2012**, *553*, 89–95, doi.org/10.1016/j.msea.2012.05.097.

70. Peroni, L.; Scapin, M.; Fichera, C.; Lehmhus, D.; Weise, J.; Baumeister, J.; Avalle, M. Investigation of the mechanical behaviour of AISI 316L stainless steel syntactic foams at different strain-rates. *Compos. Part B Eng.* **2014**, *66*, 430–442, doi.org/10.1016/j.compositesb.2014.06.001.

71. Kincses, D.B.; Károly, D.; Bukor, C. Production and testing of syntactic metal foams with graded filler volume. *Mater. Today Proc.* **2021**, *45*, 4225–4228, doi.org/10.1016/j.matpr.2020.12.163.

72. Mei, Y.; Fu, C.; Fu, Y.; Ding, Y.; Wang, E.; Yang, Q. Tensile Behavior and Performance of Syntactic Steel Foams Prepared by Infiltration Casting. *Metals (Basel).* **2022**, *12*, doi:10.3390/met12040668.

73. Anbuchezhiyan, G.; Mohan, B.; Sathianarayanan, D.; Muthuramalingam, T. Synthesis and characterization of hollow glass microspheres reinforced magnesium alloy matrix syntactic foam. *J. Alloys Compd.* **2017**, *719*, 125–132, doi.org/10.1016/j.jallcom.2017.05.153.

74. Daoud, A.; Abou El-khair, M.T.; Abdel-Aziz, M.; Rohatgi, P. Fabrication, microstructure and compressive behavior of ZC63 Mg–microballoon foam composites. *Compos. Sci. Technol.* **2007**, *67*, 1842–1853,

doi.org/10.1016/j.compscitech.2006.10.023.

75. Kubelka, P.; Kádár, C.; Jost, N. Effect of the interface on the compressive properties of magnesium syntactic foams. *Mater. Lett.* **2021**, *287*, 129293, doi.org/10.1016/j.matlet.2020.129293.

76. Akinwekomi, A.D.; Tang, C.-Y.; Tsui, G.C.-P.; Law, W.-C.; Chen, L.; Yang, X.-S.; Hamdi, M. Synthesis and characterisation of floatable magnesium alloy syntactic foams with hybridised cell morphology. *Mater. Des.* **2018**, *160*, 591–600, doi.org/10.1016/j.matdes.2018.10.004.

77. Linul, E.; Lell, D.; Movahedi, N.; Codrean, C.; Fiedler, T. Compressive properties of zinc syntactic foams at elevated temperatures. *Compos. Part B Eng.* **2019**, *167*, 122–134, doi.org/10.1016/j.compositesb.2018.12.019.

78. Li, G.; Muthyala, V.D. A cement based syntactic foam. *Mater. Sci. Eng. A* **2008**, *478*, 77–86, doi.org/10.1016/j.msea.2007.05.084.

79. Pielichowska, K.; Pielichowski, K. Phase change materials for thermal energy storage. *Prog. Mater. Sci.* **2014**, *65*, 67–123, doi.org/10.1016/j.pmatsci.2014.03.005.

80. Dincer, I.; Ezan, M.A. *Heat Storage: A Unique Solution For Energy Systems*; Green Energy and Technology; Springer International Publishing, **2018**; ISBN 9783319918938.

81. Ibrahim, D.; Marc, A.R. *Thermal energy storage systems and applications*; Wiley Periodicals, Inc, **2020**; Vol. 21; ISBN 9789896540821.

82. S. Kalaiselvam; Parameshwaran, R. *Thermal Energy Storage Technologies for Sustainability*; Elsevier Inc., **2014**; ISBN 978-0-12-417291-3.

83. Cabeza, L.F. *Advances in Thermal Energy Storage Systems: Methods and Applications*; Woodhead Publishing Series in Energy; Elsevier Science, **2020**; ISBN 9780128198889.

84. Safari, A.; Saidur, R.; Sulaiman, F.A.; Xu, Y.; Dong, J. A review on supercooling of Phase Change Materials in thermal energy storage systems. *Renew. Sustain. Energy Rev.* **2017**, *70*, 905–919, doi.org/10.1016/j.rser.2016.11.272.

85. Jarimi, H.; Aydin, D.; Yanan, Z.; Ozankaya, G.; Chen, X.; Riffat, S. Review on the recent progress of thermochemical materials and processes for solar thermal energy storage and industrial waste heat recovery. *Int. J. Low-Carbon Technol.* **2019**, *14*, 44–69, doi:10.1093/ijlct/cty052.

86. Sharma, A.; Tyagi, V. V; Chen, C.R.; Buddhi, D. Review on thermal energy storage with phase change materials and applications. *Renew. Sustain. Energy Rev.* **2009**, *13*, 318–345, doi.org/10.1016/j.rser.2007.10.005.

87. Irfan Lone, M.; Jilte, R. A review on phase change materials for different applications. *Mater. Today Proc.* **2021**, *46*, 10980–10986, doi.org/10.1016/j.matpr.2021.02.050.

88. Venkateswarlu, K.; Ramakrishna, K. Recent advances in phase change materials for thermal energy storage-a review. *J. Brazilian Soc. Mech. Sci. Eng.* **2022**, *44*, 1–17, doi:10.1007/s40430-021-03308-7.

89. Chavan, S.; Rudrapati, R.; Manickam, S. A comprehensive review on current advances of thermal energy storage and its applications. *Alexandria Eng. J.* **2021**, *61*, 5455–5463, doi:10.1016/j.aej.2021.11.003.

90. He, B.; Setterwall, F. Technical grade paraffin waxes as phase change materials for cool thermal storage and cool storage systems capital cost estimation. *Energy Convers. Manag.* **2002**, *43*, 1709–1723, doi:10.1016/S0196-8904(01)00005-X.

91. Peng, G.; Dou, G.; Hu, Y.; Sun, Y.; Chen, Z. Phase Change Material (PCM) Microcapsules for Thermal Energy Storage. *Adv. Polym. Technol.* **2020**, *2020*, 9490873, doi:10.1155/2020/9490873.

92. Zhang, H.; Wang, X. Fabrication and performances of microencapsulated phase change materials based on n-octadecane core and resorcinol-modified melamine-formaldehyde shell. *Colloids Surfaces A Physicochem. Eng. Asp.* **2009**, *332*, 129–138, doi:10.1016/j.colsurfa.2008.09.013.

93. Pasarkar, N.P.; Yadav, M.; Mahanwar, P.A. A review on the micro-encapsulation of phase change materials: classification, study of synthesis technique and their applications. *J. Polym. Res.* **2023**, *30*, doi:10.1007/s10965-022-03380-0.

94. Zhai, X.; Wu, Z.; Peng, H. Minireview on Application of Microencapsulated Phase Change Materials with Reversible Chromic Function: Advances and Perspectives. *Energy & Fuels* **2022**, *36*, 8054–8065, doi:10.1021/acs.energyfuels.2c01389.

95. Gouin, S. Microencapsulation: industrial appraisal of existing technologies and trends. *Trends Food Sci. Technol.* **2004**, *15*, 330–347, doi.org/10.1016/j.tifs.2003.10.005.

96. Gharibzahedi, S.M.T.; George, S.; Greiner, R.; Estevinho, B.N.; Frutos

Fernández, M.J.; McClements, D.J.; Roohinejad, S. New Trends in the Microencapsulation of Functional Fatty Acid-Rich Oils Using Transglutaminase Catalyzed Crosslinking. *Compr. Rev. Food Sci. Food Saf.* **2018**, *17*, 274–289, doi:https://doi.org/10.1111/1541-4337.12324.

97. Han, P.; Qiu, X.; Lu, L.; Pan, L. Fabrication and characterization of a new enhanced hybrid shell microPCM for thermal energy storage. *Energy Convers. Manag.* **2016**, *126*, 673–685, doi:10.1016/j.enconman.2016.08.052.

98. Hassan, A.; Laghari, M.S.; Rashid, Y. Micro-encapsulated phase change materials: A review of encapsulation, safety and thermal characteristics. *Sustain.* **2016**, *8*, 32, 1046, doi:10.3390/su8101046.

99. Su, J.; Wang, L.; Ren, L. Fabrication and thermal properties of MicroPCMs: Used melamine-formaldehyde resin as shell material. *J. Appl. Polym. Sci.* **2006**, *101*, 1522–1528, doi:10.1002/app.23151.

100. Nelson, G. Application of microencapsulation in textiles. *Int. J. Pharm.* **2002**, *242*, 55–62, doi.org/10.1016/S0378-5173(02)00141-2.

101. M, C.; Velraj, R.; Renganarayanan, S. Performance analysis on refrigeration system integrated with encapsulated PCM based cool thermal energy storage system. *Int. J. Energy Res.* **2007**, *31*, 1398–1413, doi:10.1002/er.1313.

102. Cabeza, L.F.; Navarro, L.; Pisello, A.L.; Olivieri, L.; Bartolomé, C.; Sánchez, J.; Álvarez, S.; Ríos, J.A.T. Behaviour of a concrete wall containing micro-encapsulated PCM after a decade of its construction. *Sol. Energy* **2020**, *200*, 108–112, doi:10.1016/j.solener.2019.12.003.

103. Lai, C.; Chen, R.; Lin, C.-Y. Heat transfer and thermal storage behaviour of gypsum boards incorporating micro-encapsulated PCM. *Energy Build.* **2010**, *42*, 1259–1266, doi:10.1016/j.enbuild.2010.02.018.

104. Hoang, H.M.; Leducq, D.; Perez-Masia, R.; Lagaron, J.M.; Gogou, E.; Taoukis, P.; Alvarez, G. Heat transfer study of submicro-encapsulated PCM plate for food packaging application. *Int. J. Refrig.* **2014**, *52*, 151-160; doi:10.1016/j.ijrefrig.2014.07.002.

105. Shchukina, E.M.; Graham, M.; Zheng, Z.; Shchukin, D.G. Nanoencapsulation of phase change materials for advanced thermal energy storage systems. *Chem. Soc. Rev* **2018**, *47*, 4156-4175, doi:10.1039/c8cs00099a.

106. Ikutegbe, C.A.; Farid, M.M. Application of phase change material foam composites in the built environment: A critical review. *Renew. Sustain.*

Energy Rev. **2020**, *131*, 110008, doi:10.1016/j.rser.2020.110008.

107. Fredi, G.; Dirè, S.; Callone, E.; Ceccato, R.; Mondadori, F.; Pegoretti, A. Docosane-organosilicamicrocapsules for structural composites with thermal energy storage/release capability. *Materials (Basel).* **2019**, *12*, 1286; doi:10.3390/ma12081286.

108. Fredi, G.; Dorigato, A.; Fambri, L.; Pegoretti, A. Detailed experimental and theoretical investigation of the thermomechanical properties of epoxy composites containing paraffin microcapsules for thermal management. *Polym. Eng. Sci.* **2020**, *60*, 1202–1220, doi:10.1002/pen.25374.

109. Timilsena, Y.P.; Akanbi, T.O.; Khalid, N.; Adhikari, B.; Barrow, C.J. Complex coacervation: Principles, mechanisms and applications in microencapsulation. *Int. J. Biol. Macromol.* **2019**, *121*, 1276–1286, doi:10.1016/j.ijbiomac.2018.10.144.

110. Sánchez-Silva, L.; sánchez, P.; Lucas, A.; Carmona, M.; Rodríguez, J. Microencapsulation of PCMs with a polystyrene shell. *Colloid Polym. Sci.* **2007**, *285*, 1377–1385, doi:10.1007/s00396-007-1696-7.

111. Jonsson, M.; Nordin, O.; Malmström, E.; Hammer, C. Suspension polymerization of thermally expandable core/shell particles. *Polymer (Guildf).* **2006**, *47*, 3315–3324, doi:10.1016/j.polymer.2006.03.013.

112. Jensen, A.T.; Neto, W.S.; Ferreira, G.R.; Glenn, A.F.; Gambetta, R.; Gonçalves, S.B.; Valadares, L.F.; Machado, F. 8 - Synthesis of polymer/inorganic hybrids through heterophase polymerizations. In; Visakh, P.M., Markovic, G., Pasquini Micro and Nano Blends, D.B.T.-R.D. in Recent Developments on Polymer Macro, Micro and Nano Blends, P.M., Eds.; Woodhead Publishing, **2017**; pp. 207–235 ISBN 978-0-08-100408-1.

113. Chern, C.S. Emulsion polymerization mechanisms and kinetics. *Prog. Polym. Sci.* **2006**, *31*, 443–486, doi:10.1016/j.progpolymsci.2006.02.001.

114. Zhang, B.; Zhang, Z.; Kapar, S.; Ataeian, P.; da Silva Bernardes, J.; Berry, R.; Zhao, W.; Zhou, G.; Tam, K.C. Microencapsulation of Phase Change Materials with Polystyrene/Cellulose Nanocrystal Hybrid Shell via Pickering Emulsion Polymerization. *ACS Sustain. Chem. Eng.* **2019**, *7*, 17756–17767, doi:10.1021/acssuschemeng.9b04134.

115. Tikkanen, A. Emulsion Polymerization Available online: https://www.britannica.com/topic/industrial-polymer-chemistry-468716/Emulsion-polymerization. accessed on January 28th 2023

116. Cho, J.-S.; Kwon, A.; Cho, C. Microencapsulation of octadecane as a

phase-change material by interfacial polymerization in an emulsion system. *Colloid Polym. Sci.* **2002**, *280*, 260–266, doi:10.1007/s00396-001-0603-x.

117. Pasupathy, A.; Velraj, R.; Seeniraj, R. V Phase change material-based building architecture for thermal management in residential and commercial establishments. *Renew. Sustain. Energy Rev.* **2008**, *12*, 39–64, doi.org/10.1016/j.rser.2006.05.010.

118. Cui, Y.; Xie, J.; Liu, J.; Wang, J.; Chen, S. A review on phase change material application in building. *Adv. Mech. Eng.* **2017**, *9*, 1–15, doi:10.1177/1687814017700828.

119. Kuznik, F.; David, D.; Johannes, K.; Roux, J.J. A review on phase change materials integrated in building walls. *Renew. Sustain. Energy Rev.* **2011**, *15*, 379–391, doi:10.1016/j.rser.2010.08.019.

120. Fredi, G.; Simon, F.; Sychev, D.; Melnyk, I.; Janke, A.; Scheffler, C.; Zimmerer, C. Bioinspired polydopamine coating as an adhesion enhancer between paraffin microcapsules and an epoxy matrix. *ACS Omega* **2020**, *5*, 19639–19653, doi:10.1021/acsomega.0c02271.

121. Pasupathy, A.; Velraj, R. Effect of double layer phase change material in building roof for year round thermal management. *Energy Build.* **2008**, *40*, 193–203, doi.org/10.1016/j.enbuild.2007.02.016.

122. Feldman, D.; Banu, D.; Hawes, D.; Ghanbari, E. Obtaining an energy storing building material by direct incorporation of an organic phase change material in gypsum wallboard. *Sol. Energy Mater.* **1991**, *22*, 231–242, doi.org/10.1016/0165-1633(91)90021-C.

123. Kuznik, F.; Virgone, J.; Johannes, K. In-situ study of thermal comfort enhancement in a renovated building equipped with phase change material wallboard. *Renew. Energy* **2011**, *36*, 1458–1462, doi.org/10.1016/j.renene.2010.11.008.

124. Mofijur, M.; Mahlia, T.M.; Silitonga, A.S.; Ong, H.C.; Silakhori, M.; Hasan, M.H.; Putra, N.; Rahman, S.M.A. Phase Change Materials (PCM) for Solar Energy Usages and Storage: An Overview. *Energies* **2019**, *12,* 3167; doi:10.3390/en12163167.

125. Su, W.; Darkwa, J.; Kokogiannakis, G. Development of microencapsulated phase change material for solar thermal energy storage. *Appl. Therm. Eng.* **2017**, *112*, 1205–1212, doi.org/10.1016/j.applthermaleng.2016.11.009.

126. Rabin, Y.; Bar-Niv, I.; Korin, E.; Mikic, B. Integrated solar collector

storage system based on a salt-hydrate phase-change material. *Sol. Energy* **1995**, *55*, 435–444, doi.org/10.1016/0038-092X(95)00074-2.

127. Choo, Y.M.; Wei, W. Salt hydrates as phase change materials for photovoltaics thermal management. *Energy Sci. Eng.* **2022**, *10*, 1630–1642, doi:10.1002/ese3.1007.

128. Styś-Maniara, M.; Nartowska, E.; Metryka-Telka, M.; Porowski, R. Inorganic Salt Hydrates as Phase Change Materials (PCM) for Thermal Energy Storage in Solar Installations. *Struct. Environ.* **2022**, *14*, 161–172, doi:10.30540/sae-2022-018.

129. Shukla, A.; Buddhi, D.; Sawhney, R.L. Solar water heaters with phase change material thermal energy storage medium: A review. *Renew. Sustain. Energy Rev.* **2009**, *13*, 2119–2125, doi.org/10.1016/j.rser.2009.01.024.

130. Javadi, F.S.; Metselaar, H.S.C.; Ganesan, P. Performance improvement of solar thermal systems integrated with phase change materials (PCM), a review. *Sol. Energy* **2020**, *206*, 330–352, doi.org/10.1016/j.solener.2020.05.106.

131. Fazilati, M.A.; Alemrajabi, A.A. Phase change material for enhancing solar water heater, an experimental approach. *Energy Convers. Manag.* **2013**, *71*, 138–145, doi.org/10.1016/j.enconman.2013.03.034.

132. Mondal, S. Phase change materials for smart textiles – An overview. *Appl. Therm. Eng.* **2008**, *28*, 1536–1550, doi.org/10.1016/j.applthermaleng.2007.08.009.

133. Fok, S.C.; Shen, W.; Tan, F.L. Cooling of portable hand-held electronic devices using phase change materials in finned heat sinks. *Int. J. Therm. Sci.* **2010**, *49*, 109–117, doi.org/10.1016/j.ijthermalsci.2009.06.011.

134. Shao, J.; Darkwa, J.; Kokogiannakis, G. Review of phase change emulsions (PCMEs) and their applications in HVAC systems. *Energy Build.* **2015**, *94*, 200–217, doi.org/10.1016/j.enbuild.2015.03.003.

135. Tan, F.L.; Tso, C.P. Cooling of mobile electronic devices using phase change materials. *Appl. Therm. Eng.* **2004**, *24*, 159–169, doi.org/10.1016/j.applthermaleng.2003.09.005.

136. Wirtz, R.; Fuchs, A.; Narla, V.; Shen, Y.; Zhao, T.; Jiang, Y. A multi-functional graphite/epoxy-based thermal energy storage composite for temperature control of sensors and electronics. *41st Aerosp. Sci. Meet. Exhib.*, **2003**.

137. Mesalhy, O.; Lafdi, K.; Elgafy, A. Carbon foam matrices saturated with

PCM for thermal protection purposes. *Carbon N. Y.* **2006**, *44*, 2080–2088, doi:10.1016/j.carbon.2005.12.019.

138. Zhong, Y.; Guo, Q.; Li, S.; Shi, J.; Liu, L. Heat transfer enhancement of paraffin wax using graphite foam for thermal energy storage. *Sol. Energy Mater. Sol. Cells* **2010**, *94*, 1011–1014, doi.org/10.1016/j.solmat.2010.02.004.

139. Jana, P.; Fierro, V.; Pizzi, A.; Celzard, A. Thermal conductivity improvement of composite carbon foams based on tannin-based disordered carbon matrix and graphite fillers. *Mater. Des.* **2015**, *83*, 635–643, doi.org/10.1016/j.matdes.2015.06.057.

140. Friederich, K.; Breuer, U. *Multifunctionality of polymer composites*; 1st ed.; William Andrew, Norwich, NY, **2015**;

141. Chung, D.D.L. A review of multifunctional polymer-matrix structural composites. *Compos. Part B Eng.* **2019**, *160*, 644–660, doi.org/10.1016/j.compositesb.2018.12.117.

142. Forintos, N.; Czigany, T. Multifunctional application of carbon fiber reinforced polymer composites: Electrical properties of the reinforcing carbon fibers – A short review. *Compos. Part B Eng.* **2019**, *162*, 331–343, doi.org/10.1016/j.compositesb.2018.10.098.

143. Akbar, M.; Curiel-Sosa, J.L. Piezoelectric energy harvester composite under dynamic bending with implementation to aircraft wingbox structure. *Compos. Struct.* **2016**, *153*, 193–203, doi.org/10.1016/j.compstruct.2016.06.010.

144. Kim, H.; Gonzalez, M. Fatigue failure of printed circuit board chemically etched copper traces in multifunctional composite structures. *J. Compos. Mater.* **2014**, *48*, 985-996, doi:10.1177/0021998313480980.

145. Gogoi, R.; Manik, G. Development of thermally conductive and high-specific strength polypropylene composites for thermal management applications in automotive. *Polym. Compos.* **2021**, *42*, 1945–1960, doi:10.1002/pc.25947.

146. Huang, C.; Huang, Z.; Lv, X.; Zhang, G.; Wang, Q.; Wang, B. Surface modification of hollow glass microsphere with different coupling agents for potential applications in phenolic syntactic foams. *J. Appl. Polym. Sci.* **2017**, *134*, 44415, doi:10.1002/app.44415.

147. Lawson, J.; Willden, C. Mixture experiments in R using mixexp. *J. Stat. Softw.* **2016**, *72*, Code Snippet 2, doi:10.18637/jss.v072.c02.

148. Galvagnini, F.; Dorigato, A.; Fambri, L.; Pegoretti, A. Development of

Novel Polypropylene Syntactic Foams Containing Paraffin Microcapsules for Thermal Energy Storage Applications. *Molecules* **2022**, *27(23), 8520*, doi:10.3390/molecules27238520.

149. Rueda, M.M.; Auscher, M.C.; Fulchiron, R.; Périé, T.; Martin, G.; Sonntag, P.; Cassagnau, P. Rheology and applications of highly filled polymers: A review of current understanding. *Prog. Polym. Sci.* **2017**, *66*, 22–53, doi:10.1016/j.progpolymsci.2016.12.007.

150. Chang, C.; Powell, R.L. Dynamic simulation of bimodal suspensions of hydrodynamically interacting spherical particles. *J. Fluid Mech.* **1993**, *253*, 1–25, doi:10.1017/S0022112093001697.

151. Qi, F.; Tanner, R.I. Random close packing and relative viscosity of multimodal suspensions. *Rheol. Acta* **2012**, *51*, 289–302, doi:10.1007/s00397-011-0597-3.

152. Qi, F.; Tanner, R.I. Relative viscosity of bimodal suspensions. *Korea Aust. Rheol. J.* **2011**, *23*, 105–111, doi:10.1007/s13367-011-0013-7.

153. Spangenberg, J.; Scherer, G.W.; Hopkins, A.B.; Torquato, S. Viscosity of bimodal suspensions with hard spherical particles. *J. Appl. Phys.* **2014**, *116*, 184902, doi:10.1063/1.4901463.

154. Ullas, A. V.; Kumar, D.; Roy, P.K. Epoxy-glass microballoon syntactic foams: Rheological optimization of the processing window. *Adv. Polym. Technol.* **2019**, doi:10.1155/2019/9180302.

155. Fredi, G.; Dorigato, A.; Pegoretti, A. Dynamic-mechanical response of carbon fiber laminates with a reactive thermoplastic resin containing phase change microcapsules. *Mech. Time-Dependent Mater.* **2020**, *24*, 395–418, doi:10.1007/s11043-019-09427-y.

156. Dorigato, A.; Fredi, G.; Pegoretti, A. Application of the thermal energy storage concept to novel epoxy–short carbon fiber composites. *J. Appl. Polym. Sci.* **2019**, *136*, 1–9, doi:10.1002/app.47434.

157. Fredi, G.; Zimmerer, C.; Scheffler, C.; Pegoretti, A. Polydopamine-Coated Paraffin Microcapsules as a Multifunctional Filler Enhancing Thermal and Mechanical Performance of a Flexible Epoxy Resin. *J. Compos. Sci.* **2020**, *4*, 174, doi:10.3390/jcs4040174.

158. Fredi, G.; Dorigato, A.; Unterberger, S.; Artuso, N.; Pegoretti, A. Discontinuous carbon fiber/polyamide composites with microencapsulated paraffin for thermal energy storage. *J. Appl. Polym. Sci.* **2019**, *136*, 1–14, doi:10.1002/app.47408.

159. Fredi, G.; Brünig, H.; Vogel, R.; Scheffler, C. Melt-spun polypropylene

filaments containing paraffin microcapsules for multifunctional hybrid yarns and smart thermoregulating thermoplastic composites. *Express Polym. Lett.* **2019**, *13*, 1071–1087, doi:10.3144/expresspolymlett.2019.93.

160. Temina Mary, R.; Soorya, N.; Dona, M.. Room temperature processable heat-resistant epoxy-oxazolidone-based syntactic foams. *Polym. Adv. Technol.* **2018**, *29*, 121–129, doi:10.1002/pat.4094.

161. Devi, K.A.; John, B.; Nair, C.P.R.; Ninan, K.N. Syntactic foam composites of epoxy-allyl phenol-bismaleimide ternary blend - Processing and properties. *J. Appl. Polym. Sci.* **2007**, *105*, 3715–3722, doi:10.1002/app.26316.

162. Xing, Z.; Ke, H.; Wang, X.; Zheng, T.; Qiao, Y.; Chen, K.; Zhang, X.; Zhang, L.; Bai, C.; Li, Z. Investigation of the thermal conductivity of resin-based lightweight composites filled with hollow glass microspheres. *Polymers (Basel).* **2020**, *12*, 1–15, doi:10.3390/polym12030518.

163. Fredi, G.; Dorigato, A.; Pegoretti, A. Novel reactive thermoplastic resin as a matrix for laminates containing phase change microcapsules. *Polym. Compos.* **2019**, *40*, 3711–3724, doi:10.1002/pc.25233.

164. Bollin, S.; Motor, F. Productivity Advantages of Lightweight Injection Molded Thermoplastics Enabled by 3M Hollow Glass Microspheres Available online: https://speautomotive.com/wp-content/uploads/2020/12/Productivity-Advantages-of-Lightweight-Injection-Molded-Thermoplastics-Bonded-by-3M-Hollow-Glass-Microspheres.pdf (accessed on Dec 2, **2022**).

165. Zeltmann, S.E.; Chen, B.; Gupta, N. Thermal expansion and dynamic mechanical analysis of epoxy matrix–borosilicate glass hollow particle syntactic foams. *J. Cell. Plast.* **2018**, *54*, 463–481, doi:10.1177/0021955X17691566.

166. Imran, M.; Rahaman, A.; Pal, S. Morphology and mechanical characterization of carbon nanotubes/epoxy based material filled with hollow glass microsphere. *Mater. Res. Express* **2020**, *7*, 25307, doi:10.1088/2053-1591/ab7164.

167. Lian, Q.; Li, K.; Sayyed, A.A.S.; Cheng, J.; Zhang, J. Study on a reliable epoxy-based phase change material: facile preparation, tunable properties, and phase/microphase separation behavior. *J. Mater. Chem. A* **2017**, *5*, 14562–14574, doi:10.1039/C7TA02816D.

168. Sundararajan, S.; Kumar, A.; Chakraborty, B.C.; Samui, A.B.; Kulkarni, P.S. Poly(ethylene glycol) (PEG)-modified epoxy phase-change polymer with dual properties of thermal storage and vibration damping. *Sustain.*

Energy Fuels **2018**, *2*, 688–697, doi:10.1039/C7SE00552K.

169. Ashby, M.F.; Johnson, K. *Materials and design : the art and science of material selection in product design*; Third edit.; Butterworth-Heinemann: Waltham, MA, 2014; ISBN 9780080982052.

170. D'Almeida, J.R.M. Evaluation of the compressive yield strength of hollow glass microsphere - Epoxy composites as a function of the microsphere/-epoxy interface strength. *Polym. Polym. Compos.* **2007**, *15*, 444–451, doi:10.1177/096739110701500603.

171. Liu, X.; Wang, G.; Pei, J.; Wang, Z.; Wu, Z. Fabrication and mechanical properties of a novel epoxy-hollow glass microsphere composite. *J. Compos. Mater.* **2018**, *52*, 1627–1632, doi:10.1177/0021998317730895.

172. Zhang, X.; Wang, P.; Zhou, Y.; Li, X.; Yang, E.H.; Yu, T.X.; Yang, J. The effect of strain rate and filler volume fraction on the mechanical properties of hollow glass microsphere modified polymer. *Compos. Part B Eng.* **2016**, *101*, 53–63, doi:10.1016/j.compositesb.2016.06.079.

173. Sutikno; Berata, W.; Wijanarko, W. Hollow glass microsphere-epoxy composite material for helmet application to reduce impact energy due to collision. *AIP Conf. Proc.* **2017**, *1855*, doi:10.1063/1.4985483.

174. Ge, H.; Jin, X.; Liu, Z.; Wang, C.; Wang, P. Compressive property and thermal stability of Hollow glass microsphere/epoxy resin lightweight composites. *J. Nanosci. Nanotechnol.* **2017**, *17*, 3217–3223, doi:10.1166/jnn.2017.13045.

175. Zeltmann, S.E.; Chen, B.; Gupta, N. Mechanical properties of epoxy matrix-borosilicate glass hollow-particle syntactic foams. *Mater. Perform. Charact.* **2017**, *6*, 1–16, doi:10.1520/MPC20150056.

176. Dando, K.R.; Cross, W.M.; Robinson, M.J.; Salem, D.R. Production and characterization of epoxy syntactic foams highly loaded with thermoplastic microballoons. *J. Cell. Plast.* **2018**, *54*, 499–514, doi:10.1177/0021955X17700093.

177. Fredi, G.; Dorigato, A.; Fambri, L.; Pegoretti, A. Multifunctional epoxy/carbon fiber laminates for thermal energy storage and release. *Compos. Sci. Technol.* **2018**, *158*, 101–111, doi:10.1016/j.compscitech.2018.02.005.

178. Zhang, L.; Zhang, J.; Wang, D.Y. Hierarchical layered double hydroxide nanosheets/phosphorus-containing organosilane functionalized hollow glass microsphere towards high performance epoxy composite: Enhanced interfacial adhesion and bottom-up charring behavior. *Polymer (Guildf).*

2020, *210*, 123018, doi:10.1016/j.polymer.2020.123018.

179. Shunmugasamy, V.C.; Anantharaman, H.; Pinisetty, D.; Gupta, N. Unnotched Izod impact characterization of glass hollow particle/vinyl ester syntactic foams. *J. Compos. Mater.* **2015**, *49*, 185–197, doi:10.1177/0021998313515290.

180. Gogoi, R.; Kumar, N.; Mireja, S.; Ravindranath, S.S.; Manik, G.; Sinha, S. Effect of Hollow Glass Microspheres on the Morphology, Rheology and Crystallinity of Short Bamboo Fiber-Reinforced Hybrid Polypropylene Composite. *JOM* **2019**, *71*, 548–558, doi:10.1007/s11837-018-3268-3.

181. Çelebi, H. Thermal conductivity and tensile properties of hollow glass microsphere/polypropylene composites. Anadolu Univ. *J. Sci. Technol. A - Appl. Sci. Eng.* **2017**, 1–1, doi:10.18038/aubtda.323483.

182. Vignali, A.; Iannace, S.; Falcone, G.; Utzeri, R.; Stagnaro, P.; Bertini, F. Lightweight poly(ε-caprolactone) composites with surface modified hollow glass microspheres for use in rotational molding: Thermal, rheological and mechanical properties. *Polymers (Basel).* **2019**, *11*, 624, doi:10.3390/polym11040624.

183. Valentini, F.; Fambri, L.; Dorigato, A.; Pegoretti, A. Production and Characterization of TES-EPDM Foams With Paraffin for Thermal Management Applications. *Front. Mater.* **2021**, *8*, 1–16, doi:10.3389/fmats.2021.660656.

184. Xing, Z.; Ke, H.; Wang, X.; Zheng, T.; Qiao, Y.; Chen, K.; Zhang, X.; Zhang, L.; Bai, C.; Li, Z. Investigation of the thermal conductivity of resin-based lightweight composites filled with hollow glass microspheres. *Polymers (Basel).* **2020**, *12*, doi:10.3390/polym12030518.

185. Ding, J.; Ye, F.; Liu, Q.; Yang, C.; Gao, Y.; Zhang, B. Co-continuous hollow glass microspheres/epoxy resin syntactic foam prepared by vacuum resin transfer molding. *J. Reinf. Plast. Compos.* **2019**, *38*, 896–909, doi:10.1177/0731684419857173.

186. Gupta, N.; Pinisetty, D. A review of thermal conductivity of polymer matrix syntactic foams - Effect of hollow particle wall thickness and volume fraction. *JOM* **2013**, *65*, 234–245, doi:10.1007/s11837-012-0512-0.

187. Afolabi, L.O.; Mutalib, N.A.A.; Ariff, Z.M. Fabrication and characterization of two-phase syntactic foam using vacuum assisted mould filling technique. *J. Mater. Res. Technol.* **2019**, *8*, 3843–3851, doi:10.1016/j.jmrt.2019.06.046.

Scientific production

- Galvagnini, F.; Dorigato, A.; Valentini F.; Fiore V.; La Gennusa M.; Pegoretti A., ***Multifunctional polyurethane foams with thermal energy storage/release capability.*** Journal of Thermal Analysis and Calorimetry. 2020, 147, 297-313, https://doi.org/10.1007/s10973-020-10367-w.
- Galvagnini, F; Valentini F.; Dorigato, A. ***Development of polymeric insulating foams for low-temperature thermal energy storage applications.*** J Appl Polym Sci. 2022, 139 (25), https://doi.org/10.1002/app.52397.
- Galvagnini, F.; Dorigato, A.; Fambri, L.; Fredi, G.; Pegoretti A., ***Thermophysical Properties of Multifunctional Syntactic Foams Containing Phase Change Microcapsules for Thermal Energy Storage.*** Polymers (Basel). 2021, 13, 1790, https://doi.org/10.3390/polym13111790.
- Galvagnini, F.; Fredi, G.; Dorigato, A.; Fambri, L.; Pegoretti, A., ***Mechanical Behaviour of Multifunctional Epoxy/Hollow Glass Microspheres/Paraffin Microcapsules Syntactic Foams for Thermal Management.*** Polymers (Basel). 2021, 13, 2896, https://doi.org/10.3390/polym13172896.
- Galvagnini, F.; Dorigato, A.; Fambri, L.; Pegoretti, A. ***Development of Novel Polypropylene Syntactic Foams Containing Paraffin Microcapsules for Thermal Energy Storage Applications.*** Molecules 2022, 27, 8520, https://doi.org/10.3390/molecules27238520.

Participation to congresses

- **MIPOL Milan polymer days (Online), 15-17 July 2020.** Poster "Multifunctional polyurethane foams with thermal energy storage/capabilities".
- **MIPOL Milan polymer days (Online), 6-8 July 2021.** Poster "Thermal-mechanical investigation of Epoxy/HGM syntactic foams incorporating encapsulated phase change materials".
- **Time Of Polymers (Ischia, NA Italy), 5-9 September 2021.** Oral presentation "Thermo-mechanical behavior of syntactic foams with thermal energy storage/release capability".
- **AIMAT2021 (Cagliari), 15-18 September 2021.** Poster "Mechanical behavior of syntactic foams incorporating Phase Change Materials for Thermal Energy Storage/Release".
- **INSTM (Sestriere, TO Italy), 23-26 January 2022.** Poster "Characterization of a multifunctional epoxy/HGM/PCM syntactic foams for thermal energy storage applications"
- **European Polymer Congress EPF 2022 (Prague), 26 June – 1 July 2022.** Oral presentation "Development and characterization of novel PP/HGM/PCM syntactic foams for thermal energy storage applications".
- **AIM (Trento), 4-7 September 2022.** Oral presentation "Development and characterization of PP/HGM/PCM syntactic foams for thermal energy storage applications".
- Member of the Organizing Secretary (Local Committee) of the **XXIV National Meeting of the ASSOCIAZIONE ITALIANA DI SCIENZA E TECNOLOGIA DELLE MACROMOLECOLE - AIM (Trento), 4-7 September 2022**

Side activities

Academic Course and Tutoring

- Update and revision of the didactic material used in the course of “Polymeric materials engineering” 2020-21, Materials and production engineering University of Trento, Department of Industrial Engineering.
- Tutor activity for the laboratory part of the course of “Polymeric materials engineering” during the second semester of the AY 2021-22, Materials and production engineering University of Trento, Department of Industrial Engineering.
- Tutor activity for the laboratory part of the course of “Polymeric and composite materials engineering. Module 1.” during the second semester of the AY 2022-23, Materials and production engineering University of Trento, Department of Industrial Engineering.

Industrial collaborations

- Collaboration in the industrial contract with Mixcycling Srl, Via dell'Artigianato 10 - 36042 Breganze (VI) Italy, 2021-23, “Sviluppo di nuovi compounds a base di miscele polimeriche di poliesteri biodegradabili e bioderivati”.
- Technical applied research for Roechling SE & Co., Via Alfred Nobel, 11, 39055 Laives BZ, “Sviluppo di materiale siliconico per il thermal management”.

Ringraziamenti

Questa tesi non è solo il riassunto di tre anni di lavoro, ma è la testimonianza delle esperienze che ho vissuto in questa parte importante della mia vita.

Quando ho cominciato questo percorso non sapevo ancora chiaramente come la mia strada si sarebbe costruita mentre la percorrevo. Non sapevo dove mi avrebbe portato e come ci sarei arrivato. Era tutto nuovo per me. Non nascondo di aver avuto dubbi e timori; ma il desiderio della scoperta, di esplorare qualcosa di nuovo mi ha fatto trovare il coraggio di buttarmi in questa avventura.

Fortunatamente non ero solo in questo mio percorso. Ho trovato un gruppo di colleghi fantastici che fin da subito mi hanno fatto sentire a casa. Quindi grazie Francesco Valentin (mio ex tutor della tesi), Giulia Fredi (per il tuo supporto), e Daniele Rigotti (per la tua allegra follia). Voi mi avete guidato nei primi mesi del mio dottorato instradandomi nella retta via. Si, anche te Rigotti.

Poco dopo ci sarebbe stato il Covid che rese tutto complicato, specie per noi che non potevamo condurre normalmente i nostri esperimenti. In quel frangente mi sono chiesto più e più volte cosa desiderassi e cosa avrei voluto ottenere da questa mia esperienza.

Qualche mese dopo si cominciò a tornare lentamente alla normalità. In quell'estate di rinascita ho conosciuto Anna, non avrei potuto essere più fortunato di così. Con lei ho condiviso e continuo a condividere tutte le splendide esperienze della vita di coppia. Solo lei è riuscita a rasserenare la mia turbolenta vita sentimentale, e a rasserenare anche questi anni di dottorato. Lei mi ha supportato e sopportato, sempre, nonostante tutto, e farò lo stesso con lei, adesso come in futuro. Grazie amore mio.

A breve giro il nostro gruppo di lavoro si sarebbe ulteriormente espanso con nuove leve. Con la loro allegria ed energia si è proprio sentita una spinta positiva dopo quel lungo periodo di chiusure forzate portando nuova linfa vitale nel lab. Quindi vorrei ringraziare Alessandro Sorze, Laura Simonini, e Davide Perin per aver scelto il lab di polimeri invece degli altri noiosissimi lab (ovviamente scherzo). Vorrei fare un ringraziamento speciale a Davide Perin, lui non è stato semplicemente un collega, lui è stato e sarà sempre un mio grandissimo amico con cui ho condiviso millanta esperienze e con cui ho sempre amato passare il tempo. Non potrò mai dimenticare il supporto e l'amicizia che hai condiviso con me e per questo ti ringrazio dal profondo del cuore. Un giorno, quando si sarà vecchi bacucchi, sono certo che ripensando alle cavolate fatte nei convegni ci rideremo su grassamente. Magari un giorno mi farai mangiare le zampe di ran… rospo.

In tutta questa vicenda Alfredo Casagranda, nostro inestimabile tecnico di laboratorio, ha giocato un ruolo fondamentale. Sarò sempre convinto del fatto che senza di lui il laboratorio sarebbe perso. Inutile dire quanto il suo aiuto sia stato importate per il mio lavoro, ma vorrei sottolineare quanto lo sia per tutti quanti. Quindi non penso di sbagliare dicendo che parlo a nome di tutti nel ringraziarti per la tua gentilezza e disponibilità.

Vorrei ringraziare anche i miei tutor Luca Fambri ma soprattutto Andrea Dorigato. Ho sempre apprezzato il poter parlare apertamente con te; anche se a volte non si era d'accordo si è sempre trovato il modo di trovare una strada comune per arrivare poi a questa tesi, dimostrazione del buon lavoro effettuato. Grazie anche per le ultime fasi del mio dottorato, il tuo supporto nel periodo in cui già lavoravo è stato fondamentale per potermi dottorare. Spero riuscirai ad essere una buona guida per i futuri dottorandi e alunni come lo sei stato già per molti negli anni passati. Il ruolo del docente è uno dei più importanti che ci sia, perché il docente ha la responsabilità di istruire le persone del domani. Stai facendo un ottimo lavoro, certo non servo io a dirtelo, e sono anche certo che continuerai a farlo. Grazie per tutto.

Vorrei ringraziare la mia famiglia per il supporto e l'interesse che hanno dimostrato negli anni di dottorato. Il sapere di avere sempre le spalle coperte mi ha sempre rassicurato del fatto che qualsiasi cosa accada, loro ci saranno sempre per me.

Vorrei ringraziare anche tutti i miei coinquilini, quelli di adesso e quelli che se ne sono andati. Con voi ho condiviso pizzate, biliardi, compleanni e serate pazze. Inconsciamente mi avete aiutato ad alleviare gli stress giornalieri. Grazie mille.

In fine vorrei fare un ringraziamento speciale al sottoscritto. Lo so, sembrerà un po' autocelebrativo, e di fatto lo è. Però è giusto che mi ricordi quanta energia e dedizione io sia stato in grado di trovare per completare questo percorso lungo e tortuoso. Le persone che ho incontrato mi hanno sicuramente aiutato, come si dice, la vita è come un fiume, a volte calmo a volte turbolento. Ma solo mettendoci del proprio pagaiando in direzione dell'obbiettivo si può sperare di arrivare. Quindi grazie a me per essere stato determinato ad iniziare, vivere e completare questo lungo percorso. Ma questo è solo l'inizio, è solo un capitolo che si chiude aprendone uno tutto nuovo. Un altro capitolo mi aspetta e con ancora più dedizione e coraggio lo dovrò affrontare. In bocca al lupo a me.